OT REPORT 75-65

STUDIES OF OXYGEN AND WATER VAPOR MICROWAVE SPECTRA UNDER SIMULATED ATMOSPHERIC CONDITIONS

OT

U.S. DEPARTMENT OF COMMERCE / Office of Telecommunications

OT REPORT 75-65

STUDIES OF OXYGEN AND WATER VAPOR MICROWAVE SPECTRA UNDER SIMULATED ATMOSPHERIC CONDITIONS

HANS J. LIEBE

U.S. DEPARTMENT OF COMMERCE
Rogers C. B. Morton, Secretary

Betsy Ancker-Johnson, Ph. D.
Assistant Secretary for Science and Technology

OFFICE OF TELECOMMUNICATIONS
John M. Richardson, Acting Director

June 1975

For sale by the Superintendent of Documents, U.S. Government Printing Office, Washington, D.C. 20402

UNITED STATES DEPARTMENT OF COMMERCE
OFFICE OF TELECOMMUNICATIONS
STATEMENT OF MISSION

The mission of the Office of Telecommunications in the Department of Commerce is to assist the Department in fostering, serving, and promoting the nation's economic development and technological advancement by improving man's comprehension of telecommunication science and by assuring effective use and growth of the nation's telecommunication resources.

In carrying out this mission, the Office

- Conducts research needed in the evaluation and development of policy as required by the Department of Commerce
- Assists other government agencies in the use of telecommunications
- Conducts research, engineering, and analysis in the general field of telecommunication science to meet government needs
- Acquires, analyzes, synthesizes, and disseminates information for the efficient use of the nation's telecommunication resources.
- Performs analysis, engineering, and related administrative functions responsive to the needs of the Director of the Office of Telecommunications Policy, Executive Office of the President, in the performance of his responsibilities for the management of the radio spectrum
- Conducts research needed in the evaluation and development of telecommunication policy as required by the Office of Telecommunications Policy, pursuant to Executive Order 11556

USCOMM - ERL

Preface

This OT-Report is Part III of the Final Report on work performed at the Institute for Telecommunication Sciences on

"Quantitative millimeter wave spectroscopy of oxygen under simulated atmospheric conditions"

with support from the following agencies:

(a) NASA Langley Research Center, Hampton, VA 23365
Order No. AAFE, L58,506 (Amendments No. 1 to 16), dated January 8, 1971, and monitored by Mr. R. E. Davis.

(b) NOAA-National Environmental Satellite Service, Suitland, MD 20233, under Order No.
NA-755-74, dated February 5, 1974,
5-13155, dated October 13, 1974,
and monitored by Mr. J. Alishouse.

(c) OT-ITS, Division of Applied Electromagnetic Science.

(d) U.S. Army Research Office, Durham, NC 27706, under MIPR No. ARO 14-74, dated May 28, 1974, monitored by Mr. E. Fliegler, USECOM-AMSEL-NLM-1, Ft. Monmouth, NJ 07703, supported part of this work during the period July 1, 1974, to May 31, 1975.

The complete Final Report consists of three parts -

Part I - OT-Report No. 73-10, May 1973 (APPENDIX A):

"Molecular attenuation and phase dispersion between 40- and 140 GHz for path models from different altitudes."

Part II - OT-Report No. 74-35, April 1974 (APPENDIX A):

"A pressure-scanning refraction spectrometer for atmospheric gas studies at millimeter wavelengths."

Part III - This Report.

Inquiries should be addressed to the author at the Institute for Telecommunication Sciences, Office of Telecommunications, U.S. Department of Commerce, Boulder, CO 80302.

CONTENTS

LIST OF FIGURES

GLOSSARY OF TERMS

See pages ix and x of Part 2.

LIST OF TABLES

STUDIES OF OXYGEN AND WATER VAPOR MICROWAVE SPECTRA UNDER SIMULATED ATMOSPHERIC CONDITIONS

Hans J. Liebe*

ABSTRACT

Atmospheric radio wave propagation in the 40 to 140 GHz band is influenced by microwave spectra of oxygen (O_2-MS) and water vapor. The report treats the complementary roles of controlled laboratory experiments and computer analysis for providing detailed molecular transfer characteristics. A pressure-scanning differential refractometer was operated at fixed frequencies between 58 and 61.5 GHz. The variability of O_2 and H_2O spectra with frequency, pressure, temperature, and magnetic field strength was studied under conditions which occur in the atmosphere. Results obtained (a) for oxygen and air on the 9^+ line, the $7^+/5^-$ and $3^+/9^-$ doublets, and the continuum spectrum and (b) for water vapor on nonresonant effects are reported. The experimental O_2-MS data are used in theoretical analyses of attenuation and dispersion rates which are extended to other lines, to frequencies identified for remote sensing applications, and to temperature and pressure sensitivities between 40 and 140 GHz.

Key Words: Atmospheric mm-wave propagation; attenuation profiles; dispersion profiles; EHF transfer characteristics; oxygen microwave spectrum; water vapor microwave spectrum.

1. INTRODUCTION

Radio wave propagation in the 40 to 140 GHz band through the first hundred kilometers of the clear atmosphere is strongly influenced by many (> 30) lines of the oxygen microwave spectrum (O_2-MS) and to a lesser extent by a nonresonant spectrum of water vapor. Attenuation, phase dispersion, and thermal noise associated with these molecular effects of air impose ultimate propagation limitations as well as

*The author is with the Institute for Telecommunication Sciences, Office of Telecommunications, U.S. Department of Commerce, Boulder, CO 80302.

affording unique system opportunities (e.g., transmission security and remote sensing of atmospheric variables). This is the last in a series of three reports which all address the problem of establishing a reliable correlation between clear air transfer properties and meteorological variables. Part 1 (Liebe and Welch, 1973)* reviewed O_2-MS theory, identified directions for experimental research, and demonstrated computer analysis of transfer properties for various path configurations. Part 2 (Liebe, 1974)* described in great detail a new experimental technique capable of measuring, under simulated atmospheric conditions, molecular attenuation and phase dispersion rates.

This Part 3 treats the complementary roles of controlled laboratory experiments and computer analysis in providing information on the complicated dependences of gaseous atmospheric microwave spectra. The report treats oxygen, air, and water vapor behaviors. Section 2 dwells upon the variability of O_2-spectra with frequency ν, pressure p, temperature T, and magnetic field strength H as they occur over the altitude range $h = 0$ to 80 kilometers. Such a description of electromagnetic properties of the atmosphere is fundamental to treatments of amplitude, phase, and directional responses of any emergent signal. In addition, above 40 kilometers height, the Zeeman-effect causes dependences upon polarization and orientation (unisotropic medium). Section 2 is organized in Paragraphs A and B, separating experimental and analytical O_2-MS studies. The variable for experiments is the gas

---

*) Referred to throughout this report as Part 1 and Part 2. Both reports have been condensed to Journal publications:
Liebe, IEEE Trans. MTT-23, 380-385, (1975); Rev.Sci.Instr. 46, July (1975)

pressure p, which is paralleled by the microwave frequency ν in analytical treatments of molecular transfer and emission characteristics. Three problem areas are investigated; namely, (a) in Sections 2.1 and 2.2, pressure-broadening of individual lines in O_2, in binary mixtures of O_2+ air components, and in air; (b) in Section 2.3, isolated line behavior as the pressure approaches zero; and (c) in Section 2.4, the band shape (O_2-MS continuum) formed by more than thirty overlapping lines. The experimental results are taken into account in Sections 2.5 and 2.6 to arrive at specific O_2-MS properties under atmospheric conditions. Section 3 discusses laboratory measurements of water vapor at 23, 30.6, and 61.2 GHz, which yield anomalous high attenuation and dispersion rates when the saturation pressure is approached.

Past experimental and theoretical studies of O_2 and H_2O microwave spectra have been carried out to a large extent at universities, as manifested by numerous Ph.D. theses (P-1 to P-17) all addressing fundamental problems related to the interaction of gas molecules with microwave radiation. Each work in its own right has furthered and refined the understanding, although invariably some frustration is expressed in regard to the lack of reliable absolute intensity data.

The ability to describe molecular transfer characteristics of air under general meteorological conditions is of great practical importance particularly for extending the radio spectrum into the 40 to 140 GHz range and for "all-weather" remote sensing of atmospheric temperature structure via satellite. Microwave radiometers are operating in two research satellites (NIMBUS 5, 6) and are planned for an operational

satellite (TIROS N). The interpretation of O_2-MS emission in terms of atmospheric temperature hinges on accuratly known dependencies of the O_2-MS upon the physical parameters, hence, providing the main impetus to our studies.

Such studies are conducted best in the laboratory under highly controlled conditions but, of course, they cannot compete with the long path lengths ($> 10^6$m, inhomogeneous) encountered in the atmosphere. The limited effective path length ($< 5 \cdot 10^2$m, homogeneous) of a laboratory microwave experiment requires extraordinary means to achieve the necessary detection sensitivity. It is easy to simulate pressure and temperature, but a new approach had to be taken to secure reliable spectroscopic information, which traditional absorption spectroscopy had not delivered. The spectrometer, as described in Part 2, utilizes dispersion instead of absorption intensities versus variable pressure instead of frequency. The usefulness of such experimental technique had been proven by studies of the 22 GHz water vapor line (Liebe, 1969). Over the 50 to 75 GHz range, the same method, however, posed several problems stemming from requirements of extreme detection sensitivity and novel data diagnostics. Changes in frequency had to be resolved to better than 1 part in 10^9, and the reduction of O_2-MS dispersion data to parameters of the band components (> 30 individual lines) as well as their reassembly to band intensities turned out to be quite challenging. By and large, the progression of experimental observations, learning, and revised measurement strategy proceeded satisfactorily, and the results of our findings are the topic of this report.

1.1 Complex Refractivity and Propagation Parameters

The interaction between EHF radiation and air is described by a complex refractivity

$$N = (n-1)10^6 = [N_o + \Delta N_d(\nu) + \Delta N_w(\nu)] - j\,[N''_d(\nu) + N''_w(\nu)], \quad (1)$$

where ν is the microwave frequency, n is the refractive index, and $j = \sqrt{-1}$, N_o is the frequency-independent refractivity, $\Delta N(\nu)_{d,w}$ are molecular dispersion spectra of dry air (O_2) and water vapor (H_2O, H_2OOH_2), respectively, while $N''(\nu)_{d,w}$ are the associated extinction spectra, all in units of parts per million [ppm].

The refractivity N_o is given by

$$N_o = N^o p = R^o p/T \quad [ppm], \quad (2)$$ †)

where R^o = 95.67(10) *) [ppm°K/torr] for O_2,
103.56(2) " for AIR,
105.60(3) " for N_2,
95.5 + 499500/T " for H_2O vapor.

Additional values of R^o for the individual air components are listed in Table 8.

The relationship to propagation parameters such as power attenuation α and phase rate ϕ is simply

$$\alpha = 0.1820\nu\, N''_{d,w} \quad [dB/km], \quad (3)$$

and

$$\phi = \phi_o + \Delta\phi = 2.095\cdot 10^{-2}\nu\,(N_o + \Delta N_{d,w}) \quad [rad/km],$$

where ν is the frequency in gigahertz [GHz].

†) Pressure proportionality is indicated in general for all appropriate parameters by a superscript°.

*) Digits in parenthesis following a numerical value represent the Standard Deviation of that value in terms of the final listed digits.

2. STUDIES OF THE OXYGEN MICROWAVE SPECTRUM

A1. THEORY (Versus Experiment)

Oxygen microwave (ν = 10 to 150 GHz) spectra of dispersion ΔN and extinction N'' are introduced as a sum of 44 lines identified by the quantum number $N^{\pm}$,

$$\Delta N_d = \sum_{N^{\pm}=1}^{43} (SF')_{N}^{\pm} \quad [\text{ppm}] ,$$
$$N''_d = \sum_{N^{\pm}=1}^{43} (SF'')_{N}^{\pm} \quad [\text{ppm}] . \tag{4}$$

The isolated line properties of strength S [Hz] and shape F', F'' [1/MHz] have been discussed in Parts 1 and 2. Theoretical treatments of the band shape composed of overlapping O_2-MS lines exist from Dillon and Godfrey (1972) and Mingelgrin (1972, 1974). The complexity of their computations, however, prevented applications to practical problems related to the atmospheric O_2-MS. Several empirical approaches to solve equation (4) for atmospheric conditions (1 to 800 torr, 180 to 320°K) which were discussed in Part 1, are fairly adequate in describing ad hoc the existing data body; but rather arbitrary assumptions disqualify them from being of general validity. Recently, Rosenkranz (1975) has come up with a manageable O_2-MS band expression. As a first order solution (in respect to pressure) of a general band shape, he derived interference coefficients Y_N^o [1/torr] attached to each line and calculable from line parameters. The coefficients Y_N^o produce with increasing pressure (overlap) a redistribution of each line contribution within the 60 GHz band.

The line shape factors for a line within the O_2-MS are given by (Rosenkranz, 1975)

$$F' = \frac{\nu}{\nu_o}\left(\frac{\nu_o-\nu+\gamma^o I^o p^2}{(\nu_o-\nu)^2+(\gamma^o p)^2} - \frac{\nu_o+\nu+\gamma^o I^o p^2}{(\nu_o+\nu)^2+(\gamma^o p)^2}\right) , \qquad (5)$$

$$F'' = p\ \frac{\nu}{\nu_o}\left(\frac{\gamma^o-(\nu_o-\nu)I^o}{(\nu_o-\nu)^2+(\gamma^o p)^2} + \frac{\gamma^o-(\nu_o+\nu)I^o}{(\nu_o+\nu)^2+(\gamma^o p)^2}\right) . \qquad (6)$$

The line strength $S = S^o p$ remains as defined in Part 1 (Eqs. 7-12; Tables 3, 7) and Part 2 (Eqs. 18, 19; Table 1). In the vicinity of a resonance $[\pm(\nu_o-\nu) \leq 50$ MHz] and at lower pressures ($p < 100$ torr, $I^o \approx 0$), the shape factors reduce to simple Lorentzians,

$$F' = \left(\frac{\nu_o-\nu}{(\nu_o-\nu)^2+(\gamma^o p)^2}\right)\frac{\nu}{\nu_o} , \qquad F'' = \left(\frac{\gamma^o p}{(\nu_o-\nu)^2+(\gamma^o p)^2}\right)\frac{\nu}{\nu_o} . \qquad (7)$$

The resonant linewidths in O_2 are (see Tables 6, 7)

$$\gamma^o \doteq (2.00-0.023N)(300/T)^{0.9} \qquad \text{[MHz/torr]} , \qquad (8)$$

whereby the quantum number N dependence is predicted by theory (Dillon and Godfrey, 1972; Mingelgrin, 1972; Pickett, 1975).

The interference coefficients are calculated as shown by Rosenkranz (1975),

$$Y_N^o = \frac{1}{d_N^{\pm}}\left\{\frac{2\ d_{N+2}^{\pm}\ a_N^o}{\nu_N - \nu_{N+2}} + \frac{2\ d_{N-2}^{\pm}\ b_N^o}{\nu_N - \nu_{N-2}} - \gamma_o^o\left(\frac{1}{\nu_N} + \frac{1}{\nu_N + 60\ \text{GHz}}\right)\right\} , \qquad (9)$$

when assuming the following:

i) the nonresonant linewidth in O_2 is

$$\gamma_o^o = 0.75(300/T)^{0.9} \qquad \text{[MHz/torr]} ; \qquad (10)$$

Table 1. Interference Coefficients $I^{o}(N^{+}_{-})$ at 252, 281, 300, and 325°K and the temperature exponents z^{+}_{-}.

	N^{+}					N^{-}				
T[°K]	252°	281°	300°	325°	z^{+}	252°	281°	300°	325°	z^{-}
N^{+}_{-}		I^{o} [1/10^{4} torr]					I^{o} [1/10^{4} torr]			
1	9.13	8.36	7.93	7.43	.8	-0.42	-0.39	-0.37	-0.34	.8
3	9.58	8.86	8.45	7.97	.7	-7.61	-6.99	-6.65	-6.24	.8
5	5.80	5.54	5.38	5.17	.5	-6.92	-6.48	-6.22	-5.91	.6
7	2.04	2.25	2.34	2.41	- .7	-3.82	-3.81	-3.77	-3.70	.1
9	- 1.13	-0.51	-0.20	0.10	9.5	-0.48	-0.91	-1.10	-1.29	-3.9
11	- 3.69	-2.72	-2.24	-1.73	3.0	2.38	1.57	1.17	0.76	4.5
13	- 5.76	-4.51	-3.88	-3.21	2.3	4.68	3.56	2.99	2.40	2.6
15	- 7.32	-5.86	-5.11	-4.32	2.1	6.51	5.14	4.45	3.71	2.2
17	- 8.69	-7.05	-6.21	-5.31	1.9	7.96	6.39	5.59	4.74	2.0
19	- 9.66	-7.90	-6.99	-6.01	1.9	9.08	7.37	6.49	5.55	1.9
21	-10.41	-8.56	-7.61	-6.57	1.8	9.92	8.12	7.18	6.17	1.9
23	-10.93	-9.04	-8.05	-6.98	1.8	10.53	8.66	7.69	6.64	1.8
25	-11.26	-9.34	-8.35	-7.26	1.7	10.91	9.02	8.03	6.96	1.8
27	-11.39	-9.49	-8.50	-7.41	1.7	11.10	9.21	8.22	7.15	1.7
29	-11.35	-9.49	-8.51	-7.44	1.7	11.09	9.24	8.27	7.21	1.7
31	-11.15	-9.36	-8.42	-7.40	1.6	10.93	9.15	8.21	7.19	1.6
33	-10.78	-9.08	-8.17	-7.17	1.6	10.59	8.88	7.98	6.98	1.6
35	-10.32	-8.76	-7.93	-7.02	1.5	10.14	8.58	7.75	6.85	1.5
37	- 9.59	-8.10	-7.29	-6.39	1.6	9.42	7.93	7.12	6.21	1.6
39	- 9.2	-8.0	-7.3	-6.6	1.3	9.0	7.8	7.2	6.5	1.3

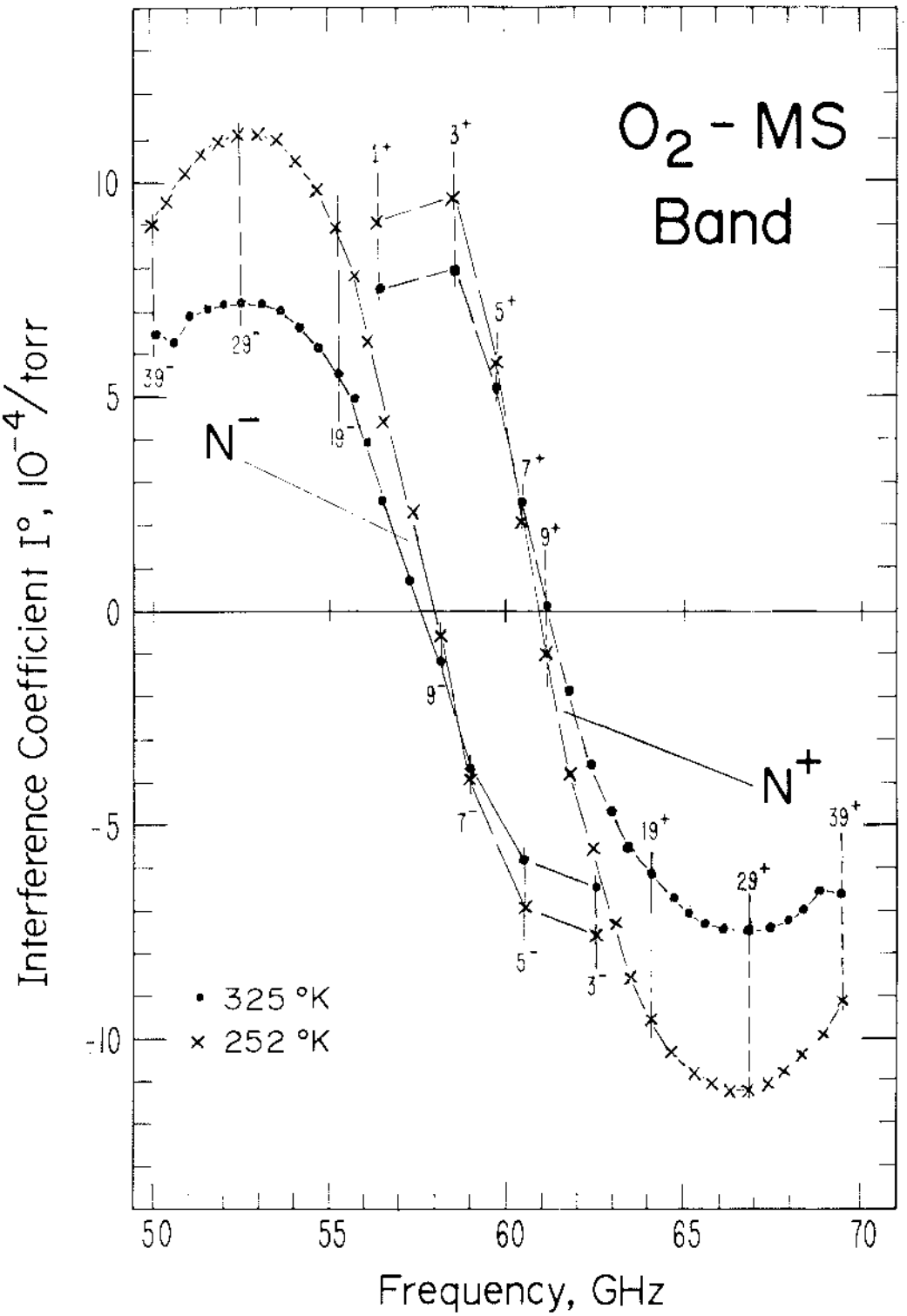

Figure 1. Interference coefficients $I^{o}_{N^{\pm}}$ for $N^{\pm}$ = 1 to 39 O_2-MS lines at temperatures chosen for experiments.

ii) the line coupling elements are obtained by the iterative procedure ($N = 43$ to 1),

$$a^o(N=43) = 0 \ , \ a^o_{N-2} = b^o_N \ \frac{2N+1}{2N-3} \exp[-2.069(4N-2)/T] \ ,$$

$$b^o_N \doteq \gamma^o_o - \gamma^o - a^o_N \ ; \qquad (11)$$

iii) the line amplitudes for the N^+ and the N^- line branches are

$$d^+ = [N(2N+3)/(N+1)(2N+1)]^{1/2} \quad (0.91 \text{ to } 1),$$

$$d^- = [(N+1)(2N-1)/N(2N+1)]^{1/2} \quad (0.82 \text{ to } 1). \qquad (12)$$

Results for I^o between $N^{\pm} = 1$ to 39 are listed in Table 1 at four experimental temperatures and depicted in figure 1. Also given is an approximate temperature exponent z defined by

$$I^o_N(T) \doteq I^o_N(300)(300/T)^z \ . \qquad (13)$$

Frequency and pressure dependencies of equation (4) are expressed explicitly while the temperature dependence is implicit in S^o, γ^o, I^o.

Equations (1) to (13) define a theoretical model of the intensity distribution by the pressure-broadened ($p \approx 1$ to 800 torr) O_2-MS under atmospheric conditions. One value of ΔN or N'' is determined, more or less, by contributions from over thirty lines and their mutual interferences (Eq. 4). The main purpose of this work is to verify and/or modify that model by reliable measurements. Experiments start with finding the parameters (S, γ, ν_o) for as many individual lines as possible. These data are obtained at lower pressures ($p < 100$ torr). The next step is to measure at higher pressures (100 to 800 torr) the band envelope and compare the results first with theoretical predictions

based on the linear addition of line terms ($I_N^o = 0$) and then find out if inclusion of interference terms ($I_N^o \neq 0$) improves the fit.

A2. EXPERIMENT (Versus Theory)

Quantitative studies are performed using dispersion data from the PRS (Pressure-Scanning Refraction Spectrometer - Part 2). Conditions have been simulated as follows:

Pressure	,	$p = 10^{-3}$ to 10^{3} torr.
Frequency of resonator R2,		ν_R = (58 to 62 GHz) ± 5 kHz.
Reference frequency by R1,		$\nu = \nu_R/2$.
Temperature	,	T = 252 to 325°K.
Magnetic field strength	,	H ≈ 0 and 0.53 G.

The variables for experimental and analytical treatments are different (see below).

	Part A Experiment Prediction	Part B Atmospheric Transfer Characteristics
Gas	O_2, Air, $O_2 + N_2$ (Ar, etc.)	AIR
Variable 1	Pressure p	Frequency ν
Variable 2	Frequency ν $\nu = \nu_R(1-N^o p)$	Altitude h (Pressure p)
Parameter 1	Temperature T	
Parameter 2	Magnetic Field Strength H when $\nu \approx \nu_o$ and $p < 3$ torr	
Result 1	$\Delta N(p) = N(\nu_R) - N(\nu_R/2)$	$\alpha(\nu)$
Result 2	$\alpha(p) = \text{fct}\ (a_1, Q, \beta)$	$\Delta\phi(\nu)$

In part A, experimental data are reduced to line parameters (strengths S_N, widths γ_N) which in turn are applied to theoretical predictions. The

task is completed once a set of parameters can reproduce satisfactorily the experimental data. The same set of line parameters is then, of course, valid for analytical treatments of transfer characteristics as given in Part B.

2.1 Self-Pressure-Broadening of O_2-MS Lines

Pressure-broadening of a line sets limits on pressure and frequency,

$$2.5 \leq p \leq 100 \text{ [torr]} \quad \text{and} \quad 5 \leq \nu_R \leq 50 \text{ [MHz]} \quad . \tag{14}$$

The Lorentzian shape (Eq. 7) is valid within these limits; below, Zeeman and Doppler broadening effects govern the line shape (Section 2.3) and above, overlapping lines interfere within the O_2-MS band (Section 2.4).

It is impossible to study properties of a pressure-broadened O_2-MS line in absolute isolation since the presence of all lines within the band adds a continuum term. For conditions specified by equation (14) one can separate line and continuum contributions and express equation (4) through (Eqs. 24 to 27 - Part 2)

$$\Delta N_d = \Delta N_L + (n_1^o + \Delta\nu n_2^o)_L p = \Delta N_L + K^o p \ , \tag{15}$$

and

$$N_d'' = N_L'' + (n_1'' - \Delta\nu n_2'')p^2 = N_L'' + K''p^2 \quad , \tag{16}$$

where

$$K^o \sim \sum_{N^\pm}^{\Gamma} S_{N^\pm} \qquad \text{and} \qquad K'' \sim \sum_{N^\pm}^{\Gamma} (\gamma S)_{N^\pm} \quad . \tag{17}$$

Quantitative experimental work relied on dispersion pressure profiles $\Delta N(p)$. The best candidate to start is the 5^+ line, which has the smallest continuum term (Table 2 - Part 2), $K^o(5^+) = -1.25 + 0.0170\ \Delta\nu$ [10^{-3} ppm/torr] at 300°K. So, introducing the theoretical value for

$K^o(5^+)$ in equation (15) will have the least error in reducing line parameters (S^o, γ^o) in case the theoretical strength values $S^o_{N\pm}$ are incorrect.

The pure line dispersion is

$$\Delta N_L = (S^o/\gamma^o)y/(1 + y^2) \qquad [ppm] \ . \qquad (18)$$

The pressure is normalized to $y = p/p_M$ with

$$p_M = \pm\Delta\nu/(\pm\gamma^o - N^o\nu_R) \doteq |\Delta\nu|/\gamma^o \quad [torr] \qquad (19)$$

being the pressure at the maximum of ΔN_L :

$$\Delta N^L_o(p_M) = S^o/2\gamma^o \qquad [ppm] \ , \qquad (20)$$

and

$$\Delta\nu = \nu_o - \nu_R \qquad [MHz] \ . \qquad (21)$$

From figure 2, we realize two important diagnostic values of $\Delta N(p)$ occurring at p_m and p_o; namely, the maximum $\Delta N_o(p_m)$ and $\Delta N_d(p_o) = 0$. The pressure p_o follows from $-N_L = K^o p_o$,

$$p_o = p_m\sqrt{A - 1} \ , \qquad (22)$$

where

$$A = S^o/K^o\Delta\nu \ . \qquad (23)$$

The pressure p_m is shifted in respect to p_M as $\Delta\nu$ changes sign and is obtained from $d(\Delta N_d)/dp = 0$ (Eq. 15) to be

$$p_m = p_M\sqrt{\frac{1}{2}[-A - 2 \pm\sqrt{(A + 4)^2 - 16}]} \qquad (24)$$

(e.g., A = 100, -100, 1, -8 yields p_m/p_M = .981, 1.021, 0 [min], 6 [max]).

Another diagnostic evolves from dispersion data pairs $\Delta N(p_1) = \Delta N(p_2)$ as shown in figure 5.4 of Part 2. The locus of $p_c = (p_1 + p_2)/2$ is a straight line for $\Delta N \geq 0.75\ \Delta N_o$ and intersects the peak value $\Delta N_o(p_m)$.

For these pairs,

$$p_c \doteq -2\Delta\nu \cdot \Delta N/(S^o + 2\Delta\nu K^o) \quad , \tag{25}$$

yielding $$p_m \doteq p_M \, A/(A + 2) \quad . \tag{26}$$

The measured values of p_m, p_o, and p_c serve as check marks for line parameter combinations.

A family of dispersion profiles recorded in the vicinity of a line is "polluted" by the phase error ΔN_ϕ. The error is induced by O_2-MS extinction as a consequence of the finite sweep speed δ and amounts to (Section 4.5 - Part 2)

$$\pm\Delta N_\phi \doteq Q^2(\pm\delta)/2\pi\nu_R^2(Q + Q_M) \quad , \tag{27}$$

where ν_R is the resonance frequency of R2,

Q is the loaded Q-value of R2, and

$Q_M = 10^6/2N''_d = 9.099\cdot10^4\nu_R/\alpha$ is the medium Q-value (e.g., $\Delta N_\phi = 0.037$ ppm for a typical PRS setting of $\nu_R = 61.2$ GHz when $\delta = 10$ kHz/μs, $Q = 360000$, $Q_M = 1137000$ [4.9 dB/km]). Dispersion pressure profiles differ by $2\Delta N_\phi$ when recorded with increasing $(+\delta)$ and decreasing $(-\delta)$ sweep speed. The systematic instrumental error can, at least in principle, be eliminated by

$$\Delta N_{true} = [\Delta N^-(+\delta) + \Delta N^+(-\delta)]/2 \quad . \tag{28}$$

In our case, the procedure of (28) was not valid since an asymmetry of the reflected R2 resonance curve caused more phase error (compared with Eq. 27) when the steeper slope was excited first and less when the reverse was true yielding, with $\Delta N_\phi^-/\Delta N_\phi^+ = g > 1$,

$$\Delta N_{true} = (g\Delta N^+ + \Delta N^-)/(1+g). \tag{29}$$

The phase error can be approximated by

$$2\Delta N_{\phi} \doteq C\, p^2/[p^2 + (\Delta\nu/\gamma^{o})^2] \qquad (30)$$

as long as $N''_d < 10^6/2Q$ (see Eq. 27). Equation (30) is a single line Lorentzian extinction pressure profile (Eq. 13 - Part 2).

True line dispersion profiles (Eq. 15) will be recorded only when the phase error is reduced below the noise level of the ΔN- detection (<0.001 ppm). This calls for untolerably low values of δ (Eq. 27). Averaged line dispersion data require knowledge of the phase error ratio g (Eqs. 28, 29), or taking advantage of specific line properties. For example, the error ΔN_{ϕ} at p_m is approximately constant ($\alpha \doteq$ const., Fig. 8) for all data recorded under constant sweep speed δ. Also, p_m is symmetric to p_M in respect to $\pm\Delta\nu_1$ (Eqs. 24, 26) for data groups below 30 MHz. These properties, in conjunction with (33), permit the data diagnostic

$$\left.\begin{aligned} \Delta N_o^{I} &\doteq [\Delta N_o(-\Delta\nu_1) - \Delta N_o(+\Delta\nu_1)]/2 \quad , \\ \gamma^{o} &\doteq 2|\Delta\nu|/[p_m(-\Delta\nu_1) + p_m(+\Delta\nu_1)] \quad , \\ n_1^{o} &\doteq [\Delta N_o(-\Delta\nu_1) + \Delta N_o(+\Delta\nu_1)]/[p_m(-\Delta\nu_1) + p_m(+\Delta\nu_1)] \quad , \end{aligned}\right\} \qquad (31)$$

and the results are independent of ± sweep direction, since the phase error cancels.

At this point it is best to discuss the relevancy of equations (15) to (31) in the light of an example. Extensive data have been recorded for the 9^+ line.

2.1.1 The 9^+ Line (252-325°K).

The strongest O_2-MS line at 300°K is 9^+. The assumed line parameters are

$$
\left.
\begin{aligned}
N^o(300) &= 0.319 \ \text{[ppm/torr]} \quad \text{(Eq. 2)}, \\
\nu_o &= 61.150567 \ \text{[GHz]} \quad \text{(Table 2 - Part 1)}, \\
S^o(300) &= 1.590 \ \text{[Hz/torr]} \quad \text{(Table 3 - Part 1)}, \\
w &= 2.33 \quad \text{(Table 4 - Part 1)}, \\
\gamma^o(300) &= 1.79 \ \text{[MHz/torr]} \quad \text{(Eq. 8)} \\
u &= .9 \quad \text{(Eq. 8)}
\end{aligned}
\right\} \quad (32)
$$

$$K^o(300) = (-3.10 + 0.0117\Delta\nu)10^{-3} \ \text{[ppm/torr]} \quad \text{(Table 2 - Part 2)}.$$

Pressure and frequency profiles are predicted for various $\Delta\nu$ and p parameters as depicted in figures 2 and 3.

Experimental conditions are identified by (a) the frequency ν_R, which was tuned symmetrically to ν_o yielding data in $\pm\Delta\nu_1$ groups between 5 and 50 MHz; (b) the temperature T, which was kept constant at 325, 300, 281, or 252°K; (c) the pressure p, which varied between 0 and 150 torr at a rate of roughly ±0.1 torr/second; and (d) the sweep speed $\pm\delta$ (Eq. 27), which was constant at each T (12 to 15 kHz/μs). Oxygen was of research quality with a purity of 99.995 percent. Dispersion $\Delta N(p)$ and relative attenuation $\alpha_r(p)$ profiles have been recorded.

Dispersion Pressure Profiles

The body of 9^+ line data consisted of 190 dispersion profile pairs $\Delta N^{\pm}(\pm\delta)$ recorded in $\pm\Delta\nu_1$ groups. Each profile consists of three contributions with various sign combinations:

$$
\left.
\begin{aligned}
\Delta N^+(-\Delta\nu_1) &= \Delta N_L + K_a^o p - \Delta N_\phi^+ , \\
\Delta N^-(-\Delta\nu_1) &= \Delta N_L + K_a^o p + \Delta N_\phi^+ \cdot g , \\
\Delta N^+(+\Delta\nu_1) &= -\Delta N_L + K_b^o p - \Delta N_\phi^+ , \\
\Delta N^-(+\Delta\nu_1) &= -\Delta N_L + K_b^o p + \Delta N_\phi^+ \cdot g .
\end{aligned}
\right\} \quad (33)
$$

The dispersion intensity was calibrated (Sect. 4.4 - Part 2) applying the refractivity N^o reported by Newell and Baird (1965) for nitrogen (Eq. 2, Table 9), which was confirmed by us. Data reduction started with the peak values $\Delta N_o(p_m)$ which proved to be most reliable of all data. The known experimental quantities are p, ν_o, $\Delta\nu$, T, and N^o; the recorded output is $\Delta N^{\pm}(p)$ with the extraordinary points $\Delta N_o^{\pm}$, $p_m^{\pm}$ and $p_o^{\pm}$. Table 2 presents an overview of the interrelationships between these quantities, all calculated with the simplifying assumption expressed in equation (15). The symmetry of p_m with respect to p_M is assured when $\pm\Delta\nu$ = 5 to 30 MHz thus setting limits on the applicability of equation (31). A plot of ΔN_o and p_m versus $\Delta\nu$ is basically nonlinear since K^o depends upon $\Delta\nu$. The results of Table 2 can be compared in figure 2 with a computer calculation based on (4) and $I_N^o = 0$.

Selected 9^+ line raw data are listed in Tables 2a-c as obtained for + sweeps at four temperatures between 252 and 325°K. The pressure range was up to 450 torr, although above about 300 torr (e.g., Fig. 27) the line loses its identity. Three parameters are determined immediately by (31), namely ΔN_o^L, γ^o, and n_1^o. The agreement of calculated values (Table 2) with experimental ones is excellent, since one input (γ^o) was the experimental result. Typical plots of extracted data points are depicted in figures 4 to 7. Each point is averaged from several (3 to 8) measurements. The error estimates were obtained with the aid of conventional propagation-of-error methods.

Figure 6 and Table 2b give an example of another diagnostic applicable to $\Delta N(p)$-profiles, that is the starting slope identified by p_s (see Fig.

2.1 - Part 2). It follows that for a Lorentzian shape plus a pressure-linear continuum term (Eq. 15)

$$p_m/p_s = 2(1 - 1/A), \tag{34}$$

transforming to the approximation (A>>1)

$$\gamma^o \doteq (|\Delta\nu|/2p_s)[A/(A+1)] + N^o\nu_R, \tag{35}$$

that supports a line width parameter. An example is given in Table 2b.

The simple concept of assuming $\Delta N_\phi^\pm$ = const. for $\Delta N_o^\pm$ and taking advantage of the line symmetry (Eq. 31) yields correct line parameters, although only one data point out of many is utilized. A computer program was written to adjust S^o and γ^o to give the best fit in the least squares sense to a large number of $\Delta N^+(p)$ or $\Delta N^-(p)$ data points. Unfortunately, the program did not converge to unique values of S^o and γ^o as evident from the example listed in Table 3. The large fluctuations are caused by the phase error ΔN_ϕ (Eq. 22), which distorts $\Delta N(p)$-profiles in a systematic way. Such analysis, however, is still useful in that the mean of each parameter agrees reasonably well with the more reliable values deduced from $\Delta N_o^+(p_m^+)$.

The analysis demonstrated in Tables 2a-c was also performed on the $\Delta N_o^-(p_m^-)$ data and the results were essentially the same with slightly larger error margins due to the larger phase error $\Delta N_\phi^- \doteq 3\Delta N_\phi^+$ (e.g., Figs. 4, 7).

In summary, it is possible to deduce 9^+ line parameters from dispersion pressure profile maxima without paying attention to the phase error $\Delta N_\phi^\pm$. The uncertainty (standard deviation from the mean) was 0.7, 1.1, and 6 percent for ΔN_o^L, γ^o, and n_1^o, respectively, for the data at 281

Table 2. 9^+ O_2MS Line calculations at T = 300°K (Parameters see Eq. 32)

$\Delta\nu$	K^o Eq. 32	A Eq. 23	p_M *) Eq. 19	p_o Fig. 2	p_o Eq. 22	p_m Fig. 2	p_m Eq. 24	p_m Eq. 26	Δp +)	ΔN_o Eq. 15
[MHz]	[ppm/torr]				[torr]					[ppm]
- 5	$-3.16\cdot10^{-3}$	+100.6	2.76	-	27.1	-	2.69	2.70	- .07	.436
+ 5	-3.04	-104.6	2.82		∞	-	2.89	2.88	+ .07	-.453
-10	-3.22	+ 49.4	5.54	38.5	38.5	5.3	5.33	5.32	- .21	.427
+10	-2.98	- 53.4	5.65		∞	5.9	5.87	5.87	+ .22	-.461
-20	-3.33	+ 23.9	11.05	53	52.9	10.2	10.18	10.2	- .87	.409
+20	-2.87	- 27.7	11.30		∞	12.2	12.18	12.2	+ .88	-.478
-30	-3.45	+ 15.4	16.58	63	62.9	15	14.7	14.7	-1.9	.390
+30	-2.75	- 19.3	16.94		∞	19	18.9	18.9	+2.0	-.493
-40	-3.57	+ 11.1	22.11	70.5	70.3	19	18.9	18.7	-3.2	.371
+40	-2.63	- 15.1	22.59		∞	26.5	26.4	26.0	+3.8	-.508
-50	-3.69	+ 8.6	27.63	77	76.2	23	22.7	22.4	-4.9	.352
+50	-2.52	- 12.6	28.24		∞	34.5	34.5	33.6	+6.3	-.522

+) $p_m = p_M \pm \Delta p$.

*) $p_M(+) = p_M(-)(1+a)/(1-a)$ where $a = N^o\nu_R/\gamma^o = 0.0110$,
$p_M(+) = 1.022\ p_M(-)$.

Table 2a. 9^+ Line data points for oxygen at T = 300°K (64 ΔN-profiles)

Δν [MHz]	ΔN_o^+	ΔN_o^-	ΔN_o^+	ΔN_o^-	p_o^+	p_m^-	p_m^+	$\bar{p}_m$	γ^o [MHz/torr]	n_1^o [10^{-3} ppm/torr] (a)
	[ppm] Figure 4				[torr] Figure 5					
5	.422	.435	-.466	-.453		2.68	2.91	2.79	1.79	-3.1
10	.412	.425	-.476	-.463		5.30	5.88	5.59	1.79	-3.3
15	.403	.416	-.485	-.472		8.0	8.9	8.45	1.78	-3.3
20	.393	.406	-.490	-.477		10.5	12.0	11.25	1.78	-3.1
25	.385	.398	-.505	-.492		12.5	15.5	14.0	1.79	-3.3
30	.377	.390	-.512	-.499		15.0	18.8	16.9	1.77	-3.2
ΔN_ϕ	+0.013									
	$\Delta N_o^L = \pm.444(3)$ *)								$\gamma^o = 1.79(2)$	$n_1^o = -3.2(2)$
40	.356	.369	-.521	-.508		20	25.5	22.75	1.76	-3.1
50	.334	.347	-.540	-.527	66	24	34	29	1.72	-3.1
100	.230	.243	-.614	-.601	84	38	90	64	1.56	-2.8
150	.136				84	39				
200	.049				66	30				
300	- .98 at 450 torr				0	>450				
400	-1.02 at 450 torr				0	>450				
500	- .74				0	159(7^+)				

*) $\sum_{i=1}^{n} [\,|\Delta N_o(+\Delta\nu)| + \Delta N_o(-\Delta\nu)\,]_i / 2n$

(a) $n_1^o = [\Delta N_o(+\Delta\nu) + \Delta N_o(-\Delta\nu)]/2\bar{p}_m$

Table 2b. 9^+ Line data points for oxygen at T = 281°K (98 ΔN-profiles)

Δν	ΔN_o^+ (−)	ΔN_o^- (−)	ΔN_o^+ (+)	ΔN_o^- (+)	p_o^+ (−)	p_m^+ (−)	p_m^+ (+)	Average $\bar{p}_m$	$\gamma^o = \Delta\nu/\bar{p}_m$	p_s^+ (−)	p_s^+ (+)	n_1^o
[MHz]	[ppm]				[torr]				[MHz/torr]	[torr] Figure 6		[10^{-3} ppm/torr] (a)
5	.441	.464	−.503	−.480	23	2.54	2.72	2.63	1.90	1.32	1.35	
7.5	.435	.458	−.512	−.489	28	3.8	4.1	3.95	1.90			−3.9
10	.432	.455	−.518	−.495	31	4.8	5.4	5.2	1.92	2.68	2.70	−3.8
15	.422	.445	−.528	−.505		7.0	8.6	7.8	1.92			−3.8
20	.413	.436	−.536	−.513	46	9.5	11.3	10.4	1.92	5.35	5.29	−3.7
25	.407	.430	−.546	−.523		11.9	14.3	13.1	1.91			−3.6
30	.395	.418	−.554	−.531	57	13.8	17.8	15.8	1.90	8.36	7.86	−3.6
ΔN_ϕ	+0.023											
	$\Delta N_o^L = \pm 0.474(3)$								$\gamma^o = 1.91(2)$	,	1.90(4)*)	$n_1^o = -3.7(2)$
35	.380	.403	−.559	−.537		15.5	21.8	18.65	1.88			−3.6
40	.372	.395	−.566	−.543	65	17.2	25.5	21.35	1.87	11.1	10.5	−3.5
45	.365	.388	−.574	−.551		19.5	29.0	24.25	1.86			−3.4
50	.355	.378	−.579	−.556	72	21	33	27	1.85	13.8	12.8	−3.3
100	.217		−.68		87	35	80	57.5	1.74			
150	.137				83	40						
200	.046				58	29						

*) Analyzed with equation (35) and averaged by $[\gamma^o(+\Delta\nu) + \gamma^o(-\Delta\nu)]/2$

Table 2c. 9^+ Line data points for oxygen at T = 252 and 325°K

$\Delta\nu$	ΔN_o^+	ΔN_o^-	ΔN_o^+	ΔN_o^-	p_o^+	p_m^-	p_m^+	$\bar{p}_m$	γ^o	n_1^o
	[ppm]				[torr]				[MHz/torr]	[10^{-3}ppm/torr]
	252°K (16 ΔN-profiles)									(a)
10	.51	.53	-.60	-.58		4.7	5.0	4.85	2.06	-5.1
20	.49	.51	-.63	-.61		8.4	10.7	9.55	2.09	-5.2
30	.46	.48	-.65	-.63		12.9	16.2	14.55	2.06	-5.2
ΔN_ϕ	+0.02									
	$\Delta N_o^L = \pm.56(1)$								$\gamma^o = 2.07(4)$	$n_1^o = -5.2(5)$
40	.44	.42	-.66	-.64		17.3	22.2	19.75	2.02	-5.6
50	.40	.38	-.67	-.65		21	29	25	2.00	-5.4
	325°K (12 ΔN-profiles)									
5	.368	.385	-.415	-.398		3.4	2.5	2.95	1.69	-2.2
10	.360	.377	-.420	-.403		6.2	5.8	6.0	1.67	-2.2
20	.345	.362	-.437	-.420		11.9	11.9	11.9	1.68	-2.4
30	.340	.357	-.460	-.443		17.0	18.2	17.6	1.70	-2.4
ΔN_ϕ	+0.017									
	$\Delta N_o^L = \pm.39(1)$								$\gamma^o = 1.68(3)$	$n_1^o = -2.3(3)$

Table 3. Fit of $\Delta N(p)$-Profiles for 9^+ Line (Oxygen, T = 281°K)

Data Input				Theoretical Assumptions		Output of Computer Fit					
Pressure Range	No. of Data Points	Sweep Direction	Freq. Dev. $\Delta\nu(9^+)$	K°	$\nu_R N^\circ$	S°			γ°		
				- +	- +	-	+	Mean	-	+	Mean
[torr]			[MHz]	[10^3 ppm/torr]	[kHz/torr]	[Hz/torr]			[MHz/torr]		
0.1 - 10	120	+	5	-3.98 -3.84	20.826 20.830	1.672	1.860	1.77	1.898	1.863	1.88
		-				1.930	1.643	1.79	1.667	1.980	1.83
0.2 - 15	176	+	10	-4.05 -3.77	20.825 20.831	1.756	1.804	1.78	2.000	1.863	1.88
		-				1.818	1.758	1.79	1.717	2.025	1.87
0.3 - 30	100	+	20	-4.19 -3.63	20.821 20.835	1.724	1.882	1.80	1.933	1.860	1.90
		-				1.922	1.689	1.81	1.704	2.076	1.89
0.6 - 45	144	+	30	-4.32 -3.50	20.818 20.838	1.695	1.891	1.79	1.979	1.806	1.89
		-				1.852	1.791	1.82	1.736	2.053	1.89
1 - 60	120	+	50	-4.60 -3.22	20.811 20.845	1.770	1.972	1.87	2.055	1.752	1.90
		-				1.925	1.843	1.88	1.693	2.142	1.91
	660			$n_1^\circ = -3.91\ 10^{-3}$				1.81(7)			1.88(5)
				$n_2^\circ = 1.38\ 10^{-5}$	.3406 ν_R						
				(Eq. 26-Part 2)							

Results of computer-fitting 9^+ Line ΔN_o-data for p = (0.5 to 2)p_m were as follows:

a) T = 281°K and assuming K° (see above) yielded
S° = 1.81(8) Hz/torr, γ° = 1.90(2) MHz/torr, $N^\circ\nu_R$ = 20(2) kHz/torr.

b) T = 300°K and assuming S° = 1.59 Hz/torr yielded
γ° = 1.80(3) MHz/torr, $n_1^\circ = 3.1(2)\cdot10^{-3}$ ppm/torr, $n_2^\circ = 1.0(6)\cdot10^{-5}$ ppm/MHztorr.

and 300°K. The error margins are about double at 252 and 325°K since the number of individual ΔN-profiles was smaller.

The Phase Error

The phase error at p_m appears as a discontinuity $2\Delta N_\phi^\pm$ at $\Delta\nu = 0$ in a plot of $\Delta N^\pm$-vs-$\Delta\nu$ (e.g., Fig. 4). The error ratio g (Eq. 29) is determined by the offset. The ratio g is also found in $\Delta N^\pm(p)$-profiles recorded at $\Delta\nu = 0$. Here, the line contribution is zero (Eq. 18) and the continuum term $n_1^o p$ is offset by $\Delta N_\phi^\pm$ (e.g., Fig. 7). The ratio g remains constant, at least for pressures up to 100 torr (Fig. 7). The operation of (29) can now be performed upon the recorded data $\Delta N^\pm(p)$ which then are treated as true molecular information.

The functional form of $\Delta N_\phi^\pm(p)$ is proportional to O_2-MS attenuation α (Eq. 27, Fig. 8). The line attenuation dominates when $p < p_m$ and equation (30) is a good approximation. The constant C is determined by averaging the "C of best fit" for the differences $\Delta N^+ - \Delta N^-$ (e.g., Fig. 5.6 - Part 2). The value of C was constant to within 4 percent for $\pm\Delta\nu(9^+) = 5$ to 30 MHz. With C known, it is possible to reconstruct $\Delta N(p)$ from $\Delta N^+(p)$ and vice versa.

Obviously, the phase error ΔN_ϕ can be reduced by slower sweep speeds δ (Eq. 27). The first PRS design, however, did not permit operation below $\delta \doteq 11$ kHz/μs. A new digital phase meter has just been completed (APPENDIX C) that can be operated as low as 1.5 kHz/μs with a detection sensitivity of $\Delta N_{min} < 0.004$ ppm. An example is shown in figure 14. The error $2\Delta N_\phi$ at p_m reduces hereby from 0.24 ΔN_o at $\delta = 11.4$ kHz/μs (Fig. 12) to 0.035 ΔN_o at $\delta = 1.52$ kHz/μs according to the ratio of δ.

Attenuation Pressure Profiles

The theoretical profiles are expressed through equations (3), (4), (6). An example for the 9^+ line, which assumes $I_N^o = 0$, is depicted in figure 8. A comparison of attenuation α and dispersion ΔN favors the latter for line studies, the reason being that $\alpha(p)$ lacks extraordinary points and a distinction between + and - $\Delta\nu$ data.

The peak detector at ν_R generates a voltage a_1 (APPENDIX C, Fig. A1) simultaneously with $\Delta N^{\pm}(p)$-profiles. The voltage a_1 relates to attenuation α by (Eqs. 39, 29 - Part 2)

$$a_1(p) = a_o/\{[\alpha(p)L_R/4.343] + 1]\}^{\beta} . \qquad (36)$$

The relation between a_1 and α requires knowledge of the detector law β and the effective length $L_R(Q)$, both of which are very difficult to measure accurately. The best we were able to achieve was ± 5 percent for Q and ± 10 percent for β. This accuracy cannot compete with the dispersion results.

Various biased and unbiased point-contact and Schottky-barrier diodes have been employed at ν_R with conversion efficiencies between 80 and 400 mV/mW. The detection law varied between $\beta = 1.0$ and 1.5 since the diode is always subjected to the full reflected power (0.5 to 5 mW).

Table 4 and figure 9 exhibit two examples of attenuation pressure profiles, just to demonstrate the difficulties of any undertaking to obtain absolute data. The first is a result of fitting 9^+ pressure profiles α_x [$\alpha_x \equiv a_1(p)$, but calibrated in decibel with precision attenuator] to the expression (Eq. 32 - Part 2)

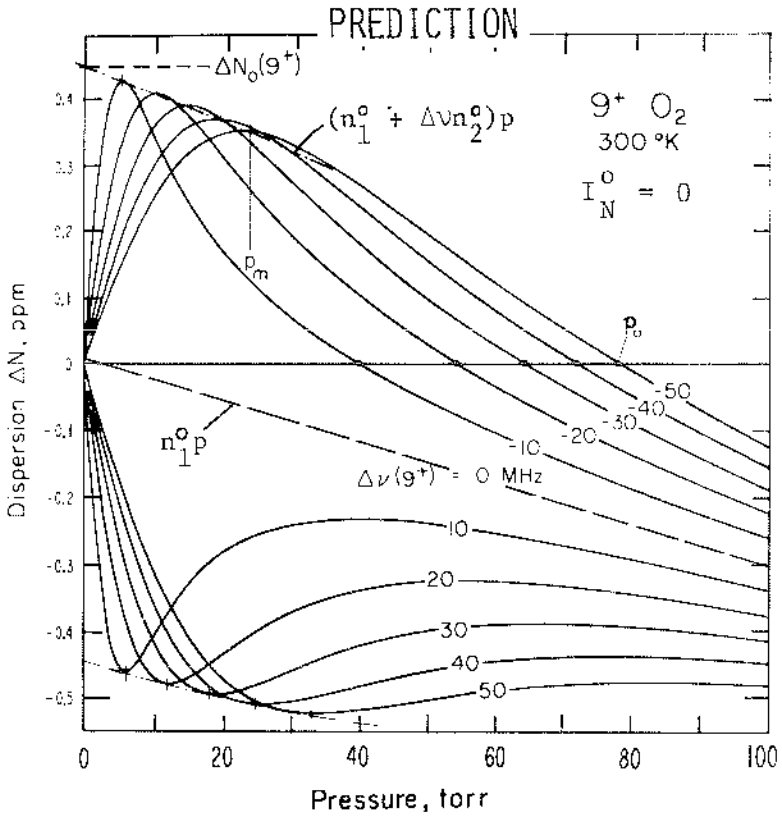

Figure 2. O_2-MS dispersion pressure profiles around the 9^+ Line as predicted for detection by the PRS.

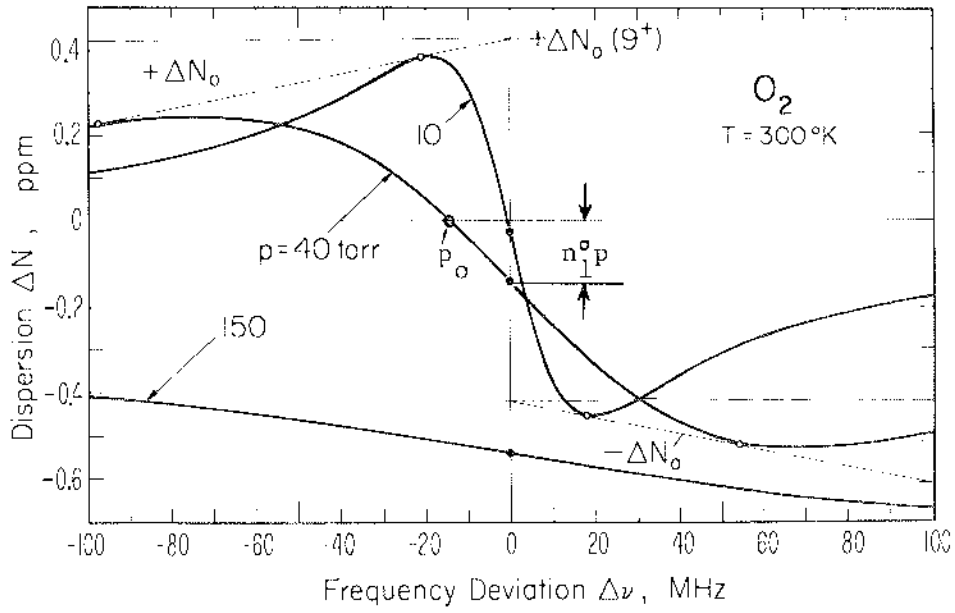

Figure 3. Calculated frequency profiles for the 9^+ O_2-MS Line at 10, 40, and 150 torr (Mingelgrin, 1972). Assumed was γ^o = 1.95 MHz/torr (Table 7).

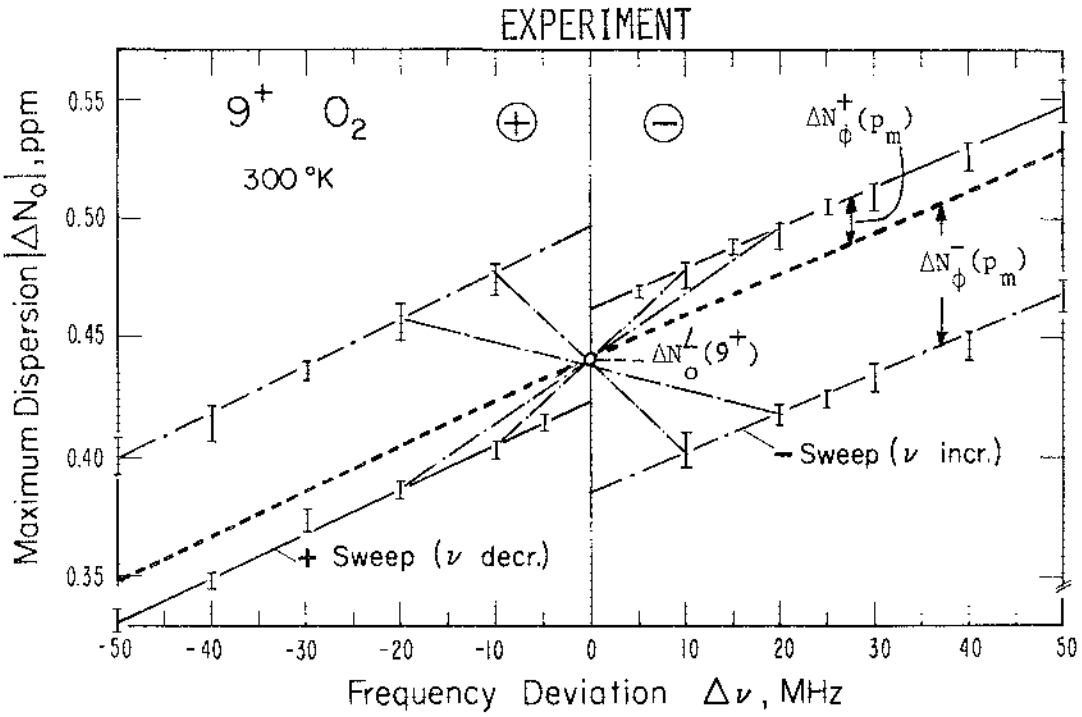

Figure 4. Measured peak dispersion ΔN_o in vicinity of 9^+ Line (see Table 2a).

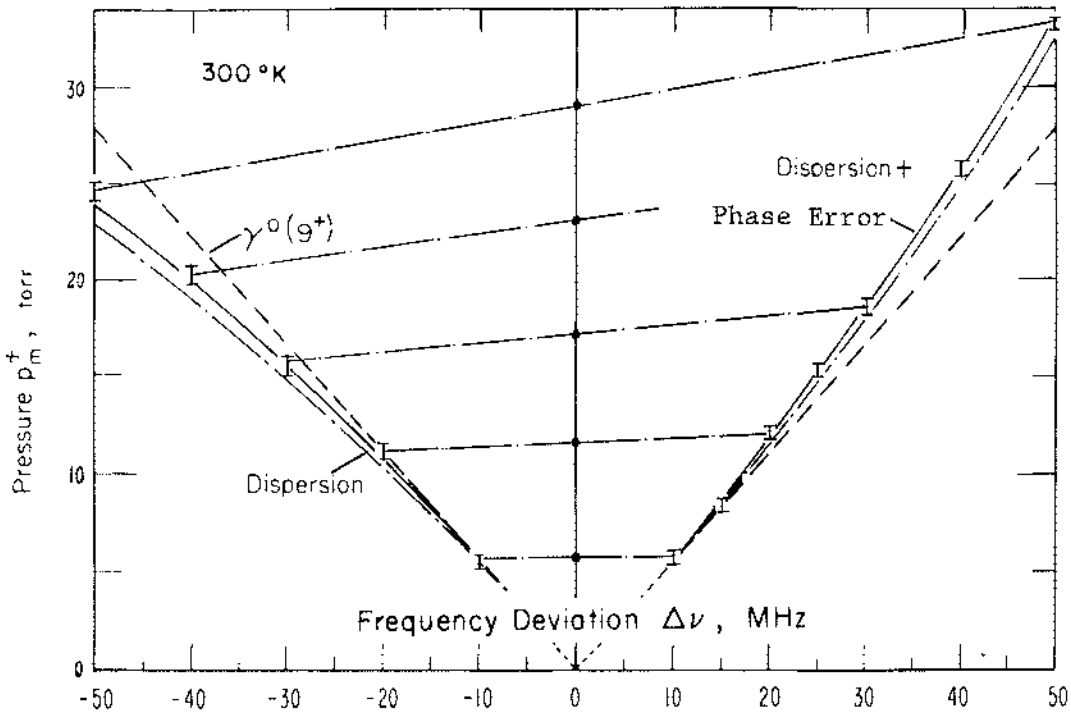

Figure 5. Measured pressure p_m^+ at peak dispersion ΔN_o in vicinity of of 9^+ Line (see Table 2a).

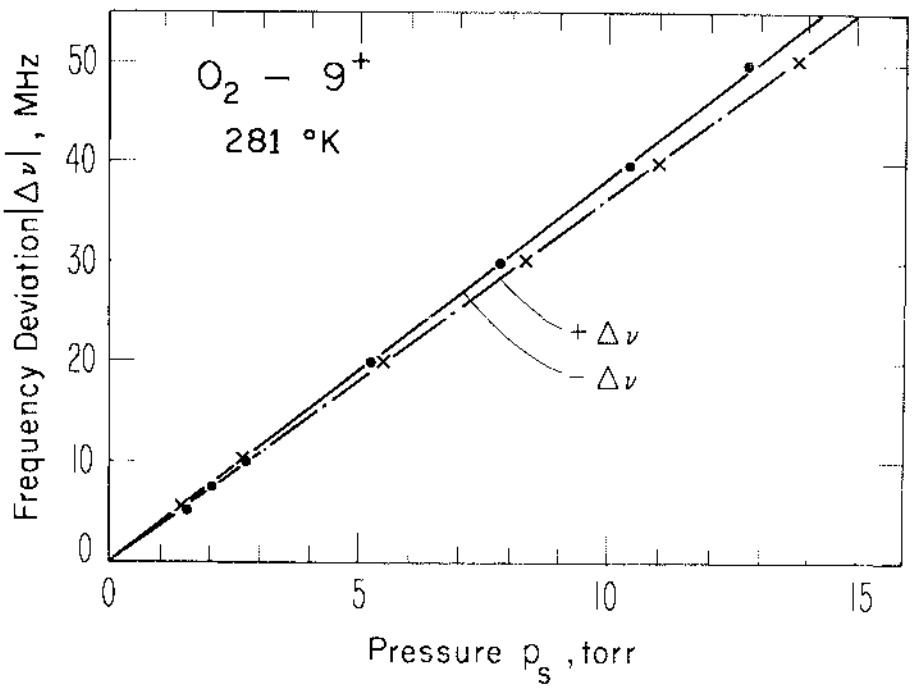

Figure 6. Wing response pressure p_s (see Fig. 2.1 - Part 2) versus the frequency deviation $\Delta\nu(9^+)$.

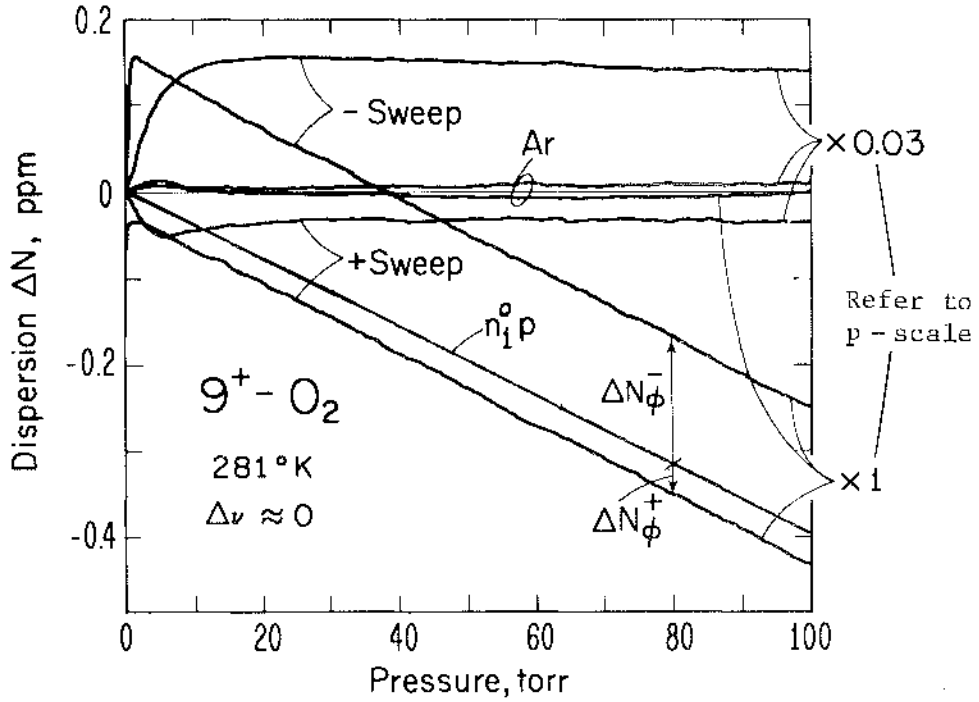

Figure 7. Dispersion pressure profiles at the 9^+ Line center displaying the continuum term $n_1^o p$ and the phase errors ΔN_ϕ^+ and ΔN_ϕ^-.

$$\alpha_x = 4.343(\beta/2)\{[1 + QN''10^{-6}]^2 + [2Q(N^o p + \Delta N)10^{-6}]^2\} . \qquad (37)$$

The best fit was obtained using "dispersion" line parameters (Table 2a) and $Q = 3.25 \cdot 10^5$, $\beta = 1.20$. The measured parameters for this experiment were $Q = 3.45(20) \cdot 10^5$ and $\beta = 1.2(1)$. Although the agreement is reasonable, we can state for sure that this type of procedure does not add much to support the "dispersion" line results.

The second example in figure 9 depicts a family of attenuation profiles recorded at 252°K. The measured vacuum Q-value was $4.0(3) \cdot 10^5$, but varied probably slightly as $\Delta\nu$ was tuned. The vertical scale is calibrated in dB/km from the known maximum line value $a_o(9^+)$, which is measured at $\Delta\nu = 0$ as a constant over a limited pressure range (1.5 to 15 torr). From figure 22 we read $a_o = 3.45$ dB, which converts to $\alpha_o(9^+) = 3.45^{1.1}/0.312 = 12.5$ dB/km in agreement with the dispersion result (Table 2c; Eq. 14 - Part 2) $22.26\ \Delta N_o = 12.5(2)$ dB/km.

The Amplitude Error

The $a_1^{\pm}$-profiles are dependent upon the sweep speed δ in similar manner as the dispersion profiles. The increase of $a_1(Q)/a_1(\delta=0)$ to $a_1(Q_G)/a_1(\delta=0)$ (see Eq. 40) tends to record less attenuation than the true molecular value. This error is not more than -0.4 dB/km for typical PRS conditions (see Fig. A3). The amplitude error, too, is smaller for the + sweep direction, although the difference between $a_1^+(p)$ and $a_1^-(p)$ profiles was never more than 3 percent. The error can be estimated by substituting different f_T for different Q_G. For the example (Fig. A3), $Q = 4 \cdot 10^5$ drops to $Q_G = 1.6 \cdot 10^5$ when $\alpha = 20$ dB/km at 60 GHz, which is equivalent to changing f_T from 2.5 to 1 kHz (error < -0.1 dB/km).

Table 4. Example of Fitting Attenuation Pressure Profiles in the Vicinity of the 9^+ Line (T = 300°K, O_2).

$\Delta\nu(9^+)$	-20 MHz			-30 MHz		
p	α_x	α_c *)	Differ. $\alpha_x - \alpha_c$	α_x	α_c *)	Differ. $\alpha_x - \alpha_c$
[torr]	[dB]		[%]	[dB]		[%]
0	0	0	0	0	0	0
3	.20	.186	7.0	.10	.009	2
6	.62	.591	4.7	.35	.328	6.3
9	1.02	.995	2.5	.65	.625	3.9
12	1.33	1.308	1.7	.96	.919	4.3
15	1.55	1.535	1.3	1.22	1.175	3.7
18	1.70	1.695	.3	1.42	1.385	2.5
21	1.80	1.809	- .5	1.57	1.554	1.0
24	1.88	1.892	- .6	1.70	1.689	.7
27	1.93	1.925	- .3	1.80	1.794	.3
30	1.99	2.001	- .5	1.88	1.879	.1

*) Calculated attenuation using the experimental parameters

$Q = 325{,}000$ and $\beta = 1.20$,

and the 9^+ line parameters:

$S^\circ = 1.59$ Hz/torr, $\gamma^\circ = 1.79$ MHz/torr, and K'' (see Eq. 26 of Part 2).

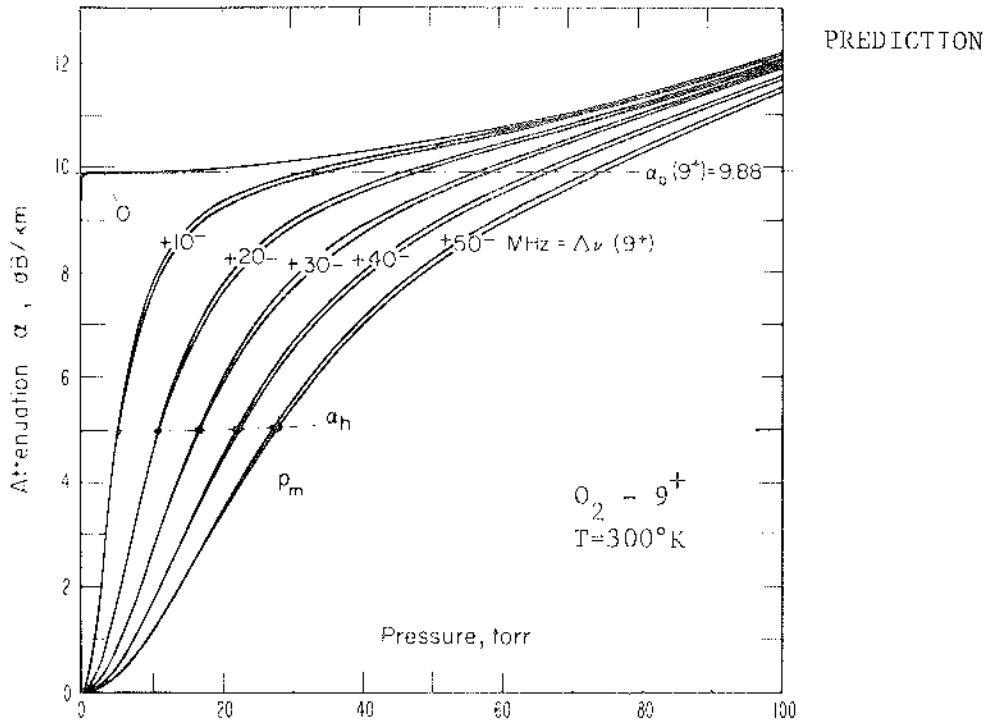

Figure 8. O_2-MS attenuation pressure profiles around the 9^+ Line as predicted for detection by the PRS.

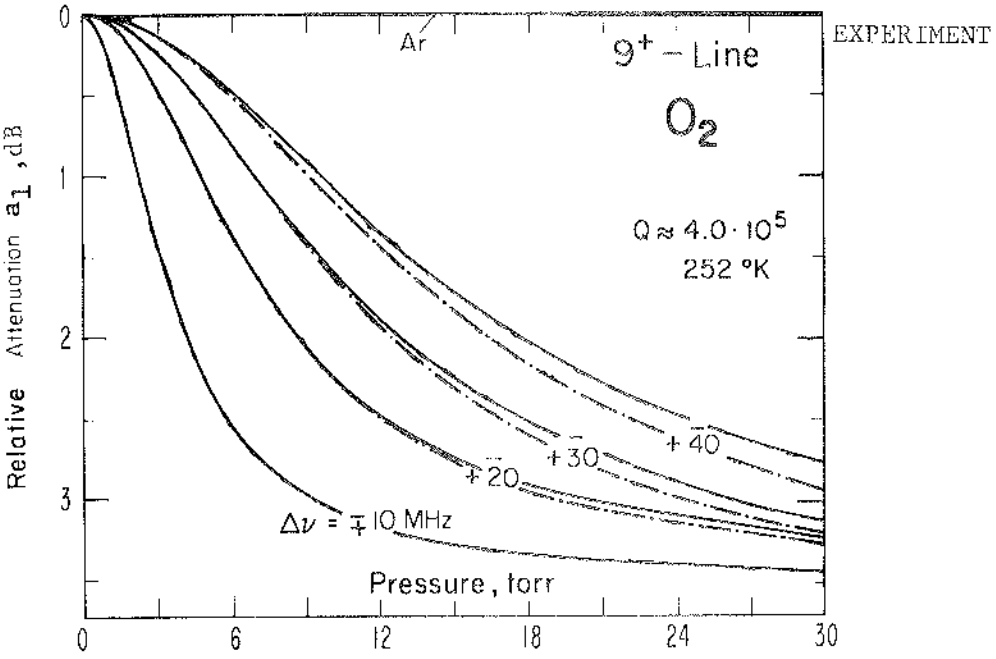

Figure 9. Recorded attenuation pressure profiles for the 9^+ Line. Effective path length L_R = 0.312 km; detection law $\beta \approx 1.1$. Also, see figure 22.

2.1.2 The Four O_2-MS Doublets (300°K)

For eight O_2-MS lines the separation is only about 1/5 of the normal frequency spacings (Table 5). These neighboring lines are called a doublet since they keep their identity as an overlapping line pair before merging with increasing pressure into the unstructured continuum (Fig. 28). The doublets provide the opportunity to study over a limited pressure range the overlap of two lines in quasi-isolation. The idea of measuring nonlinear overlap on such a two-line system had to be abandoned since Rosenkranz (1975) showed theoretically that, to first order, appreciable interference is only expected between neighboring lines in either the N^+ or N^- branch. However, the doublet is a good candidate to check the N-number dependence of the width (Eq. 9) since the spread in N is considerable for three doublets (Table 5).

Doublet pressure profiles are predicted based on equation (4), the line parameters listed in Table 1 - Part 2, and assuming $Y_N^o = 0$. Examples are in figures 10, 11 ($7^+/5^-$), 13 ($3^+/9^-$), and 15 ($1^+/15^-$). Data analysis is more complicated than for a line. Equation (15) for dispersion becomes

$$\Delta N = \Delta N_{L1} + (\Delta N_{L2} + K^o p) \ . \qquad (38)$$

Data, recorded for $^+\Delta\nu$ = 5 to 15 MHz and p < 15 torr, however, can be treated as a line (Sect. 2.1.1) since the contribution of line 2 is still pressure-linear.

The attenuation pressure profiles for a doublet (Fig. 10) are not too much different from those of a line (Fig. 8) except for a cross-over pressure p_x where the attenuation is constant over some frequency

range ($\sim$ 40 MHz in the $7^+/5^-$ example). Experimentally, the pressure p_x can serve as check point for the validity of a theoretical prediction, even when the data a_1 (Eq. 36) are recorded as relative attenuation.

The dispersion pressure profiles are significantly different in the vicinity of one or the other line (Fig. 11). The doublet dispersion displays two extraordinary points, $\Delta N_o(p_m)^{L1}$ and $\Delta N_o(p_m)^{L2}$, that are sensitive to the width parameter of line 1 and 2, respectively. A wrong value of γ_N^o in the prediction will cause noticeable discrepancies with the experimental data. The profile at $\Delta\nu = 0$ is, up to 100 torr, mostly the contribution from the other partner in the doublet. The $3^+/9^-$ doublet is well suited to study N-dependence of the linewidth. Predictions that assumed the same width parameter (1.79 MHz/torr) for both lines did not agree with measured data.

Results

Recorded dispersion profiles for $7^+/5^-$ and $3^+/9^-$, which were restricted in $\pm\Delta\nu$ (5 to 15 MHz) and p (< 15 torr), have been analyzed for line parameters. Data analysis was by equation (31), and the results are summarized in Table 5. The same phase error problem existed as for the 9^+ line. Two examples (Figs. 12 and 14) are representative of details of many individual data runs. The $7^+/5^-$ averaged data points agree well with predictions based upon equations (4), (7), (8), and $I_N^o = 0$. Deviations from a pressure-linear overlap of the two doublet lines are not detectable. This finding is supported by the pressure p_o that is kind of a balance point between the two line contributions.

Very recent results on the $3^+/9^-$ doublet profitted from smaller phase errors due to reduced sweep speeds δ possible with the new phase meter (APPENDIX C). It can operate at a sampling rate f_T = 1 kHz. For the example, figure 14, the low Q mode of R2 (Sect. 3.5.2 - Part 2) was used. The reduction in phase error is significant, especially when compared with figure 12. The slight positive slope of the N_2-baseline is caused by a sloping power mode of the doubler generating ν_R = 58.4 GHz (Eq. 64 - Part 2) that was later avoided by more careful tuning and by operating with less sweep width in the high Q mode.

Under <u>any</u> circumstance, it is of advantage to operate the PRS at the highest Q-values that possibly can be achieved. The reason for this is that the two competing requirements of low sweep speed and sufficient sweep width have to be met by observing (Eqs. 36, 52 - Part 2)

$$\Delta N/\Delta t \approx 10 f_T/Q_G \tag{39}$$

where

$$1/Q_G = (1.1 \cdot 10^{-5} \alpha/\nu_R) + 1/Q \tag{40}$$

(ν_R in GHz, α in dB/km from figures 8, 10, 11, 13, 15, etc). This adjustment causes the R2 resonance curve to be swept to ten times its bandwidth, which assures minimum phase and amplitude detection errors.

Although the number of observations made on the 7^+, 5^-, 3^+, 9^- lines are not enough for indisputable conclusions, the results (Table 5) do support two assertions: i) the line width depends upon the quantum number N (Gardiner et al., 1975) and ii) the strengths S_N^o agree within 5 percent with the theoretical values.

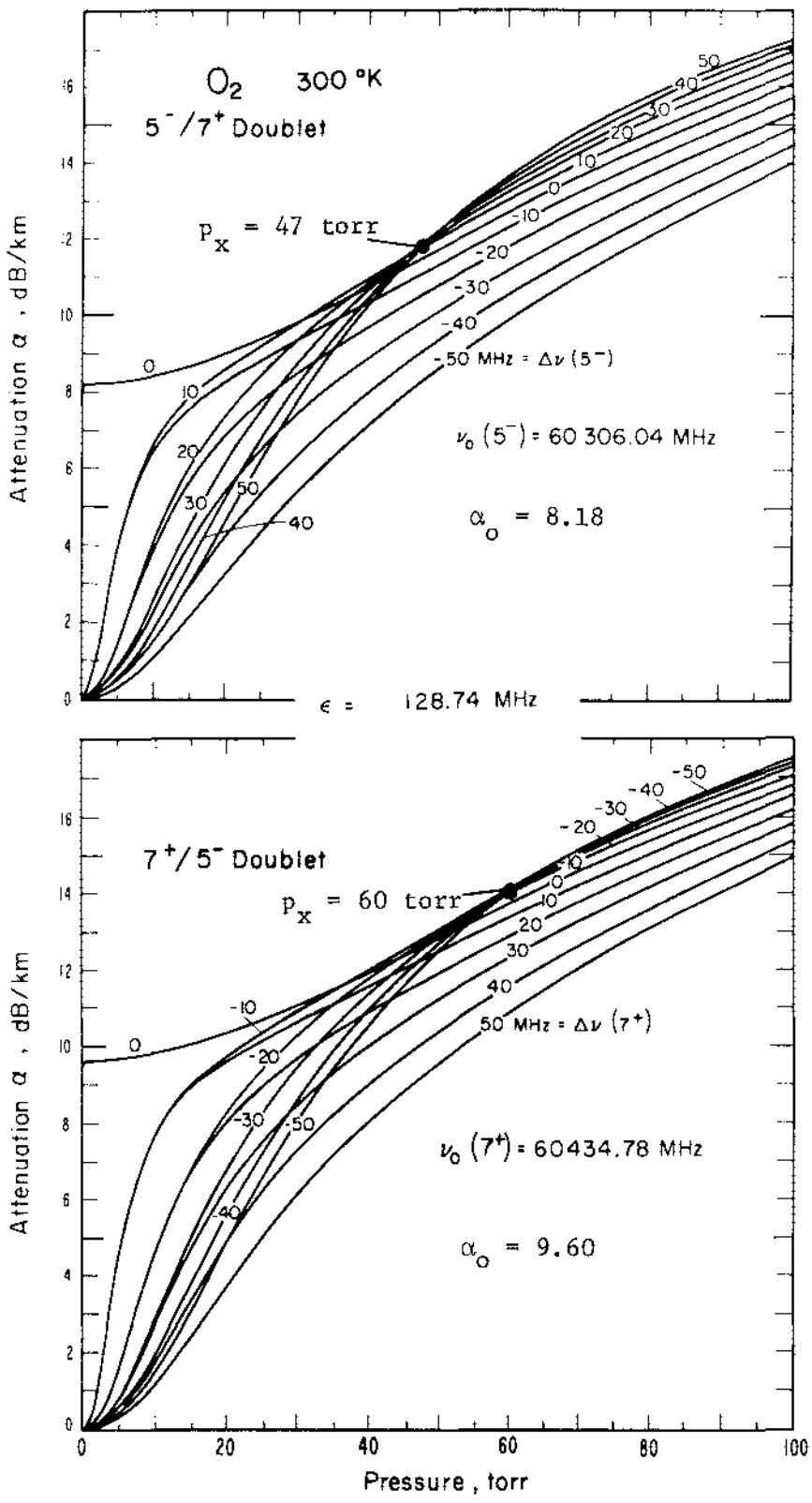

Figure 10. Computer plots of experimental $5^-/7^+$ and $7^+/5^-$ Doublet attenuation pressure profiles. $S°(7^+)/S°(5^-) = 1.16$.

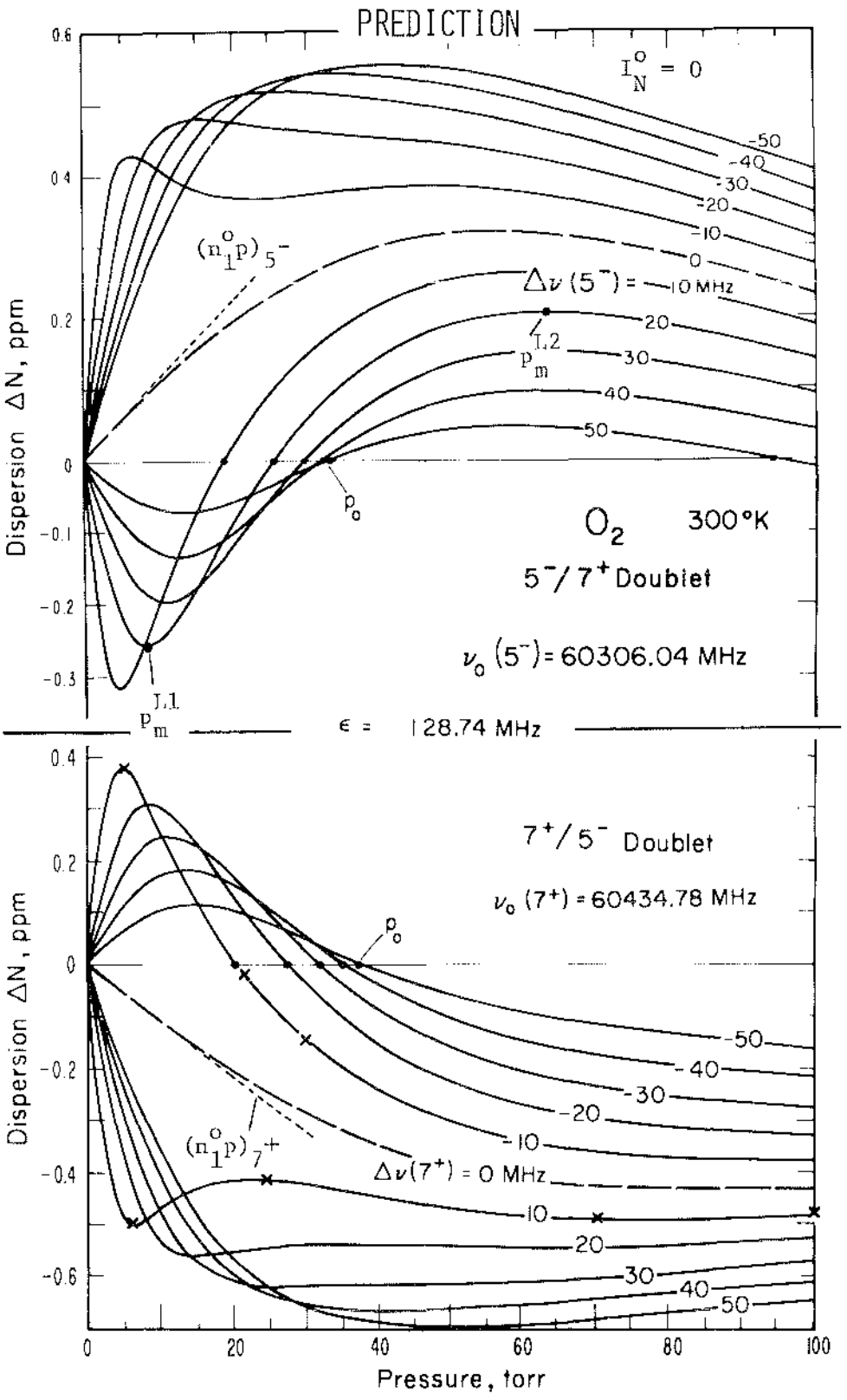

Figure 11. Computer plots of experimental $5^-/7^+$ and $7^+/5^-$ Doublet dispersion pressure profiles, ϵ - Difference between 5^- and 7^+ Line centers.
x see figure 12 .

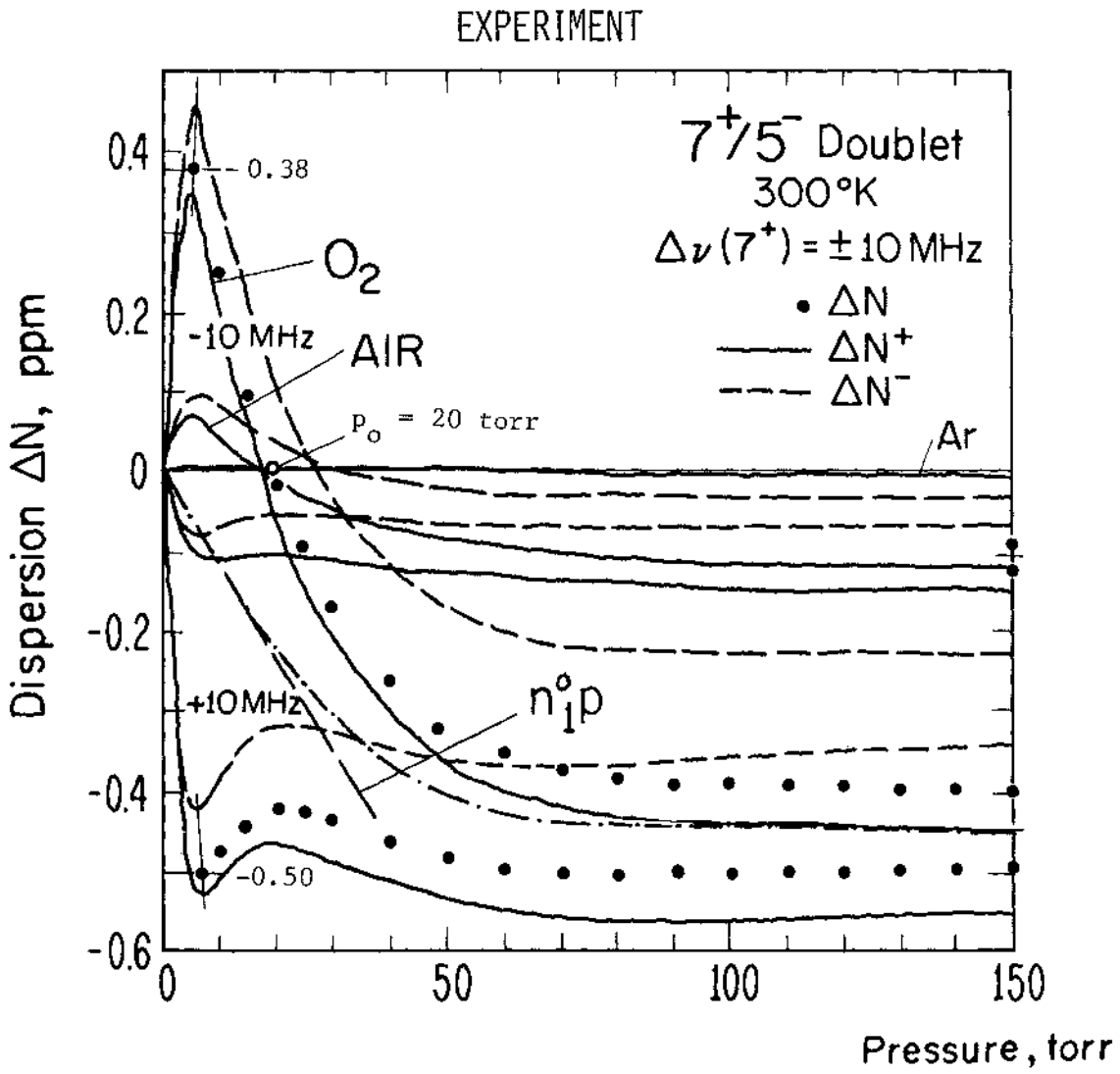

δ = 11.4 kHz/μs

Figure 12.

Measured $7^+/5^-$ Doublet dispersion pressure profiles for O_2 and AIR at $\Delta\nu(7^+) = \pm 10$ MHz. Averaged by the measured ratio, $g = \Delta N^-_\phi / \Delta N^+_\phi = 3$ (Eq. 29). Predictions see figure 11.

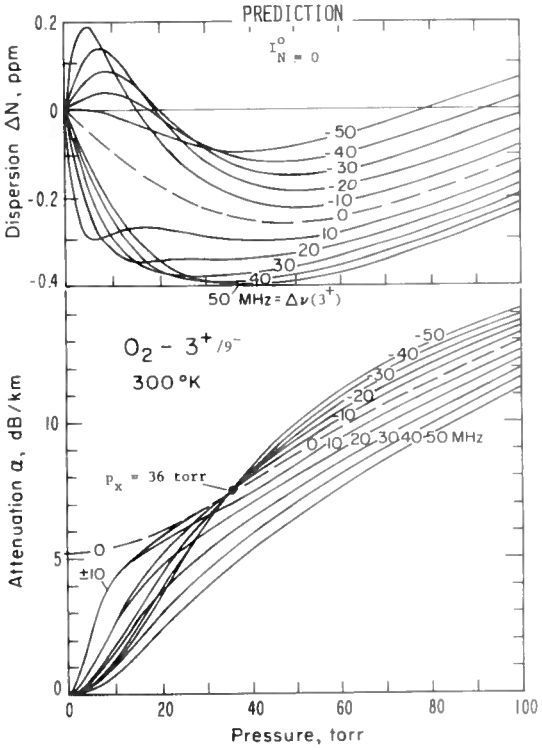

Figure 13. Computer plot of experimental $3^+/9^-$ doublet pressure profiles. ε = 123 MHz; $S^o(3^+)/S^o(9^-)$ = 0.612 .

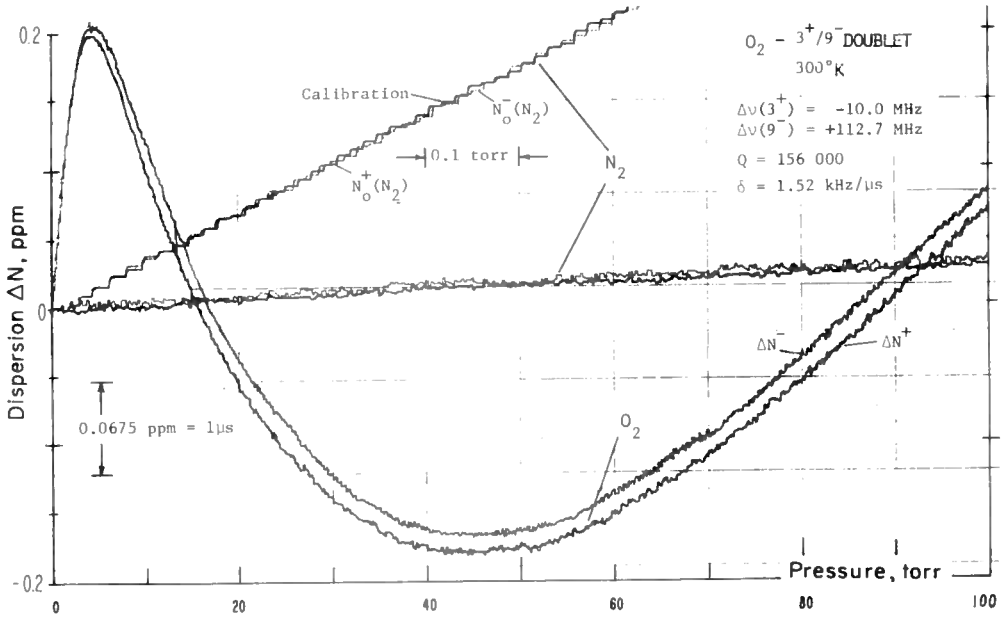

Figure 14. Measured dispersion profile of $3^+/9^-$ doublet at $\Delta\nu(3^+)$ = -10 MHz using the new phase meter (APPENDIX C).

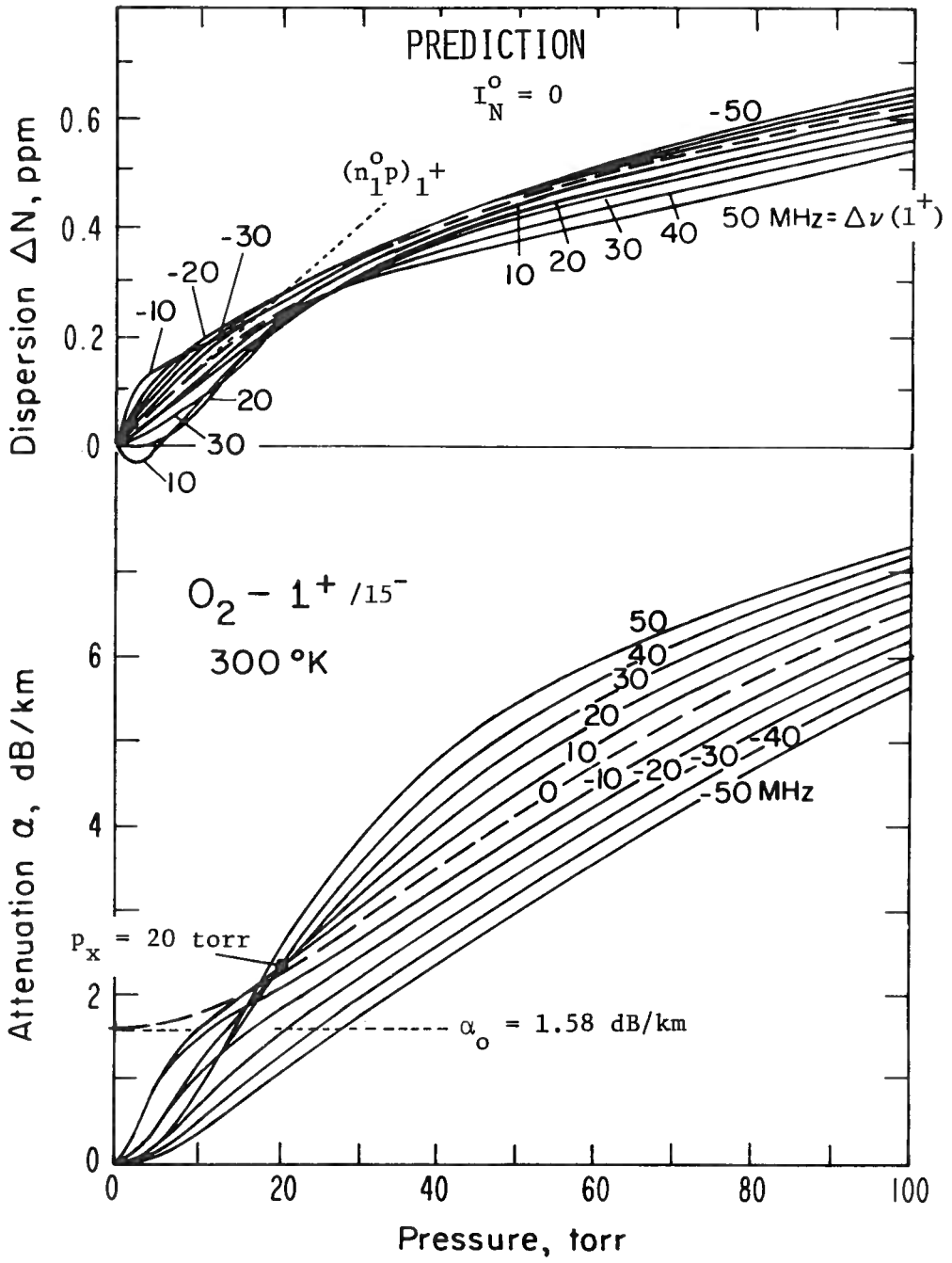

Figure 15. Computer plot of experimental $1^+/15^-$ Doublet pressure profiles (ε = 98 MHz; $S°(1^+)/S°(15^-)$ = 0.412).

Table 5. Overview of O_2-MS Doublet Data at 300°K

$N^{\pm}$	ν_o [GHz] (a)	Theory S^o [Hz/torr] (a)	Theory n_1^o [10^{-9}/torr] (b)	Experiment ΔN_o^L [ppm]	Experiment γ^o [MHz/torr]	Experiment n_1^o [10^{-9}/torr]	Experiment S^o [Hz/torr] (c)	Example
3^-	62.486 255	.9634						
13^+	62.411 223	1.2272						
7^+	60.434 776 (d)	1.5626	-11.2	.43(1)	1.82(3)	-11.2(2)	1.57(5)	Figs. 10-12
5^-	60.306 044	1.3487	+10.0	.35(1)	1.86(4)		1.30(7)	Figs. 10,11
3^+	58.466 580	.9251	- 9.40	.233(5)	1.92(3)		.90(2)	Fig. 13
9^-	58.323 885	1.5150	+ 9.25	.42(1)	1.79(4)		1.50(8)	
15^-	56.363 393	.8539	+ 1.41					Fig. 14
1^+	56.264 778	.3487	-12.6					

(a) Table 1 - Part 2
(b) Table 2 - Part 2
(c) Equation (20)
(d) See Table 10

2.1.3 Summary of Line Parameters (O_2-O_2)

After all the complications connected with the PRS and the understanding of its output, we can finally report some results. The quintessence of the studies of self-pressure-broadened lines is given in Tables 5 to 7. The actual deduced numbers indicate that dispersion profiles are suited for quantitative work. Line parameters (γ^o and ΔN_o^L) and continuum term (n_1^o) were inferred from a large number of reliable and reproducible data points. The width γ^o is the only line parameter directly measurable; derivation of the strength S^o from ΔN_o^L requires prior knowledge of γ^o (Eq. 20). The uncertainties in terms of standard deviation from the mean are small for line parameters; namely, 1 to 2 percent for γ^o and 2 to 3 percent for S^o. The larger uncertainties associated with 252 and 325°K results reflect a smaller body of raw data and, at 252°K, difficulties in maintaining drift-free stable PRS operation. Data scattering due to instrumental instabilities and S/N limitations make up the main error sources; errors in p, T, N^o, and ν are at least one order of magnitude less significant.

The conclusions to be drawn from comparison with theory for conditions specified by (14) are enumerated as follows

1. The Lorentzian shape (Eq. 7) is valid.
2. The strength parameters $S^o(300)$ are correct for the lines studied (9^+, 7^+, 3^+, 9^-, 5^-).
3. The temperature dependence of the strength, $\vartheta(9^+)$ predicts at 252°K slightly higher values than measured (w - Eq. 32).

4. The width parameter γ^o is proportional to pressure and decreases with higher quantum numbers N (3^+ to $9^{\pm}$) which is tentatively expressed in (8).
5. The width $\gamma^o(9^+)$ varies as $T^{-0.9}$ at p = const.
6. Line and continuum intensities can be separated.
7. The continuum coefficient n_1^o supports the findings expressed under 2 and 3.
8. Nonlinear overlap up to pressures of 150 torr is not detectable as expected from the magnitude of I^o (Table 1).
9. A pressure-induced shift of the line frequency ν_o is smaller than ± 20 kHz/torr if it exists at all. Such non-existence is predicted by theory (Dillon and Godfrey, 1972; Pickett, 1975).
10. Attenuation pressure profiles play only the role of supplementary information due to their limited quantitative value.

We concede that line measurements are by no means completed and that for reliable analysis of atmospheric O_2-MS transfer characteristics additional lines need to be studied with particular emphasis on low temperatures (180 to 260°K). One way to improve on the reliability of line parameters is by extending the PRS frequency setting to $\pm \Delta\nu \geq 0.5$ MHz (e.g., Fig. 18) when the earth magnetic field, present in the laboratory, is compensated for, thus removing Zeeman splitting (Sect. 2.3). A constructive approach to remaining uncertainties is to assume the validity of the statements 1 to 9 for <u>all</u> lines in order to predict O_2-MS band structure (Sect. 2.5), and then deal with the feedback from continuum data (Sect. 2.4) to direct more work to lines, the band components.

Table 6. 9^+ Lorentzian Line Parameters for O_2-O_2

Temperature		252°K	281°K	300°K	325°K	Remarks
Observed:	Table	2c	2b	2a	2c	
ΔN_o	[ppm]	.56(1)	.474(3)	.444(3)	.39(1)	Eq. 20
γ^o	[MHz/torr]	2.07(3)	1.91(2)	1.79(2)	1.68(3)	u = 0.90(3)
S^o	[Hz/torr]	2.32(8)	1.81(3)	1.59(3)	1.31(5)	w = 2.25(20)
n_1^o	[10^{-9}/torr]	-5.2(5)	-3.7(2)	-3.2(2)	-2.3(2)	
α_o	[dB/km]	12.5	10.55	9.88	8.7	$\alpha_o = 22.26\ \Delta N_o$ Eq. 14 - Part 2
Theory:						
S_T^o	[Hz/torr]	2.396	1.855	1.590	1.315	Table 3 - Part 1
$(n_1^o)_T$	[10^{-9}/torr]*)	-5.58	-3.91	-3.10	-2.35	Table 2 - Part 2
Comparison:						
S^o/S_T^o	[%]	97(3)	98(2)	100(2)	100(4)	
$n_1^o/(n_1^o)_T$	[%]	93(9)	95(5)	103(5)	98(8)	

*) $n_1^o = [K^\circ(-\Delta\nu) + K^\circ(+\Delta\nu)]/2$

Table 7. O_2-MS Line Width Parameters Versus The Rotational Quantum Number N
Additional reported values see Table 6 - Part 1.

N		γ^o (T = 300°K)				
		Theory +)	Experim. 1	Experim. 2		Predicted *)
		[MHz/torr]				
				N^+	N^-	
1	a)	(2.37)	2.05(5)			1.98
3		(2.35)	2.01(5)	1.92(3)		1.93
5		2.05	1.96(8)		1.86(4)	1.89
7		2.10	1.91(8)	1.82(3)		1.84
9		1.95	1.87(5)	1.79(2)	1.79(4)	1.79
11		1.95	1.82(7)			1.75
13		1.91	1.78(9)			1.70
15		1.71				1.66
17		1.73				1.61
19		1.58				1.56
21		1.60				1.52
23		1.52				1.47
25						1.43
27						1.38
29						1.33
31						1.29
33						1.24
35						1.20 b)
37						1.15
39						1.10
41						1.06
43						1.01
		(Mingelgrin, 1972; and P-13)	(Gardiner et al., 1975) EPR at 9.4 GHz		(This Report	

*) Eq. (8): $(2.00 - 0.023\ N)^+$ based upon Experiment 1 but adjusted to match 9^+ value of Experiment 2.

+) Also, see P-7 (Dillon, 1969) and Dillon-Godfrey (1972).

a) Values too high due to classical treatment (R. Gordon, private communication, 1973).

b) No experimental or theoretical evidence for further decrease.

2.2 Foreign Gas Pressure Broadening (AIR)

The relative concentration of atmospheric air remains constant up to 80 km height (Table 9) except for water vapor. We separate the total atmospheric pressure into a dry and a water vapor term,

$$p = p_d + p_w \ , \tag{41}$$

and treat dry air (AIR) as one homogeneous gas.

Changing from oxygen, which has been treated exclusively so far, to atmospheric air requires two adjustments in the theoretical O_2-MS scheme (Sect. 2.1.1 - Part 2). First, all line strengths S_N are reduced by $\xi r_1 = 0.2090$, the product of the portion of O_2^{16} molecules and the relative concentration of O_2 in AIR; second, the pressure-broadened widths γ_N^o are modified by broadening efficiencies m_k for atmospheric constituents other than oxygen. The atmospheric line widths, replacing equation (8), become

$$\gamma_a^o p = m_d \gamma_N^o (300/T)^u p_d + m_w \gamma_N^o (300/T)^v p_w \ . \ ^{*)} \tag{42}$$

2.2.1 Comparison of AIR-to-O_2 Data.

In connection with O_2 dispersion and attenuation profiles, we have repeated the same experiment with AIR on numerous occasions (e.g., Fig. 12). We can write for O_2 that

$$\Delta N_o(p_m) = \Delta N_o^L k_A, \tag{43}$$

where

$$k_A \doteq \{1 - A/[1 + (\tfrac{A}{A+2})^2]\}/(1 - A/2) \tag{44}$$

using (26), (15), (19), (20), (23), and neglecting refractive tuning $\nu_R N^o$. This approximation is valid for $\pm\Delta\nu$ = 5 to 30 MHz. Since the experimental parameter A is the same for O_2 and AIR (Eqs. 23, 20, 17),

---

* A reduction of the nonresonant width parameter γ_o^o (Eq. 10) may be necessary leading to slightly different I_N^o-values (Eq. 9)

the ratio of peak dispersion for AIR and O_2 becomes simply

$$\Delta N_o(AIR)/\Delta N_o(O_2) = 0.2090/m_d. \qquad (45)$$

Dispersion ratios for a Lorentzian line are

$$\Delta N(AIR)/\Delta N(O_2) = 0.2090(\Delta\nu^2 + \gamma^2)/[\Delta\nu^2 + (m_d\gamma)^2] \qquad (46)$$

which reduces at p = const. $>> \Delta\nu/\gamma^o$ to

$$\Delta N(AIR)/\Delta N(O_2) \doteq 0.2090/m_d^2, \qquad (47)$$

and at $p = p_M$ to

$$\Delta N(AIR)/\Delta N_o(O_2) = 0.4180/(m_d^2 + 1). \qquad (48)$$

The evaluation of AIR/O_2 dispersion ratios in the vicinity of the 9^+ line and $7^+/5^-$ doublet are given in Table 8. Equation (45) in particular, determines the broadening efficience of AIR to be $m_d = 0.94(2)$. For attenuation follows

$$\alpha(AIR)/\alpha(O_2) = 0.2090\ m_d[\Delta\nu^2 + (\gamma^o p)^2]/[\Delta\nu^2 + (m_d\gamma^o p)^2], \qquad (49)$$

which for $\Delta\nu = 0$ and $\gamma^o p >> \Delta\nu$ reduces to

$$\alpha(AIR)/\alpha(O_2) = 0.2090/m_d\ . \qquad (50)$$

A good approximation to convert O_2 into AIR intensities is a multiplication with the factor 0.225.

2.2.2 Broadening by Individual Air Components.

The indirect determination of a broadening efficiency m_d for AIR using selected dispersion ratios was confirmed by direct measurements of m for eleven air constituents. The measurements were made in two steps. First, oxygen was admitted to generate the self-pressure-broadened dispersion profiles $\Delta N^{\pm}$. The second step was to stabilize the O_2 pressure at $p_m^{\pm}$ and then to slowly introduce a foreign gas with increasing total pressure $p = p_m^{\pm} + p_2$ while the dispersion profiles $\Delta N_f^{\pm}$ were recorded (Fig. 16).

The broadening effect on the 9^+ line was studied at 281°K for binary mixtures of O_2 with N_2, Ar, CO_2, Ne, He, CH_4, Kr, N_2O, Xe, and H_2O vapor. The experiments were done at $\pm\Delta\nu = 5$ MHz in order to approach isolated line behavior ($K^o p_m \doteq 0.001$ ppm ≈ 0). This permits for data analysis the application of (Eq. 17 - Part 2)

$$m = p_m\{[(2\Delta N_o/\Delta N_f) - 1]^{1/2} - 1\}/p_2 \ . \qquad (51)$$

The results listed in Table 9 are based upon $\Delta N_o^+/\Delta N_f^+$ ratios, although they were found to be independent of the + or - sweep direction. The individual broadening efficiences add up (weighted average) for a standard dry air composition to

$$\sum_{k=1}^{11} (mr)_k \equiv m_d = 0.929(5), \qquad (52)$$

in agreement with the value found from dispersion ratios.

The influence of water vapor on O_2-MS line broadening is important in tropospheric wave propagation. The O_2-H_2O efficiency on the 9^+ line was measured to be

$$m_w = 1.25(10). \qquad (53)$$

The temperature dependencies of $m_d\gamma_N^o$ and $m_w\gamma_N^o$ have not been studied. For air calculations it was assumed that

$$u = 0.9 \qquad \text{and} \qquad v = 1 \ . \qquad (54)$$

Mingelgrin (1972) did "ab initio" calculations of O_2-Ar line broadening and obtained at 298°K that m(Ar) = 0.817, which compares favorably with our result (Table 9).

Refractivity measurements on eleven atmospheric constituents were performed at 61.2 GHz and the refractivity coefficients R_k^o (Eq. 2)

determined by a comparison with nitrogen refractivity for which R^o = 105.6 ppm°K/torr (Newell and Baird, 1965) was assumed. The results are included in Table 9. The weighted average

$$\sum_{k=1}^{11} (R^o r)_k \equiv R^o(\text{AIR}) = 103.49 \text{ ppm°K/torr} \qquad (55)$$

verifies a direct refractivity measurement of AIR at 30.6 GHz.

Relative attenuation pressure profiles were recorded simultaneously with foreign gas dispersion profiles. Figure 17 depicts an example. O_2-to-AIR data (Sect. 2.1.1) and attenuation of a variable mixing ratio $O_2 + N_2$, both can be analyzed for efficiencies m_d, $m(N_2)$, respectively. The ratio at p_m = 5.2 torr, for example, is $\alpha(\text{AIR})/\alpha(N_2) = (.42/1.67)^{1.1}$ = 0.22 yielding m_d = 0.95, which confirms a smaller line width in AIR than in O_2. Analysis for $m(N_2)$ was not attempted.

2.3 Doppler and Zeeman Line Broadening

In this section we briefly elucidate the intensity distribution of 9^+, 7^+, 3^+, and 1^+ lines in the vicinity of a line center ($\pm\Delta\nu$ = 0 to 1 MHz), and with the pressure below 10 torr. In the atmosphere, the magnetic field strength $H \sim 0.3$ to 1 G is omnipresent thus introducing the complications of Zeeman splitting (Sect. 2.3.3 - Part 1). In the laboratory, it is possible to compensate to $H \approx 0$ (Sect. 3.5.4 - Part 2) and study the simpler case of approaching Doppler-broadening with an unsplit line (Sect. 2.4.3 - Part 1).

The H = 0 case is of experimental value in several respects: (a) Pressure-broadening of a quasi-isolated (p = 0.5 to 10 torr) O_2-MS line can be studied, which facilitates data analysis by avoiding the

Table 8. Ratios of AIR-to-O_2 Dispersion between 61.4 and 60.4 GHz.

Line $N^{\pm}$	Temp. T	Freq. Dev. $\Delta\nu$	$p_m(O_2)/p_m(AIR)$	$\Delta N_o(AIR)/\Delta N_o(O_2)$	m_d	p	m_d*
	°K	MHz			Eq.(45)		Eq.(47)
9^+	300	-100	0.94	0.22	0.95	≤450	0.94
	300	-10	0.94	0.225	0.93		
	300	+10	0.94	0.218	0.96		
	300	+50	0.92	0.221	0.94		
	300	+100	0.91	0.225	0.93	≤450	0.94
	300	+216	0.93	0.219	0.95		
	281	-3.5	0.96	0.218	0.96		
	281	+7.5	0.96	0.216	0.97		
	252	-100	0.92	0.230	0.91		
7^+	300	-10	0.92	0.220	0.95	150	0.95
		0	--	--	--	150	0.95
		+10	0.93	0.219	0.95	150	0.95
		+16	0.94	0.225	0.93		
		+116	0.92	0.222	0.94		
9^+	300	-200	--	--	--	≤450	0.95
		-300	--	--	--	≤450	0.96
		-400	--	--	--	≤450	0.94
		-500	--	--	--	≤450	0.96
			0.94(2)		0.94(2)		0.95(1)

*Average of ten $[\Delta N(AIR)/\Delta N(O_2)]_p$ - ratios between 150 and 450 torr.

Table 9. Broadening Efficiency $m(9^+)$ and Refractivity N° Measured at ν = 61 156 MHz, T = 281°K, p ≤ 20 torr, for Different Air Components, and the Relative Concentration r of Dry Air Components.

k	Component		r	N°(281)	R°	m(9+)
			ppm by vol	ppm/torr	ppm°K/torr	
1	Oxygen	O_2	209 460 (±60)	0.3405	95.67 (a)	1
2	Nitrogen	N_2	780 840	0.3758	105.60*	0.911(5)
3	Argon	Ar	9 340	0.3549	99.73	0.805(5) +)
4	Carbon Dioxide	CO_2	320‡	0.6335	178.0	0.89(1)
5	Neon	Ne	18.18	0.08659	24.33	0.61(1)
6	Helium	He	5.24	0.0450	12.65	0.70(1)
7	Methane	CH_4	1.2-2‡	0.5672	159.4	1.03(1)
8	Krypton	Kr	1.14	0.5428	152.5	0.68(1)
9	Hydrogen	H_2	0.5‡	--	48.9	--
10	Nitrous Oxide	N_2O	0.5‡	0.7138	200.6	0.88(1)
11	Xenon	Xe	0.087	0.8636	242.7	0.63(1)
	Dry Air	AIR	10^6	0.3696	103.5 (b)	$\sum_{k=1}^{11}(rm)$=0.929(5)
	Water Vapor	H_2O	variable	6.666	fct(T) (Eq.2)	1.25(10)

*Reference value; all measured R^o are relative to the $R^o(N_2)$ - value given by Newell and Baird (1965).

+) m(Ar) = 0.817, calculated by Mingelgrin (P-13).

‡ Average value (a) - See Table 13

(b) Measured at $\nu/2$ = 30.6 GHz

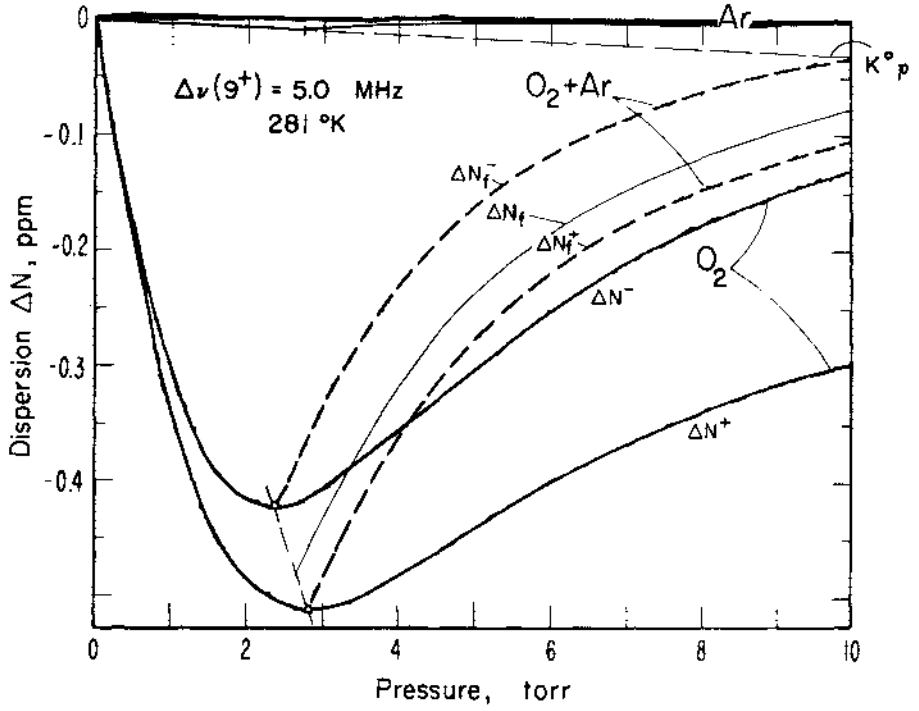

Figure 16. Recorded 9^+ line dispersion pressure profiles for foreign gas (Ar) broadening studies (see also Fig. 2.2 and Eq. 17 of Part 2).

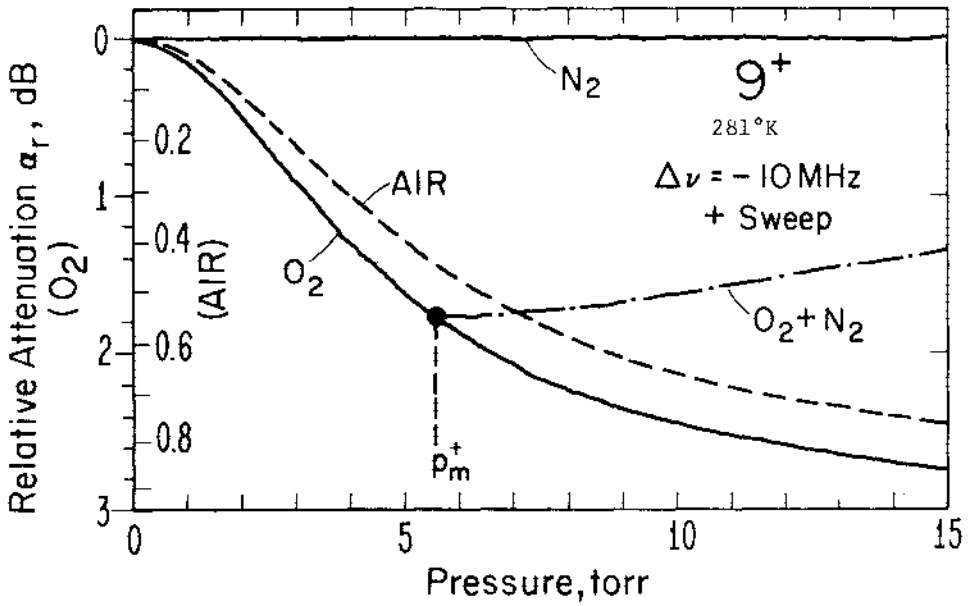

Figure 17. Recorded 9^+ attenuation pressure profile for O_2, AIR, and O_2+N_2 mixtures for foreign-gas-broadening studies. Detection law $\beta \approx 1.1$; $Q \approx 4.2 \cdot 10^5$.

continuum; (b) the transition frequency ν_o can be determined more accurately from $\Delta N(p\to 0) = 0$; (c) the relative maximum line attenuation a_o (Fig. 22) at $\Delta\nu = 0$ is well defined; and (d) the resolving power of the PRS can be evaluated. Figure 18 illustrates such a case for the 9^+ line. The Doppler width is $\gamma_D(9^+) = 67.2$ kHz. The rates for maximum attenuation and dispersion to approach zero are 0.68 and 0.61 times $S^o p/\gamma_D$, respectively, when $p < 0.01$ torr. Pure pressure-broadening (Sect. 2.1) exists for all $\Delta\nu$ when $p > 0.5$ torr.

The anomalous Zeeman effect splits the line $N = 3^\pm, 5^\pm, \ldots$ into $3(2N\pm1)$ components that are spread as a function of H over a 1 to 2 MHz wide band to either side of the line center ν_o. Each Zeeman component undergoes the gradual transition from pressure to Doppler broadening. By a judicious choice of the orientation between H and the magnetic field vector $\mathcal{E}$ of radiation, assumed linearly polarized, one can selectively excite two types ($\sigma^\pm$ and π) of Zeeman transitions. For example, the 9^+ line splits into 19π ($H \parallel \mathcal{E}$) or $38\sigma^\pm$ ($H \perp \mathcal{E}$) components. Figures 19 and 23 depict pressure profiles for π and σ-types of the 9^+ and 3^+ lines under the field strength (0.53 G) present in the laboratory. Pure pressure-broadening (Sect. 2.1) exists for $\pm\Delta\nu \geq 2$ MHz and $p > 4$ torr. Individual Zeeman components are not resolved.

The normal Zeeman effect of the $1^\pm$ lines has the simplest splitting pattern, either two σ or one π component whereby only the σ components shift away from the line center. Figure 24 gives examples of predicted pressure profiles for the 1^+ line. For the σ-type split we note a resolution of the two components on the 0 to 1 torr pressure scale.

Experiments on this line may permit identification of the predominant type of polarization inside the Fabry-Pérot resonator interaction cell and thus provide guidance for a magnetic field simulation (Sect. 3.5.4 - Part 2).

All predicted pressure profiles are calculated by approximating the transition from Lorentzian to Gaussian shape (Voigt profile) with a Lorentzian having the linewidth $\gamma = [\gamma_D^2 + (\gamma^o p)^2]^{1/2}$ (Waters, P-12).

Experimental results at the 9^+ and 7^+ line centers are shown in figures 20 to 22 for several examples. It is apparent that dispersion profiles are sensitive to frequency changes smaller than 5 kHz and that they depend upon the magnetic field strength H. While profiles for pressure-broadening are relatively easy to interpret because of γ^o, S^o, and N^o, this task becomes more difficult when $\gamma \neq \gamma^o p$. Low pressure (< 1 torr) profiles close to a line center serve three purposes:

1) to evaluate the PRS resolving power,
2) to determine the transition frequency ν_o at $H \approx 0$,
3) to measure the intensity distribution for $H \approx 0$ and H.

PRS Resolving Power. The prediction for 9^+ at $\Delta\nu = \pm 20$ kHz, based upon a 67 kHz finite Doppler width, yields $p_m = 0.045$ torr at H = 0 (Fig. 18). The experiment produces for the same condition $p_m = 0.06$ torr (Fig. 20) which indicates a finite resolved width of $\gamma_{min} \doteq 90$ kHz close to the theoretical limit. The maximum detectable dispersion gradient is $d(\Delta N)/dp = 7.5$ ppm/torr. The conventional expression of resolving power is a Q-value, $Q_{res} = \nu_o/2\gamma_{min} \doteq 6.8 \cdot 10^5$. Frequency profiles can be constructed from dispersion pressure profiles with a pressure resolution of .01 torr.

Table 10. 9^+ and 7^+ Line Center Frequencies

9^+ Line (Fig. 19), H ≐ 0

T	ν_o	R_F	I_F
°K	MHz	MHz	MHz
252	61 150.583(5)	15.056 414(1)	40. 883 845
281	.575(5)	412(1)	783
300	.565(5)	410(1)	830
325	.559(5)	408(1)	855
		x_H = 2028	
Exp.	.570(10)		
Th.	.567	Table 2 - Part 1	

7^+ Line H = 0.53 G

300	60 434.782(5)	15.009 065(1)	-40.883 822
		x_H = 2016	
Exp.	.776(10)		
Th.	.778	Table 2 - Part 1	

Transition Frequency. The frequency ν_o is defined by assuming for H ≐ 0 that $\Delta N = 0$ for p ≐ 0 to 0.1 torr. This is not exactly true since at $\Delta\nu(9^+) = 0$, first the refractive tuning (-19 kHz/torr) produces a small positive dispersion ΔN_L until next the negative continuum $n_1^o p$ takes over. For example, 9^+, O_2, 300°K, H = 0 yields:

p, torr	0	0.5	1	2	3	3.5
ΔN, ppm·10^{-3}	0	8.0 (Max)	6.5	3.0	0.3	-1.0 .

On the other hand, the speed $\delta \doteq \pm$ 16 kHz/μs forces a shift upon

Table 11. Measured Peak Dispersion ΔN_o, Pressure p_m, and Width γ^o Around the 9^+ Line Center ($\Delta\nu = \pm 5$ MHz, $T = 281°K$, ^{o}Oxygen, $H = 0.53$ gauss, + Sweep).

$\lvert\Delta\nu\rvert$	ΔN_o^+			D	p_m^+			$\Delta\nu/p_m^+$		
	-	+	Mean	Differ.	-	+	Mean	-	+	Mean
[MHz]		[ppm]				[torr]			[MHz/torr]	
0.10	.343	-.400	.372	-.057	.08	.10	.09	1.25	1.00	1.13
0.25	.410	-.435	.423	-.025	.18	.20	.19	1.39	1.25	1.32
0.50	.426	-.450	.438	-.025	.28	.32	.30	1.79	1.56	1.68
1	.434	-.479	.457	-.045	.53	.61	.57	1.89	1.64	1.77
2	.441	-.490	.466	-.049	1.06	1.12	1.09	1.89	1.79	1.84
2.5	.442	-.495	.468	-.053	1.31	1.42	1.37	1.91	1.76	1.84
3.5	.441	-.499	.470	-.058	1.81	1.97	1.89	1.93	1.78	1.85
5	.441	-.503	.472	-.062	2.54	2.72	2.63	1.97	1.84	1.90
5-30	Table 2b:		.474(3)							1.91(2)

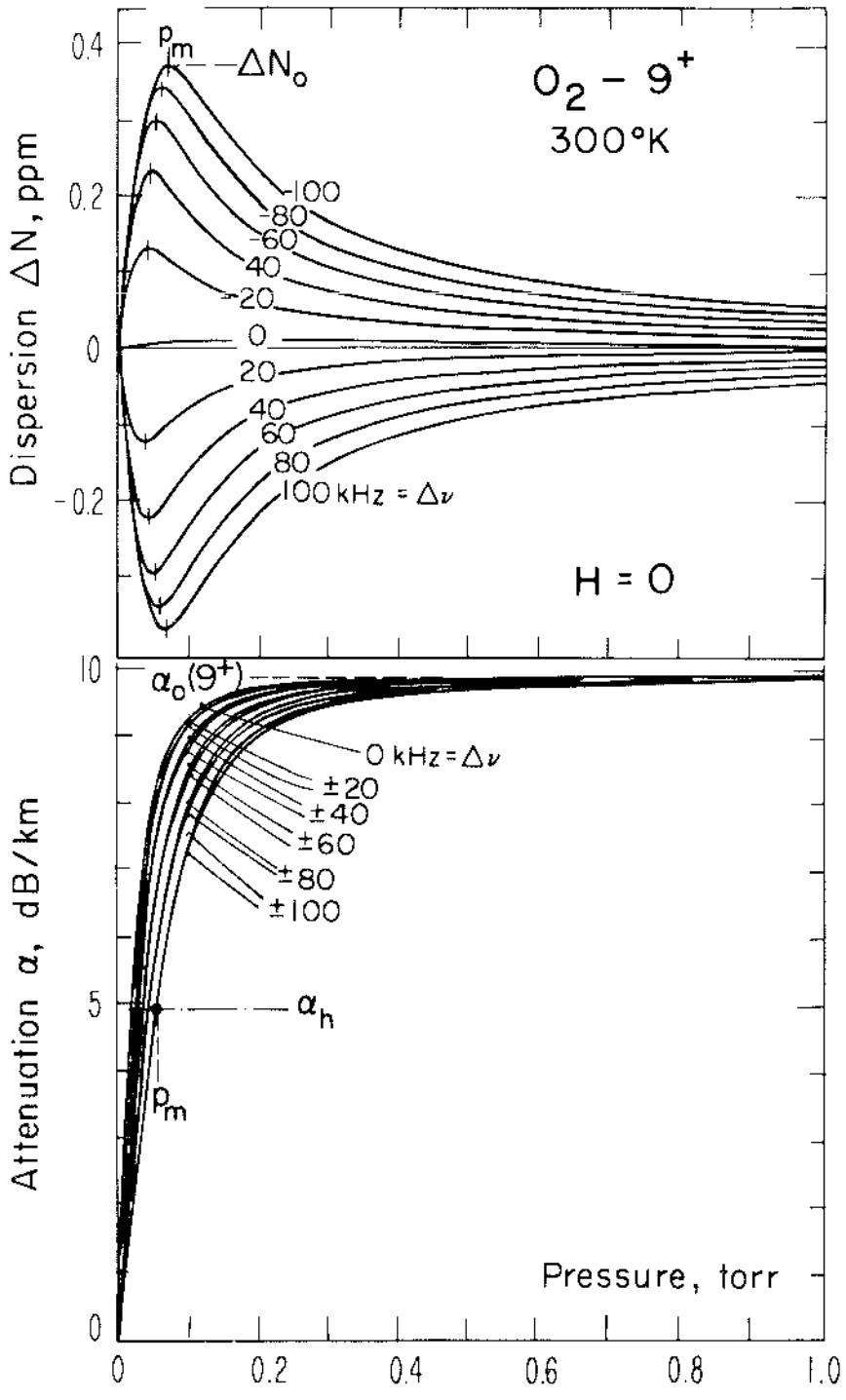

Figure 18. Computer plot of experimental pressure profiles for Doppler-broadened (H = 0) 9^+ Line Center (see Fig. 10 - Part 1).

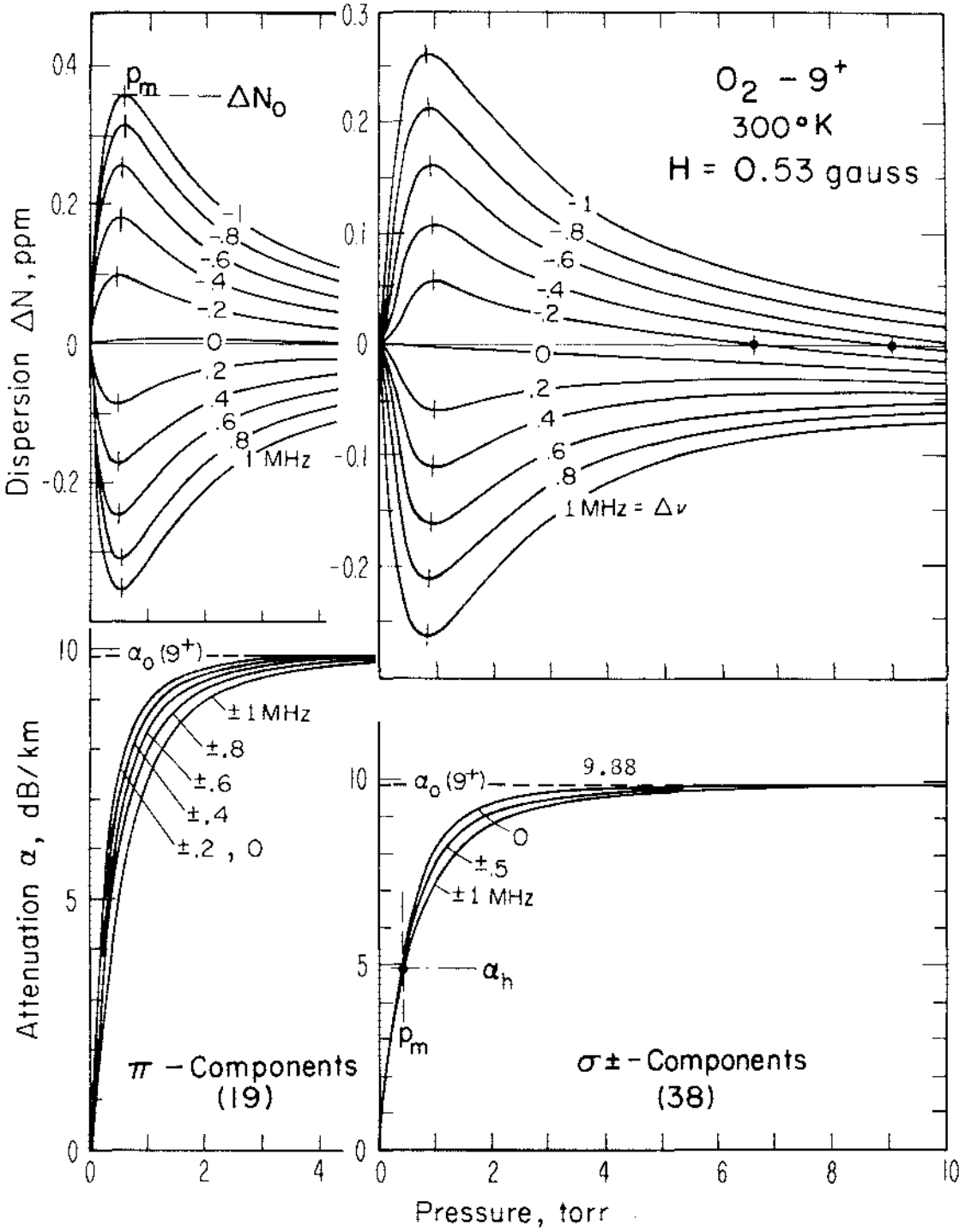

Figure 19. Computer plot of experimental pressure profiles for Doppler- and Zeeman-broadened 9^+ Line Center.

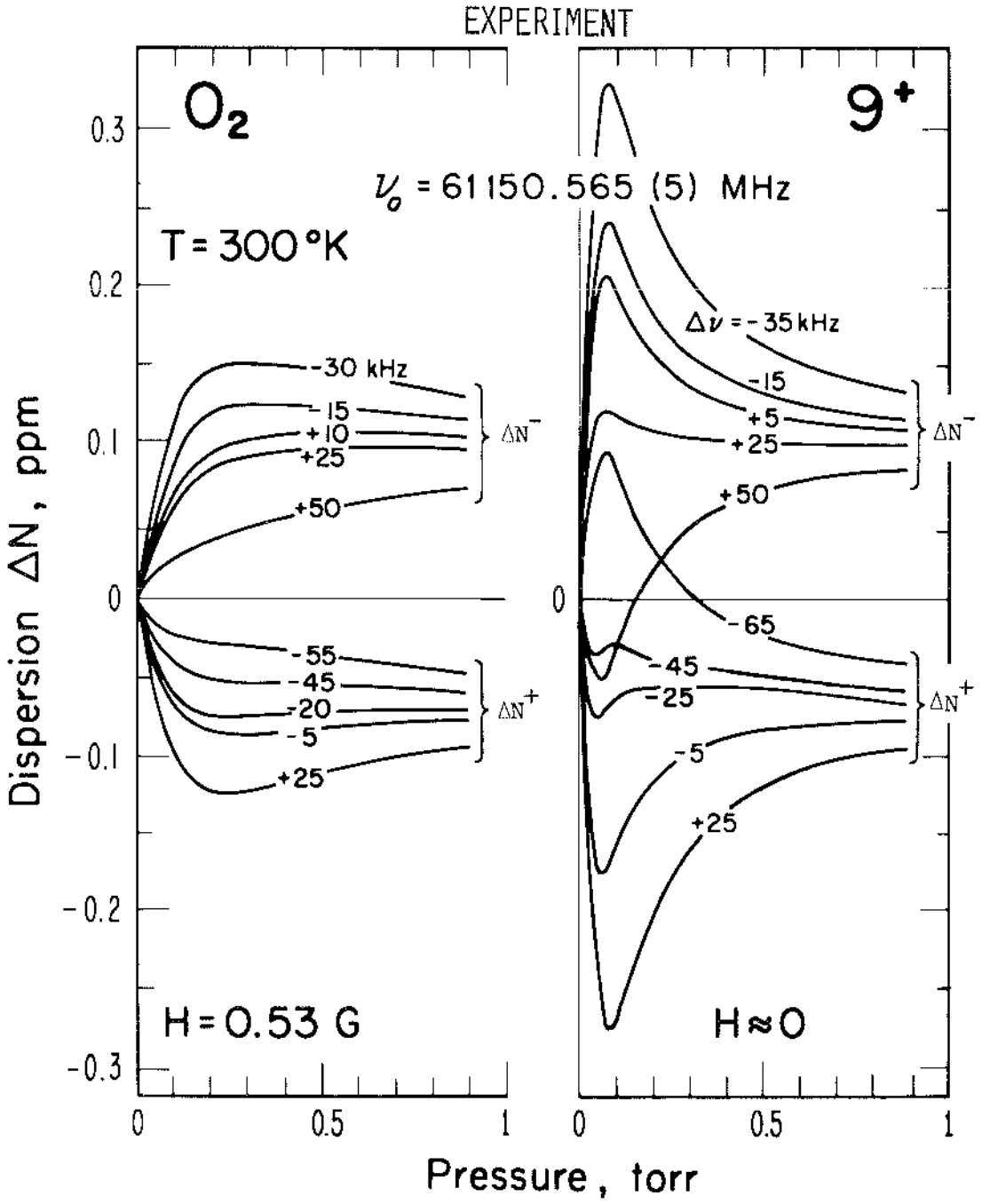

Figure 20. Recorded dispersion pressure profiles for ± sweep direction around the 9^+ Line center for compensated (H≈0) and uncompensated (H = 0.53 gauss) earth's magnetic field strength.

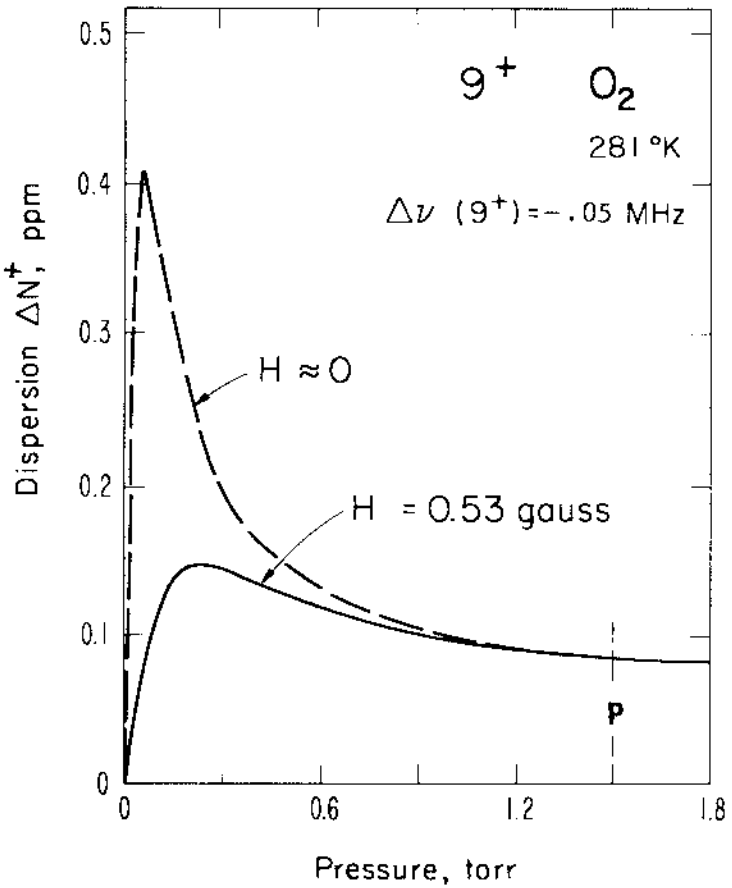

Figure 21. Recorded dispersion pressure profile close to the 9^+ line center for compensated ($H \approx 0$) and uncompensated ($H = 0.53$ gauss) earth's magnetic field strength. Also, see Fig. 20.

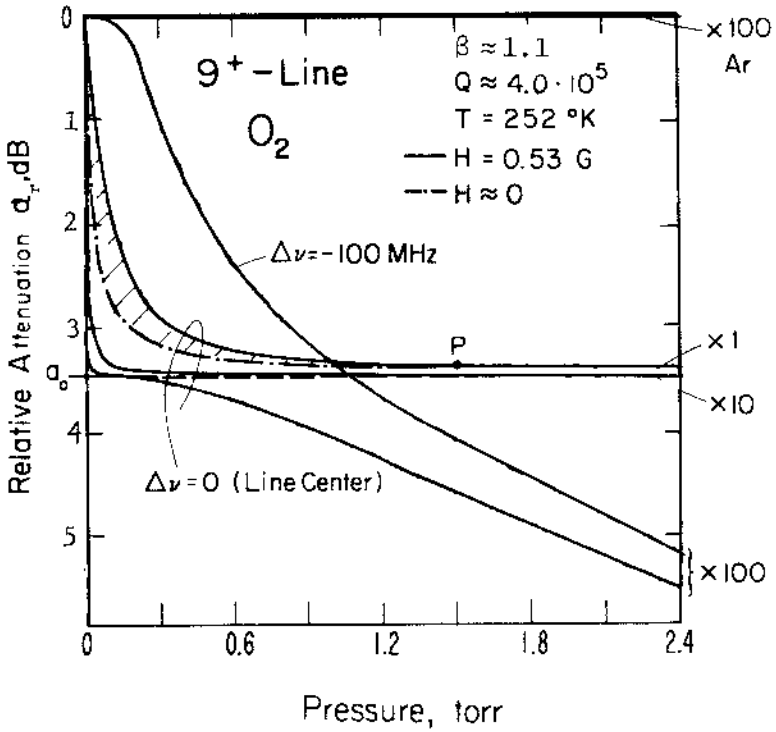

Figure 22. Recorded attenuation pressure profiles showing at the line center the influence of the magnetic field strength H=0.53 gauss up to the pressure P (1.5 torr). Also, see Fig. 9.

$\nu_R(\delta=0)$ with the difference $|\nu_R(+\delta) - \nu_r(-\delta)| = 28(4)$ kHz, which is sufficient to produce close to a line center vastly different dispersion profiles (Fig. 20). The center ν_o was determined when the setting $\Delta\nu(9^+) = \pm 14$ kHz produced $\Delta N^- + \Delta N^+ \doteq 0$ for $p = 0$ to 0.1 torr. The results are listed in Table 10 and there was no difference for $H = 0$ and $H = 0.53$ G. The very slight systematic temperature dependence of ν_o indicates that the above procedure was somewhat erroneous although not more than other reported values. The line contributions $+\Delta N_L^-(+ 14$ kHz) = $-\Delta N_L^+(- 14$ kHz) probably did not cancel completely because of $g \neq 1$ (Eq. 29, Fig. 7).

Intensity Distribution. The $\Delta N(p)$-profiles have the potential for absolute intensity measurements. A puzzling problem is whether or not overlap interference exists between Zeeman components in analogy to the pressure-broadened O_2-MS band shape. That question surfaced when Waters (1973) measured emission from well-resolved ($\gamma \approx 3$ MHz, $h > 40$ km) O_2-MS lines originating in the upper stratosphere. On the edges of the band, thermal emission from high N-number lines penetrates the lower atmosphere. Against the continuum background, a peak emission T_o at the line centers was measured toward zenith to be (Waters, 1973)

N-number	31^-	29^-	27^-	25^-				23^-
Measured T_o, °K	6.5	10	13	11	22	40	95	5
Calculated T_o, °K	2.8	5	7.8	7				2.4
Observation height h, km	0	0	0	0	3.3	4.9	11.8	0 ,

which is consistently higher when compared with calculations based upon Lenoir's (1968) formulation. Another plausible explanation for the

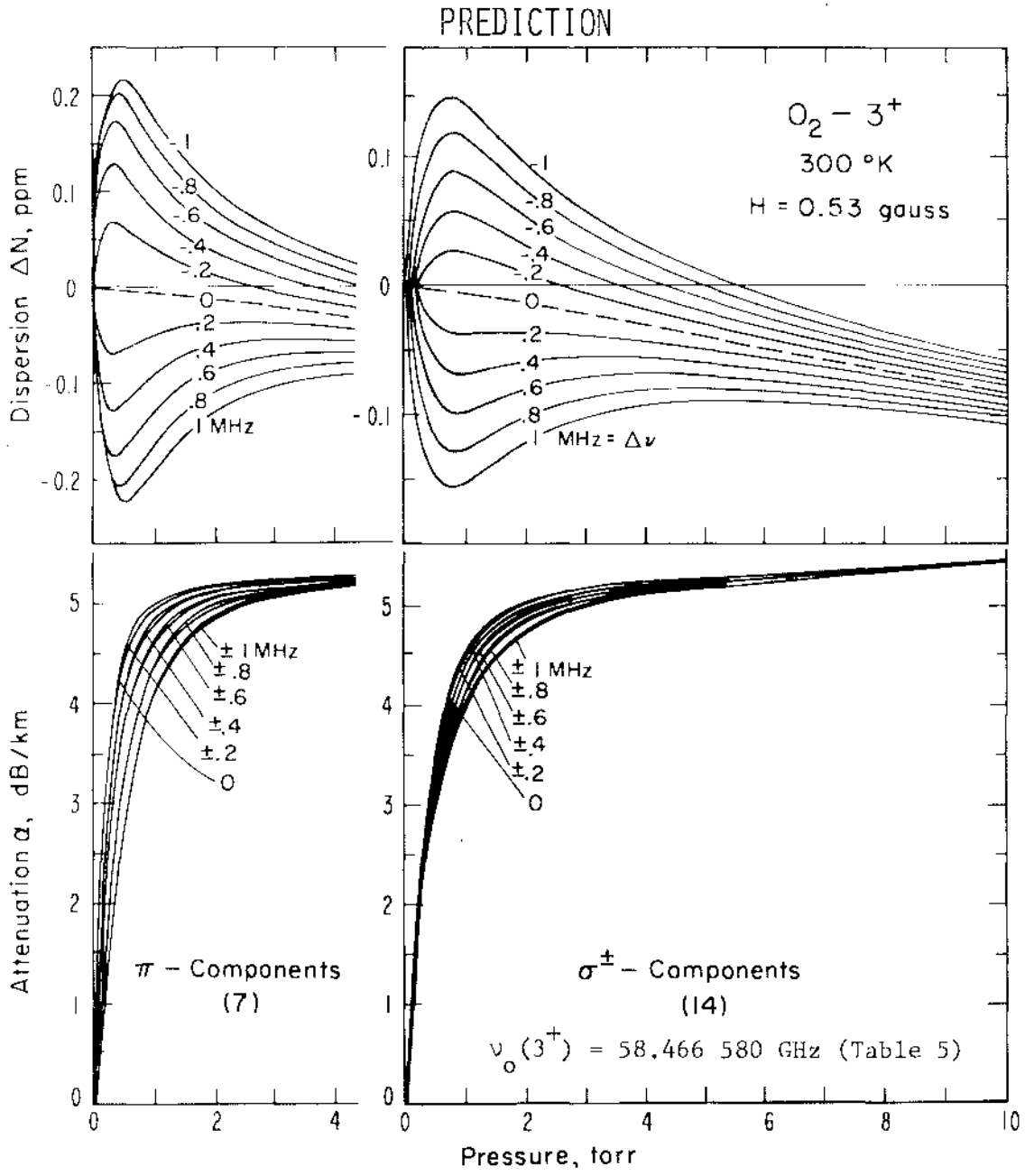

Figure 23. Computer plot of experimental pressure profiles for Doppler- and Zeeman-broadened 3^+ Line center.

PREDICTION

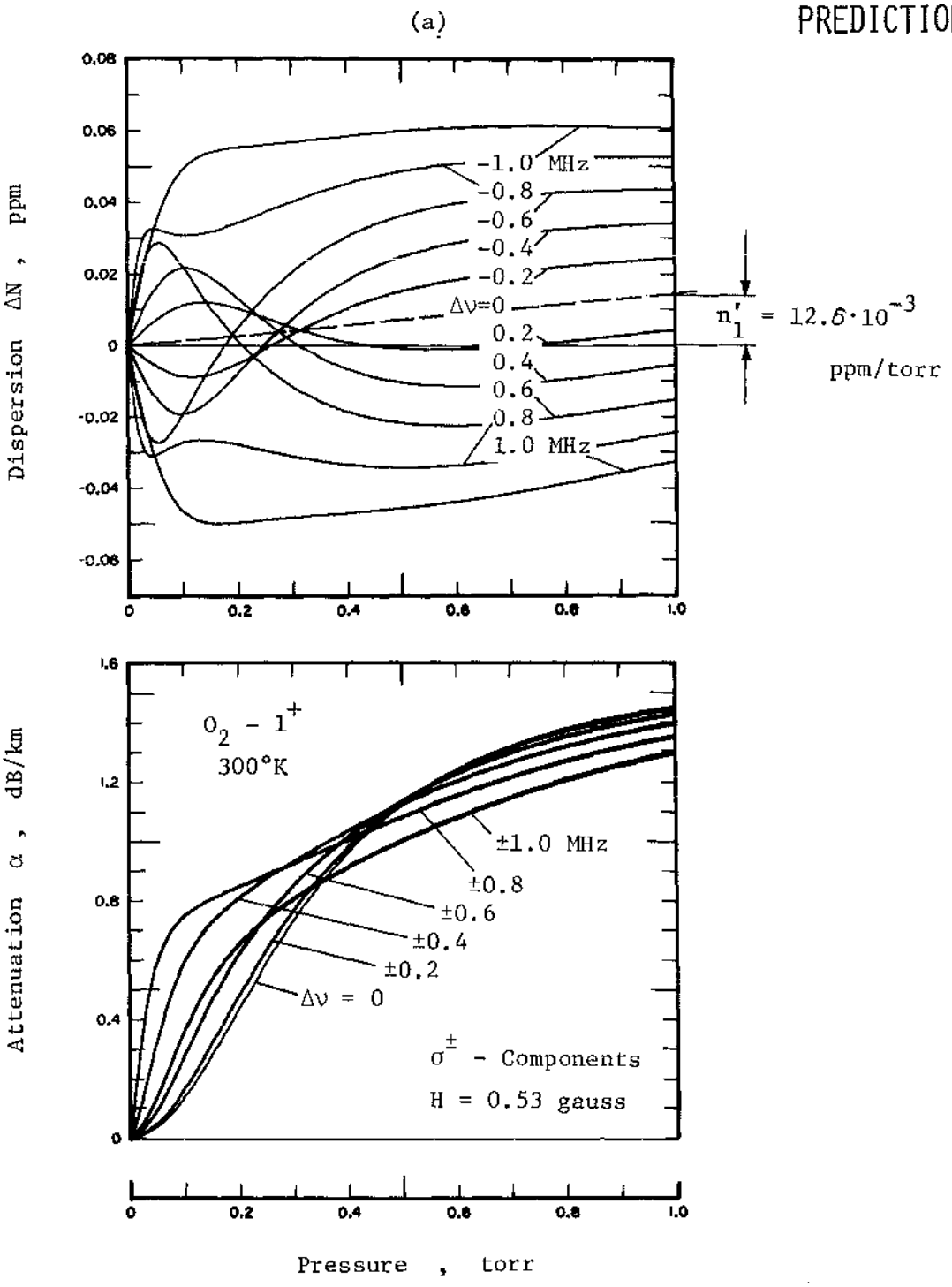
(a)
Dispersion ΔN , ppm
0.08
0.06
0.04
0.02
0
-0.02
-0.04
-0.06
-1.0 MHz
-0.8
-0.6
-0.4
-0.2
Δν=0
0.2
0.4
0.6
0.8
1.0 MHz
0
0.2
0.4
0.6
0.8
1.0
$n_1' = 12.6 \cdot 10^{-3}$
ppm/torr
Attenuation α , dB/km
1.6
1.2
0.8
0.4
0
$O_2 - 1^+$
300°K
±1.0 MHz
±0.8
±0.6
±0.4
±0.2
Δν = 0
$\sigma^{\pm}$ - Components
H = 0.53 gauss
0
0.2
0.4
0.6
0.8
1.0
Pressure , torr

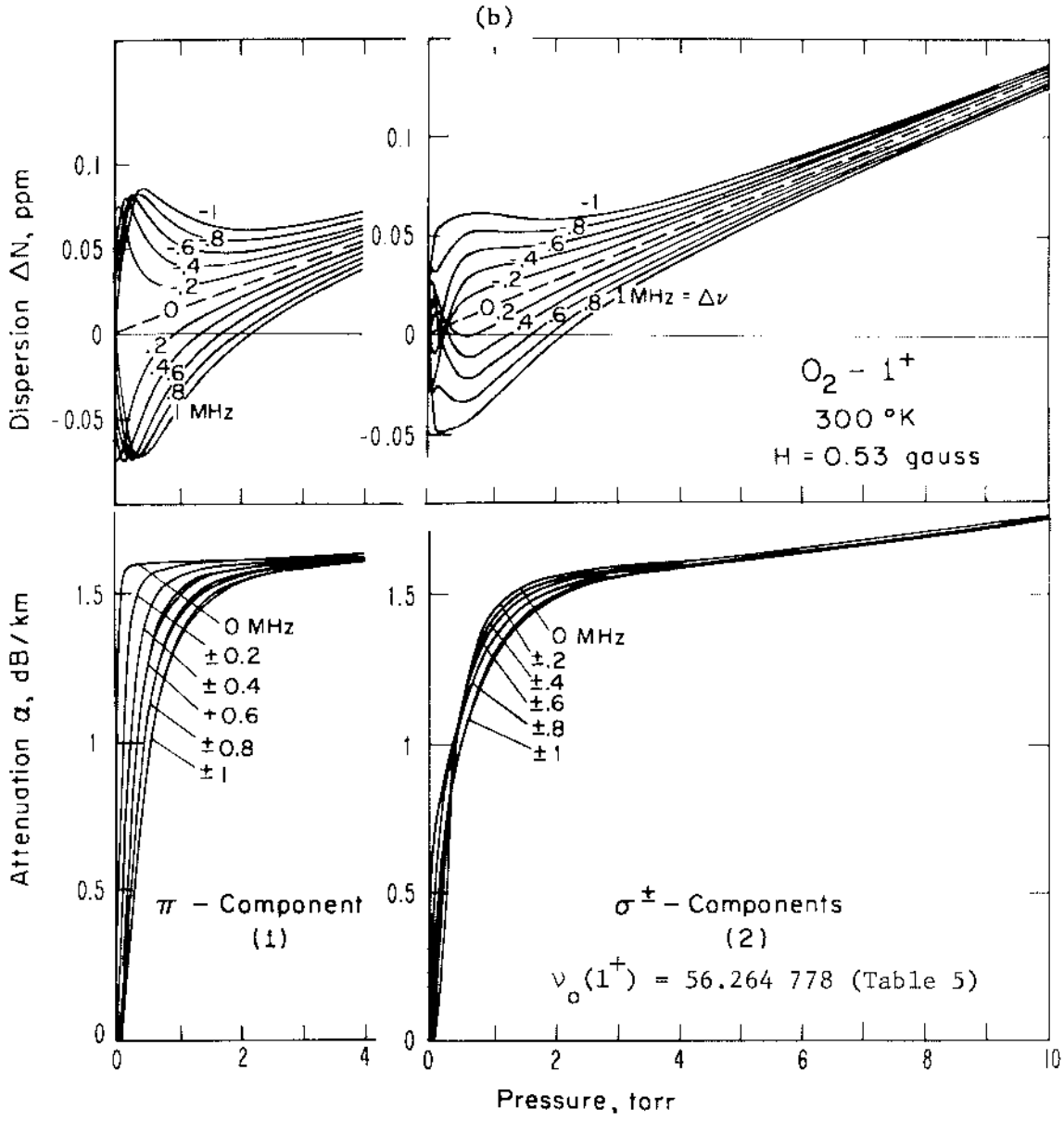

(a) p = 0 to 1 torr , $\sigma^{\pm}$

(b) p = 0 to 10 torr , $\sigma^{\pm}$ and π

Figure 24. Computer plot of experimental pressure profiles for Doppler- and Zeeman-broadened 1^{+} Line center (normal Zeeman effect).

enhanced center intensities can lie in assumed width parameters different from equation (8) (Rosenkranz, private communication 1975).

Predictions of pressure profiles are given in figures 19, 23, 24 for the 9^+, 3^+, and 1^+ lines. When it comes to interpreting experimental data quantitatively one has to unravel several competing influences:

a) The orientation and polarization of $\vec{\varphi}_g(TEM_{001})$ for the Fabry-Pérot resonator in respect to H is not known. Hence our results are some mixture between π- and σ-states.

b) Fast passage effects upon the resonator response [phase error $\Delta N_\phi^+(\alpha,\delta)$] and the molecular resonance have to be considered. Both effects arise when a frequency is swept through a resonance (circuit and/or molecular) in a time period short relative to the relaxation process. Molecular relaxation, which depends upon pressure (collision rate) and field strength (power saturation) should play no role for sweep speeds $\delta < 20$ kHz/μs and input powers of 15 dB below 1 to 3 mW at ν_R (typical PRS values) when O_2 pressure is above 10 mtorr (McGurk et al., 1974).

c) Dispersion detection by the frequency shift of ν_R is nonlinear when the line quality value $Q_L = \nu_o/\gamma$ becomes larger than the resonator Q-value Q. The consequence is an enhancement of experimental dispersion intensities (Dillon and Liebe, 1971). For example, this is the case when $p < 0.15$ torr for 9^+, 300°K, and O_2 ($Q_L \doteq Q \doteq 4 \cdot 10^5$).

d) The resonator cell R_2 causes wall broadening,

$$\gamma_w \doteq (2.30 \cdot 10^3/d[cm])(T/M)^{1/2} \doteq 0.5 \text{ kHz} \qquad (56)$$

As a consequence of a) to d), we cannot quote absolute dispersion values close to a line center; however, all theoretical predictions are qualitatively fulfilled. Table 11 demonstrates the decrease of maximum dispersion and apparent line width approximately as predicted for the π-state in figure 19.

In summary, good reproducible dispersion data have been obtained at line centers but that their quantitative value remains questionable. Some clarification is expected in the future from I^+ line studies (Fig. 24) and a considerably reduced sweep speed δ.

2.4 Continuum Spectra

The pressure range for atmospheric O_2-MS continuum spectra lies between > 100 to 800 torr. Lines and doublets lose their identity when increasing pressure makes them coalesce into a relatively unstructured band shape centered at 60 GHz and about ± 10 GHz wide. The continuum requires overlapping line theory which considers collisional couplings between the rotational states. Dillon and Godfrey (1972) predicted such couplings to be insignificant. Mingelgrin (1972, 1974), however, found differences of 21 percent between the envelope of a sum by all O_2-MS lines and scattering calculations of a general band shape theory (Figs. 9, 21 -Part 1). A serious disadvantage of his approach is the fact that the physical variables are implicit parameters in a complex, time consuming calculation procedure. Only very recently, Rosenkranz (1975) has come up with an elegant and practical O_2-MS band solution which we adopted (Sect. 2A). He showed that the properties of resolved lines contain enough information to extrapolate the process of pressure-broadening to 800 torr, simply by limiting collisional coupling to adjacent rotational states and assuming pressure proportionality of the interference term (Eq. 8).

Since the work on this project was almost completed before Dr. Rosenkranz kindly provided us with a preprint of his paper, we had most of the predictions and analytical treatments already developed based on the sum of non-interfering O_2-MS lines. In the following, a distinction is made between "Linear Model" ($I_N^o = 0$) and "Overlap Model" (I_N^o - Table 1). The interference terms I_N^o force the band narrower than the sum of individual lines. An overview of the conditions for all treated continuum frequency spectra and pressure profiles is given in Table 12. Before testing the two "Models" with experimental results, we want to point out that, at a selected frequency ν, the "Linear M." can be converted into the "Overlap M." by

$$\alpha = \alpha_{Linear} + x^o p \quad \text{and} \quad \Delta N = \Delta N_{Linear} + y^o p \ . \qquad (57)$$

A few examples of the conversion coefficients x^o, y^o at T = 300°K are listed below (see Table 14).

ν	x^o		y^o	Figure
	O_2	AIR	O_2	
[GHz]	[10^{-3}dB/km torr]		[10^{-4}ppm/torr]	
61.141	8.7	2.0	6.3	27
58.875	5.0	1.1	0.6	30
58.437	11	2.5	4.5	29
54.943	- 1.6	- .36	4.4	30
53.647	- 2.8	- .63	4.3	30

2.4.1 Frequency Spectra at Sea Level

At ground level, more or less all O_2-MS lines are contributing to one pair of α, ΔN-values. The band shape is not a very sensitive function of the line widths γ_N. Differences between the "Overlap" and

the "Linear" model are most pronounced at sea level pressures. To find the maximum differences between the two models for an experimental confirmation, we calculated some frequency spectra (Fig. 25). The straightforward band calculation using Rosenkranz's (1975) method agrees well with Mingelgrin's (1972) more rigorous treatment. The complete O_2-MS extends over the 0 to 140 GHz range with three contributions:

i) 0 to 5 GHz - nonresonant,

ii) 40 to 80 GHz - band,

iii) 110 to 130 GHz - 1^- line.

These spectral features make it difficult to establish the non-dispersive O_2 refractivity. As evident from Table 13, reported O_2 refractivities vary slightly throughout the microwave range, although in agreement with the O_2-MS (Fig. 25a). We decided to define the 9 GHz refractivity as non-dispersive reference. Table 14 lists numerical values of "Overlap" and "Linear" results for one O_2 condition and frequencies between 20 and 140 GHz. The numbers can be used to calculate the pressure-linear conversion coefficients x^o, y^o (Eq. 57).

2.4.2 Pressure Profiles at Selected Frequencies

The key to a general atmospheric O_2-MS lies in the results of line studies. Only there is it possible to obtain absolute spectroscopic parameters (width, strength) of the band components. For continuum data, one deals with summarized values of all lines plus the theoretical refinement of interference. The coefficients I_N^o, however, cannot be measured directly. Rosenkranz (1975) supported his model by three types of absorption data: (a) zenith attenuations (Table 10 - Part 1),

(b) satellite (NIMBUS 5) measurements of atmospheric brightness temperature T_H at 54.9 GHz (Eqs. 58, 59), and (c) laboratory attenuation measurements by Poon (1974) at 58.82 GHz (O_2, 295°K, 0-320 torr). Direct measurements of α and ΔN between 100 and 800 torr are the most sensitive test. The discrepancies Overlap-to-Linear are, for example (Table 14), for O_2 attenuation -40, 0, +18, 0, -80% at 50, 55.4, 60, 63.6, 100 GHz, respectively; and for O_2 dispersion 2.5, 26, 82, 38, 2.5% at 50, 57, 60, 62, 70 GHz, respectively. A main objective of this project was the confirmation of O_2-MS theory at frequencies selected by NASA and NOAA for temperature soundings. Figure 29 illustrates the differences Overlap-to-Linear for the three NIMBUS 5 O_2-MS channels (Sabatini, 1972).

Measurements of dispersion and relative attenuation pressure profiles have been conducted, so far, under the following conditions:

$N^{\pm}$	ν, GHz	p, torr	T, °K	Example
9^+	$61.15^{+0.1}_{-0.5}$	0 - 450 (760)	300, 282, 252	Fig. 26, 27
7^+	$60.4^{+0.3}_{-0.01}$	0 - 450	300	Fig. 28
	58.87	0 - 150	300	Fig. 30
3^+	58.4	0 - 800	300	Fig. 29 .

Dispersion measurements are sensitive to better than ± 0.005 ppm and the accuracy depends upon the assessment of the phase error ΔN_ϕ. The phase error ratio g found from line studies (Fig. 7) was extrapolated, but there was no way to check if g remained constant up to 800 torr. This uncertainty has been considerably reduced by the new phase meter. Averaged dispersion results (Eq. 29) are compared with either PREDICTIONS, $N(\nu_R) - N(\nu_R/2)$, or THEORY, $\Delta N(\nu)$. In the case of THEORY,

Table 12. Overview of Treated O_2-MS Continuum Data

Figure, Table	ν [GHz]	Δν	p [torr]	T [°K]	O_2	AIR	α	ΔN	Theory Linear	Theory Overlap	Experiment Predict.	Experiment Measured
25a	0 - 140		760	300	x		x	x	x	x		
25b	20 - 140		760	300	x		x	x	x	x		
T 13	20 - 140		760	300			x		x	x		
T 12	0 - 72				x			x				x
33	40 - 140		760,570,380,190	200, 300		x						
34	40 - 140		760,570,380,190	200, 300		x						
31c	50.300	0±0.1	0 - 800	250 - 300	x		x	x	x			
32	52.800	0±0.1	0 - 800	300		x	x	x	x			
31c	52.800	0±0.1	0 - 800	250 - 300	x		x	x	x			
31c	53.647	0±0.1	0 - 800	200 - 300	x		x	x	x			
30	53.647	0	0 - 800	300	x		x	x	x	x	x	
T 15	53.647	0	0 - 400	200 - 300		x	x		x			
32	54.900	0±0.1	0 - 800	300		x	x	x	x			
31b	54.943	0±0.1	0 - 400	200 - 300	x		x	x	x			
30	54.943	0	0 - 400	300	x		x	x	x	x	x	
T 16	54.943	0	0 - 200	200 - 300		x	x		x			
31b	54.960	0±0.1	0 - 800	250 - 300	x		x	x	x			
31b	55.500	0±0.1	0 - 800	250 - 300	x		x	x	x			
31a	57.950	0±0.1	0 - 800	250 - 300	x		x	x	x			
29	58.437	0	0 - 800	300	x		x	x	x	x	x	x
31a	58.800	0±0.1	0 - 800	250 - 300	x		x	x	x			
32	58.800	0±0.1	0 - 800	300		x	x	x	x			
30	58.865	0	0 - 200	300	x		x	x	x	x	x	x
31a	58.875	0±0.1	0 - 200	200 - 300	x		x	x	x			
30	58.875	0	0 - 200	300	x		x	x	x	x	x	
T 17	58.875	0	0 - 100	200 - 300		x	x		x			
28	60.435	0±0.3	0 - 1000	300	x		x	x	x		x	
27	61.141	0	0 - 800	300	x		x	x	x	x	x	x
26	61.151	0±0.3	0 - 1000	300	x		x	x	x		x	

Table 13. Reported Oxygen Microwave Refractivity At 760 torr and 300°K (see Fig. 25).

Frequency ν [GHz]	0	9	23.6	24	30.6	48	72
Refractivity N_o [ppm]	-	242.4(2) Reference	-	242.6(2)	242.8(1)	243.1(1)	240.3(2)
Refract.Modul. R^o/T [ppm °K/torr]	-	95.67(10)	-	95.75(10)	95.86(5)	95.96(5)	94.85(10)
Dispersion ΔN [ppm]	+0.39[a)]	0	+0.4(1)	+0.2(2)	+0.4(1)	+0.7(1)	-2.1(2)
Author	Mingelgrin 1972	Essen 1953 *)	Part 1 p 60 1973	Essen-Froome 1951 *)	This Report	Newell-Baird 1964	Froome 1955 *)

a) Maximum Nonresonant O_2-MS Contribution, using Eq. 24 of Part 1 and corrected Debye Shape Factor, $F'_o = \gamma_o^2/(\nu^2 + \gamma_o^2)$.

*) Cited by Boudouris (1963).

Table 14. O_2-MS Attenuation α and Dispersion ΔN at 300°K, 760 torr (Fig. 25b).

Frequency ν [GHz]	α [dB/km]		ΔN [ppm]	
		$I^o = 0$		$I^o = 0$
20	0.022	0.021	0.138	0.138
25	0.039	0.040	0.198	0.198
30	0.067	0.076	0.278	0.278
35	0.116	0.144	0.391	0.390
40	0.212	0.293	0.563	0.561
42	0.278	0.400	0.661	0.658
44	0.375	0.564	0.785	0.780
46	0.525	0.825	0.949	0.940
48	0.784	1.279	1.178	1.161
50	1.317	2.195	1.523	1.486
51	1.876	3.076	1.775	1.713
52	2.981	4.606	2.111	2.000
53	5.335	7.367	2.550	2.343
54	10.16	12.18	3.059	2.693
55	18.80	19.72	3.486	2.923
56	31.31	29.43	3.526	2.828
57	43.90	38.53	2.971	2.355
58	53.83	46.18	2.077	1.666
59	60.56	51.37	0.958	0.793
60	64.59	54.57	-0.231	-0.127
61	64.71	54.76	-1.577	-1.160
62	60.17	52.12	-2.939	-2.135
63	47.00	44.27	-4.094	-3.108
64	30.25	32.03	-4.348	-3.513
65	17.33	21.37	-4.006	-3.424
66	9.297	13.81	-3.463	-3.109
67	5.047	9.091	-2.947	-2.746
68	2.998	6.342	-2.538	-2.422
69	2.002	4.735	-2.232	-2.160
70	1.468	3.738	-2.002	-1.953
72	0.922	2.593	-1.679	-1.653
74	0.644	1.958	-1.461	-1.445
76	0.478	1.559	-1.304	-1.292
78	0.369	1.288	-1.183	-1.175
80	0.294	1.094	-1.088	-1.082
90	0.128	0.625	-0.805	-0.803
100	0.091	0.464	-0.660	-0.659
110	0.208	0.503	-0.552	-0.551
115	0.912	1.153	-0.469	-0.467
116	1.507	1.730	-0.441	-0.438
117	2.778	2.982	-0.414	-0.410
118	5.262	5.479	-0.438	-0.431
119	6.406	6.722	-0.606	-0.598
120	3.855	4.229	-0.700	-0.695
121	1.997	2.365	-0.685	-0.682
122	1.136	1.486	-0.655	-0.653
123	0.714	1.049	-0.630	-0.629
125	0.348	0.663	-0.596	-0.595
130	0.105	0.392	-0.548	-0.548
140	0.019	0.028	-0.501	-0.501

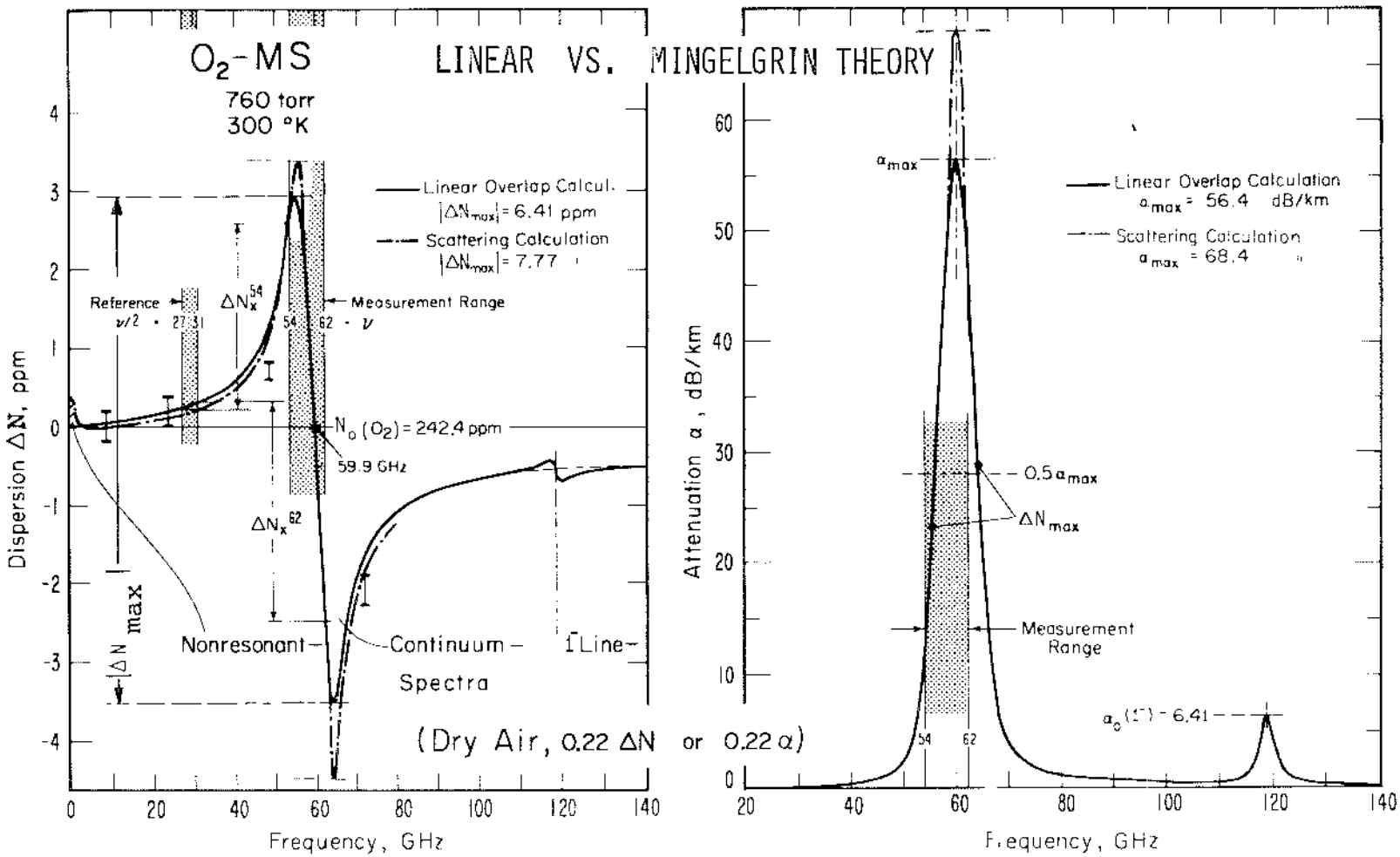

Figure 25a. The O_2 Microwave Spectrum of dispersion ΔN and attenuation α between 0 and 140 GHz and the frequency range of the measurements. The experimental dispersion ΔN_x is measured as difference in refractivity at ν and ν/2.
T : Reported O_2 refractivities - see Table 13.
Scattering calculations by Mingelgrin (1972, 1974, and Fig. 9 - Part 1).

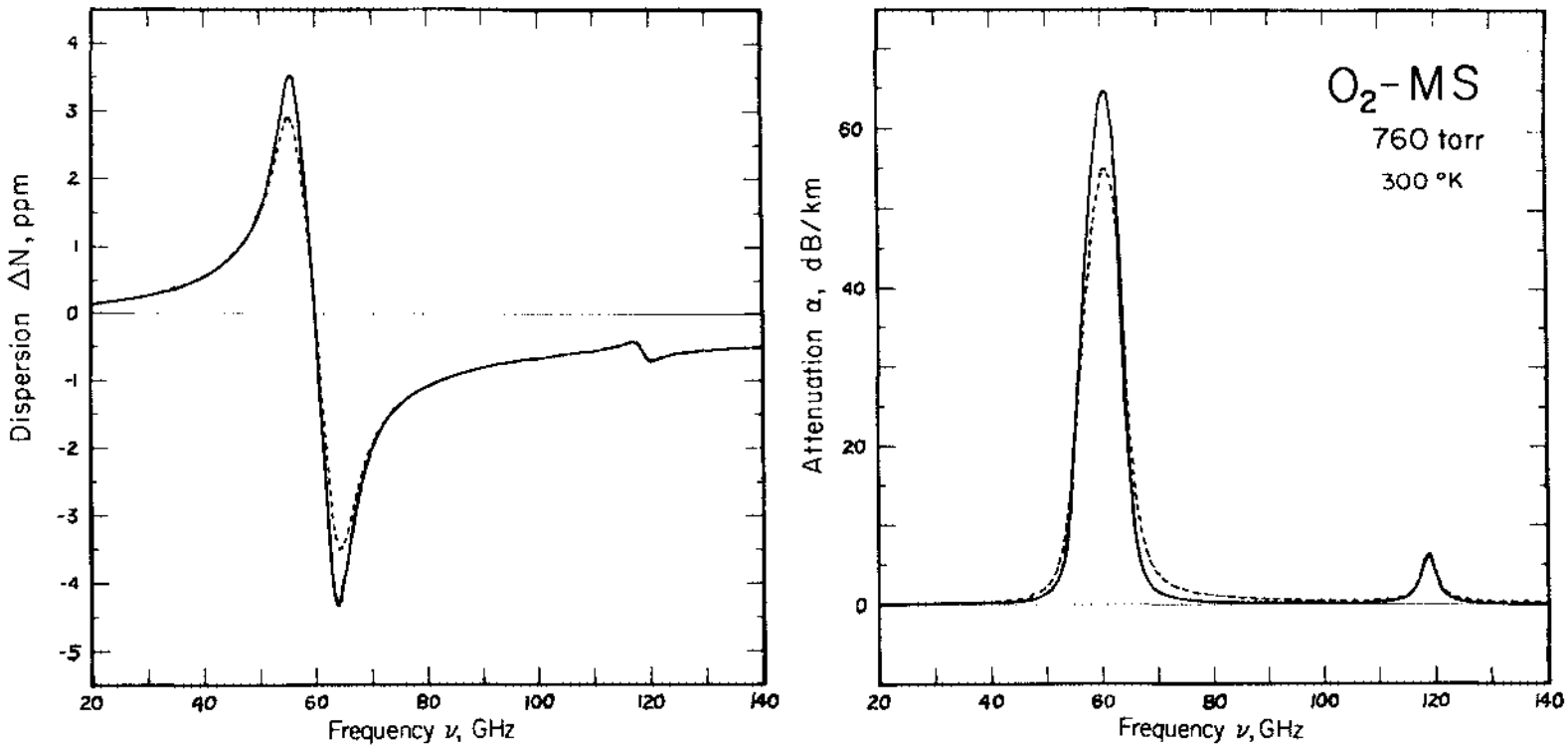

Figure 25b. The O_2-MS microwave spectrum of dispersion ΔN (Eqs. 4, 5, 9) and attenuation α (Eqs. 3, 4, 6, 9) between 20 and 140 GHz.

Solid line : I_N^o - Figure 1, Table 1.

Dashed line: $I_N^o = 0$.

Numerical values see Table 14.

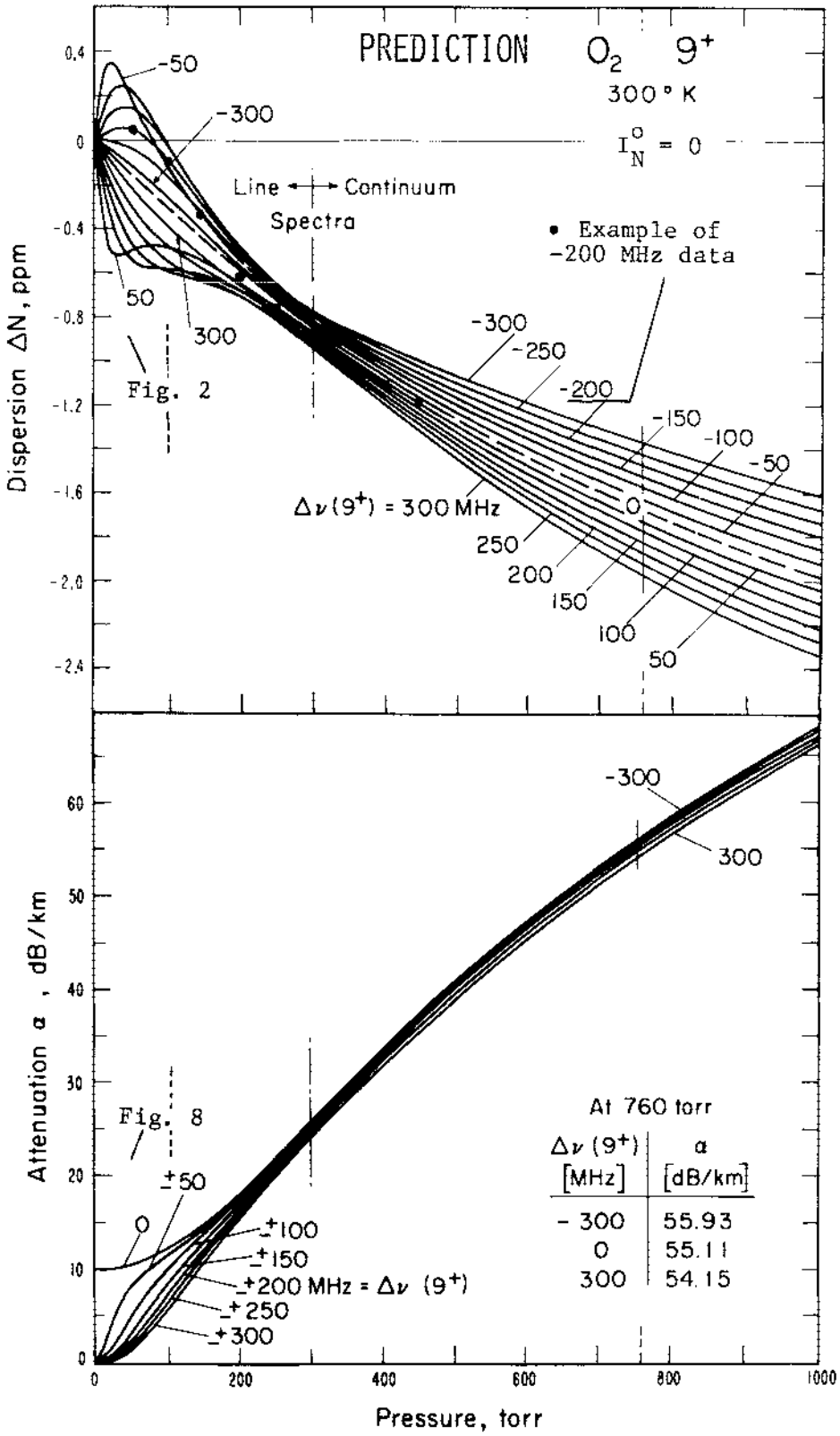

Figure 26. Computer plot of experimental O_2-MS Continuum pressure profiles in the vicinity of the 9^+ Line (61.15 ± 0.3 GHz).

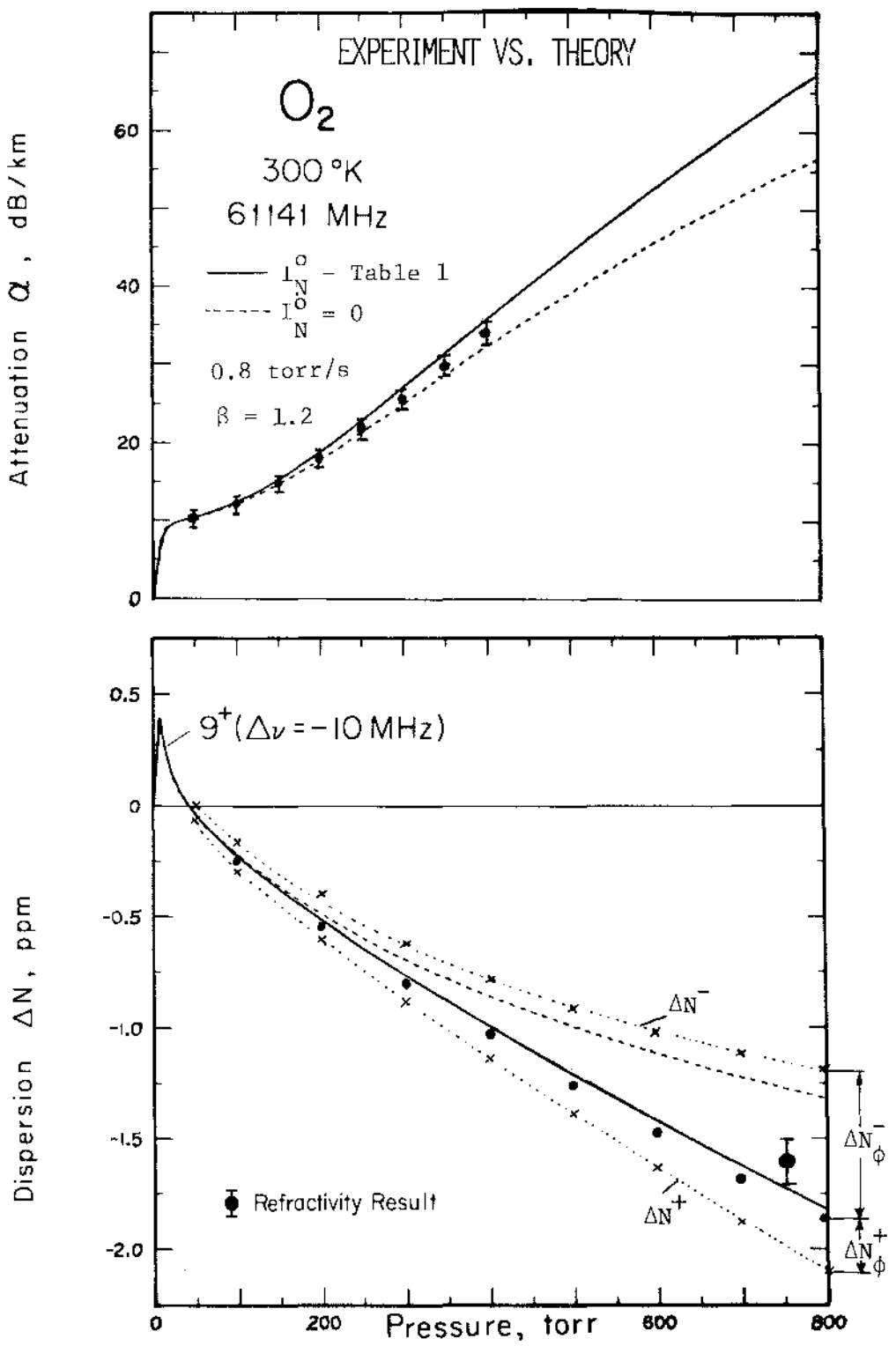

Figure 27. Comparison of experimental and theoretical continuum pressure profiles at 61.1406 GHz [$\Delta\nu(9^+)$ = - 10 MHz].

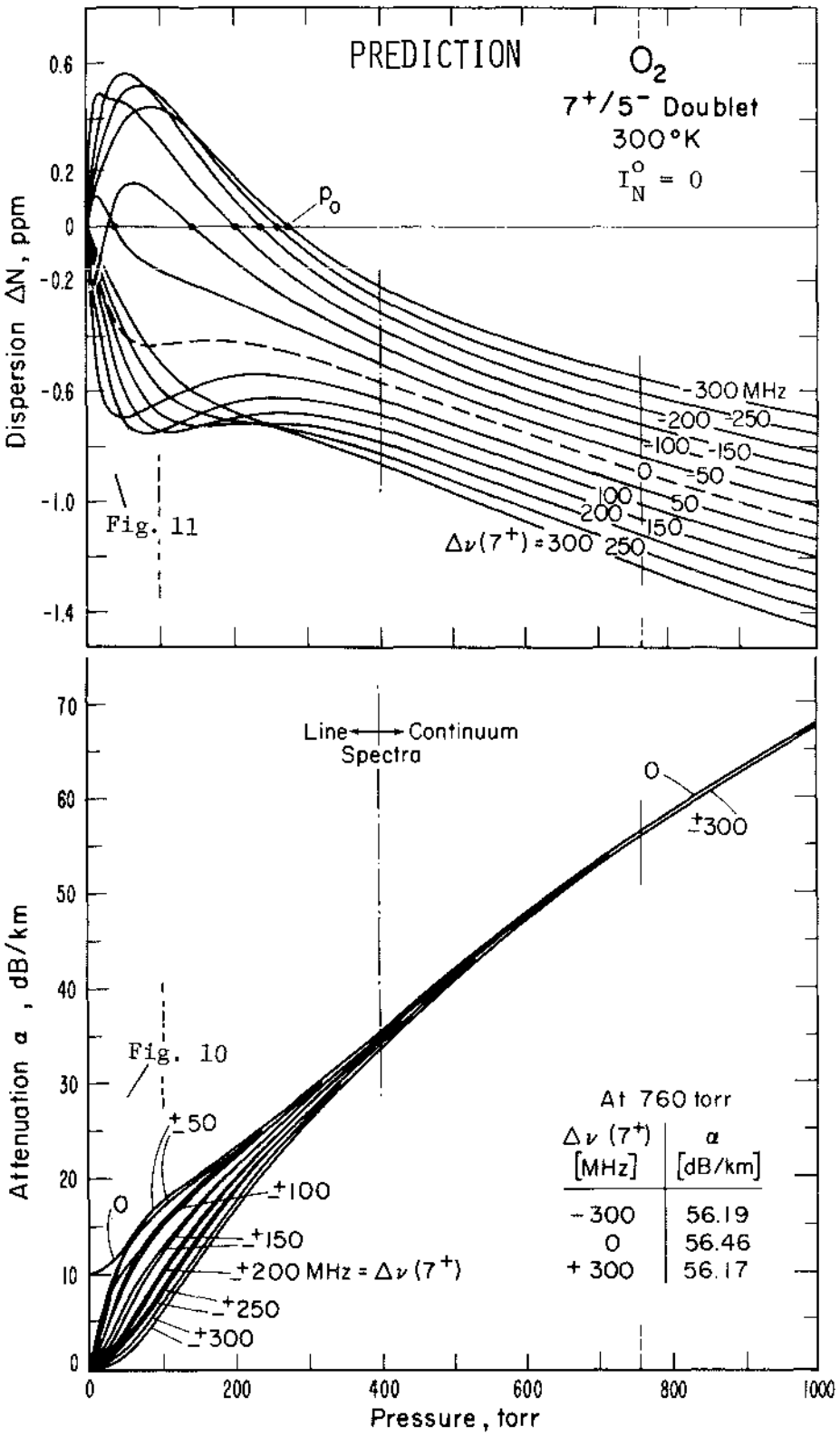

Figure 28. Computer plot of experimental O_2-MS continuum pressure profiles in the vicinity of the $7^+/5^-$ Doublet ^{2} (60.4 ± 0.3 GHz).

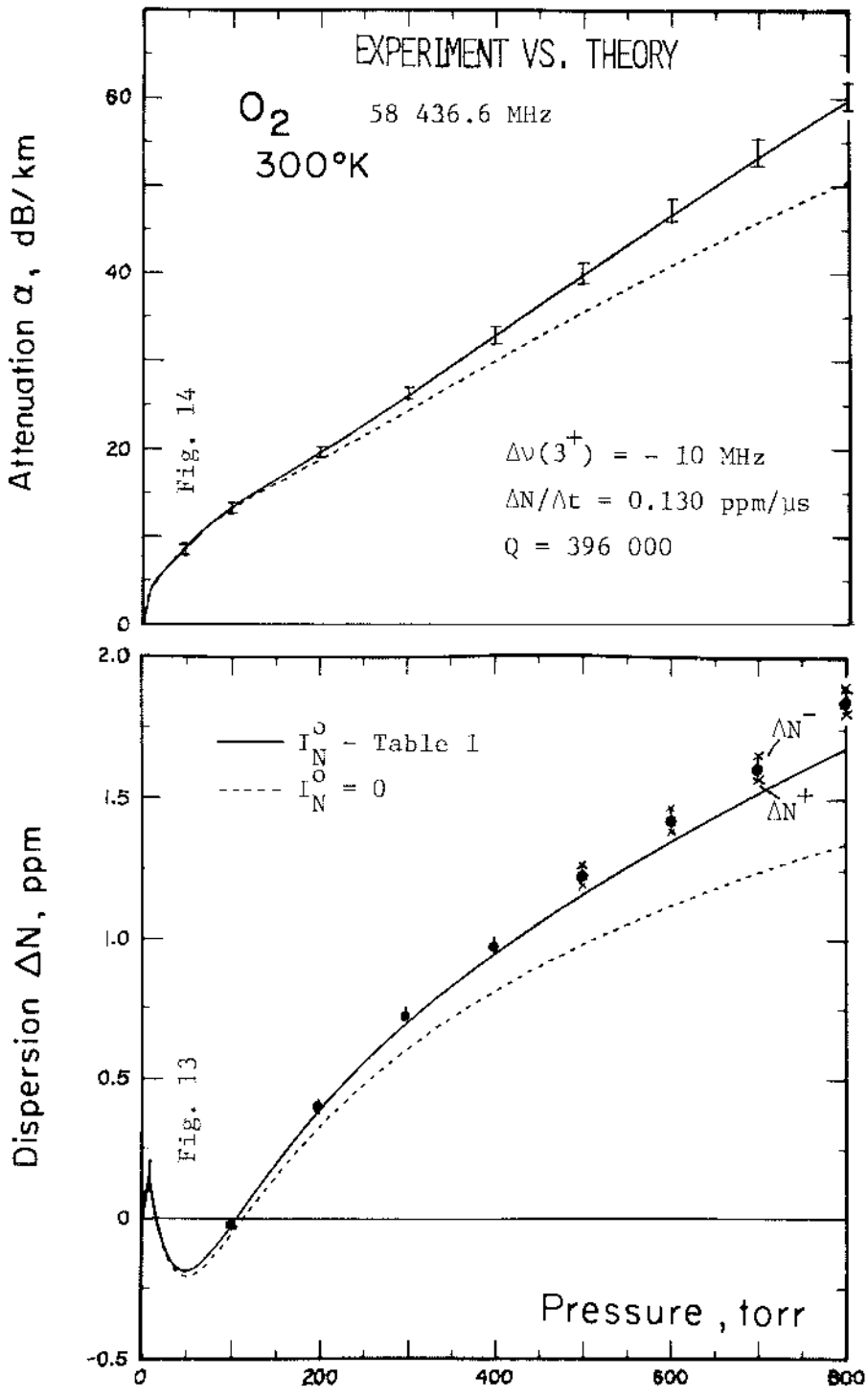

Figure 29. Comparison of experimental and theoretical continuum pressure profiles at 58.4356 GHz [$\Delta\nu(3^+)$ = - 10 MHz]

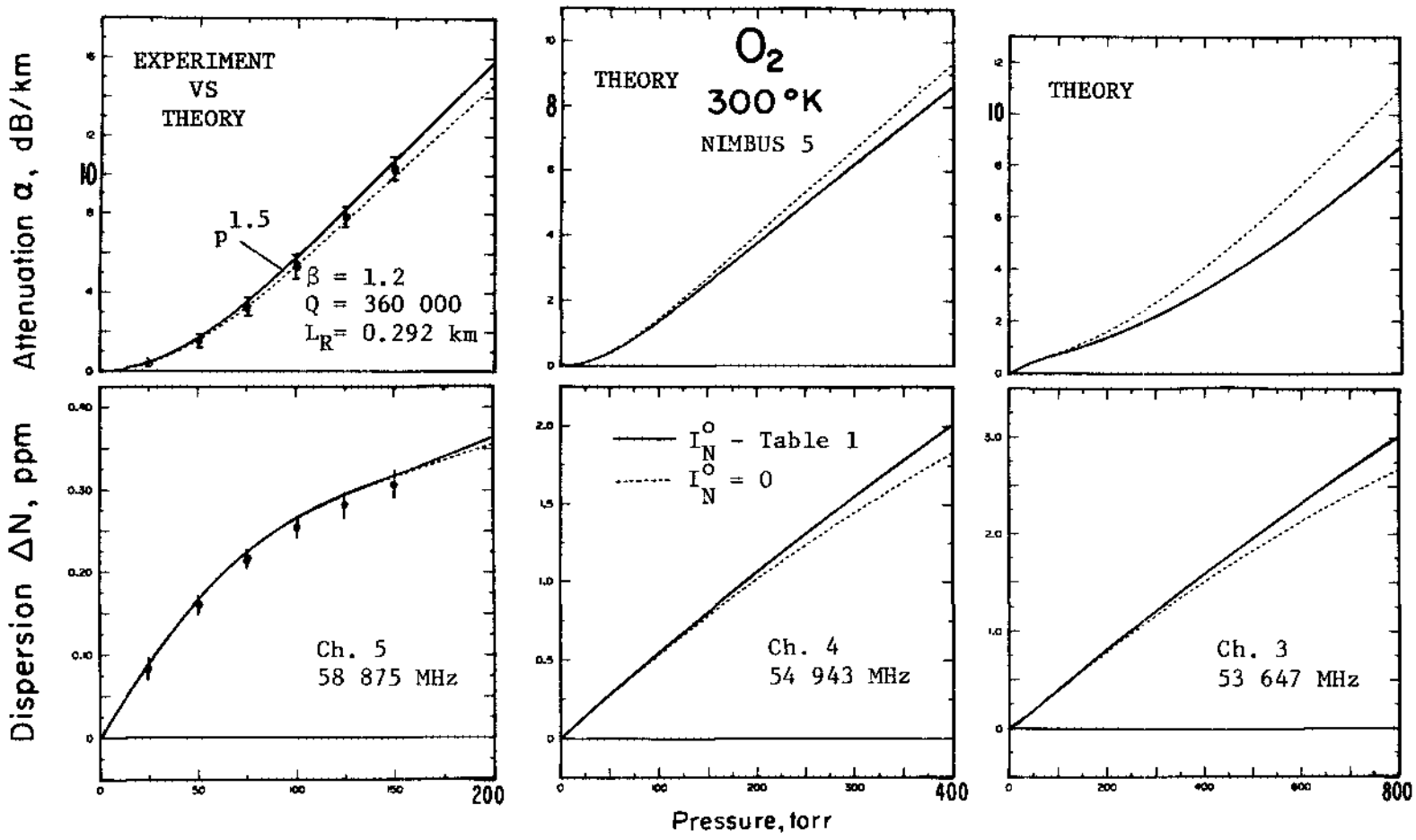

Figure 30. Theoretical continuum pressure profiles with and without interference at the three NIMBUS 5 oxygen channels (Sabatini, 1972).

the O_2-MS dispersion contribution at $\nu/2$ is subtracted from the experimental result (e.g., $-3.46 \cdot 10^{-4}$ ppm/torr for O_2, 58.4/2 GHz, 300°K).

Attenuation measurements are sensitive to 0.01 dB/km, and the accuracy was estimated ± 11 percent when the absolute intensity was obtained from measured values of Q and β (Eq. 36) and was improved to ± 3 percent when relative attenuation profiles $a_1(p)$ were taken at $\Delta\nu = 0$. At a line center, the maximum attenuation of that line, α_o, is constant over a pressure range, particularly when $H \approx 0$ (Fig. 8, 10). The value α_o was calibrated using "dispersion" line parameters (Sect. 2.1.4). The measurement range was initially limited to 30 dB/km, but was extended to 75 dB/km by the improved peak detection of the new design (Fig. A1).

Results are expressed as agreement with "Linear" or "Overlap" O_2-MS models. Under all circumstances (see above), a better fit to the data was obtained when considering the interference coefficients based upon Rosenkranz's (1975) theory (see Figs. 27, 29). The results at 58.4 GHz are most reliable since they were obtained with much less phase error due to the new phase meter (APPENDIX C). The O_2 dispersion result at 61.14 GHz, 760 torr, 300°K was confirmed by a refractivity measurement which involved the readings $[\nu_R(p=0)-\nu_R(p=760)]/\nu_R(p=0) \equiv N(\nu_R)$, correcting $N(\nu_R)$ for a small pressure-tuning of R2 [$4 \cdot 10^{-10}$/torr when checked against $N_o(N_2)$] and taking the difference $N(\nu_R)-N(9\ \text{GHz}) \equiv \Delta N$.

This concludes the description of completed experimental studies on O_2 and AIR. The O_2-MS theory, introduced in Section 2A, can now be applied with some confidence to practical problems.

B. ANALYSIS

2.5 Transfer and Emission Characteristics of Air (40 -140 GHz)

The transfer properties of the clear, dry atmosphere are expressed through cumulative attenuation, phase dispersion, and phase delay along a ray path $h_o \rightarrow h_1$ (Eq. 43) - Part 1):

$$A = \int_{h_o}^{h_1} \alpha(\ell)\,d\ell \quad [\text{Np}], \quad \Delta\Upsilon = \int_{h_o}^{h_1} \Delta\phi\,d\ell \quad \text{and} \quad \Upsilon_o = \int_{h_o}^{h_1} \phi_o\,d\ell \quad [\text{rad}], \qquad (58)$$

where α, $\Lambda\phi(\Delta N)$ are spectra of O_2 whose dependency upon frequency ν and physical parameters p, T, H has been the main topic of this report ($d\ell$ - path increment over which α = const. and $\Lambda\phi$ = const.; 1 Np $\hat{=}$ 8.686 dB). The transfer function of the medium is defined by (Eq. 1 - Part 1):

$$\tau \equiv \exp\left\{-\left[A + j\,(\Upsilon_o \pm \Delta\Upsilon)\right]\right\} \quad . \qquad (58a)$$

Equation (58) is a filter function that governs the propagation of signals through the atmosphere and can, in principle, be compensated by an equalizer.

Atmospheric emissivity due to molecular attenuation is commonly expressed by a power-equivalent temperature,

$$T_A = \int_h^{\infty} W(\ell)\; T(\ell)\; d\ell, \qquad (59)$$

where the kinetic temperature structure is $T(\ell)$ and its weighting function is

$$W(\ell) = \alpha(\ell)\, \exp(-\Lambda) \quad . \qquad (59a)$$

Equation (59) represents a random noise signal that (a) determines the ultimate detection sensitivity of a receiver and (b) is basic to remote sensing atmospheric temperature structure $T(\ell)$ by radiometric means. The weighting function shows band pass behavior filtering $T(\ell)$ selectively with altitude as a function of frequency. The solution of (59) requires height profiles of pressure and temperature to

calculate $\alpha(\ell)$. At selected frequencies ν and $\nu \pm 0.1$ GHz between 59 and 50 GHz, we demonstrate in figure 31 the variability of α (and ΔN) for pressures up to 800 torr at temperatures between 200 and 300°K. The ν are those chosen in NIMBUS 5 and future TIROS N satellites for temperature soundings. The results are for the "Linear" O_2-MS model, although they may be converted to the more probably "Overlap" model using equation (57). Weighting functions have been calculated at frequencies between 50 and 67 GHz, usually for the U.S. Standard Atmosphere 62, by many workers (e.g., Meeks and Lilley, 1963; Poon, 1974; Malota and Stein, 1974).

Two simplifying assumptions can be made to make $W(\ell)$ tractable. These are

i) $p(h) = p_o \exp(-h/H)$, $\bar{H} = 0.0293\ T_a$ (59b)

(e.g., scale height $\bar{H} = 7$ km when $T_a = 239°K$);

ii) $\alpha(\nu) \doteq a(\nu)\left(\frac{p}{p_o}\right)^{x(\nu)} \left(\frac{T}{T_o}\right)^{y(\nu)}$ (59c)

(pressure and temperature exponents x, y for small variations of p and T are listed in Table 18).

The altitude range over which $W(\ell)$ is significant determines for an opaque ($\mathbf{A}_o > 3$Np) atmosphere the weighted mean temperature T_A that can be received. With the help of(59 b,c) one can calculate the parameters that govern the maximum W_m. These are (Poon, 1974)

the pressure $p_m = (x/a\bar{H})^{1/x}$, (59d)

the height $h_m = (\bar{H}/x)\ln \mathbf{A}_o$, (59e)

the attenuation $\alpha_m = x/\bar{H}$, (59f)

and the opacity $\mathbf{A}_m = 1$ [Np]. (59g)

The conditions at the peak of a weighting function are solely described by a, x, and $\bar{H}$. The values of a and x can be deduced from $\alpha(p,T)$ of which, in Tables 15 to 17, an overview is given for the three NIMBUS 5 frequencies. The reliability of those numbers is compared below with some first measurements at T = 300°K.

α[dB/km]					ν	p
Linear	(Table)	x	Overlap	Measured	[GHz]	[torr]
.925	(15)	1.40	.673	.9(2)[a]	53.647	400
.926	(16)	1.25	.854	.9(2)[a]	54.943	200
1.22	(17)	1.65	1.32	1.5(6)[a]	58.875	100
1.22	(17)	1.65	1.32	1.26(8)[b]	58.875	100

a) Poon (1974). b) This report, $\alpha(\text{AIR}) = 0.225\ \alpha\ (O_2)$ from Fig. 30.

Our direct attenuation measurements at remote sensing frequencies are scant, so far, for several reasons. First of all, these frequencies lie between line centers so that the absolute calibration is at best 10 percent since it relies on measured values of Q and β (see p. 79). Most of the effort was spent on improving the accuracy of line measurements. Other factors are the time consuming multiple tunings when the PRS frequency is changed in big steps, which may even go to a point where it becomes necessary to replace the end piece of the Fabry-Pérot resonator (Fig. 3.9 - Part 2) in order to keep the coupling ($\sim\nu^2$) in the desired 1 to 2 percent range. With some certainty now about line parameters, we will spend more effort on these important continuum measurements, preferably to be conducted in the 200 to 250°K temperature range.

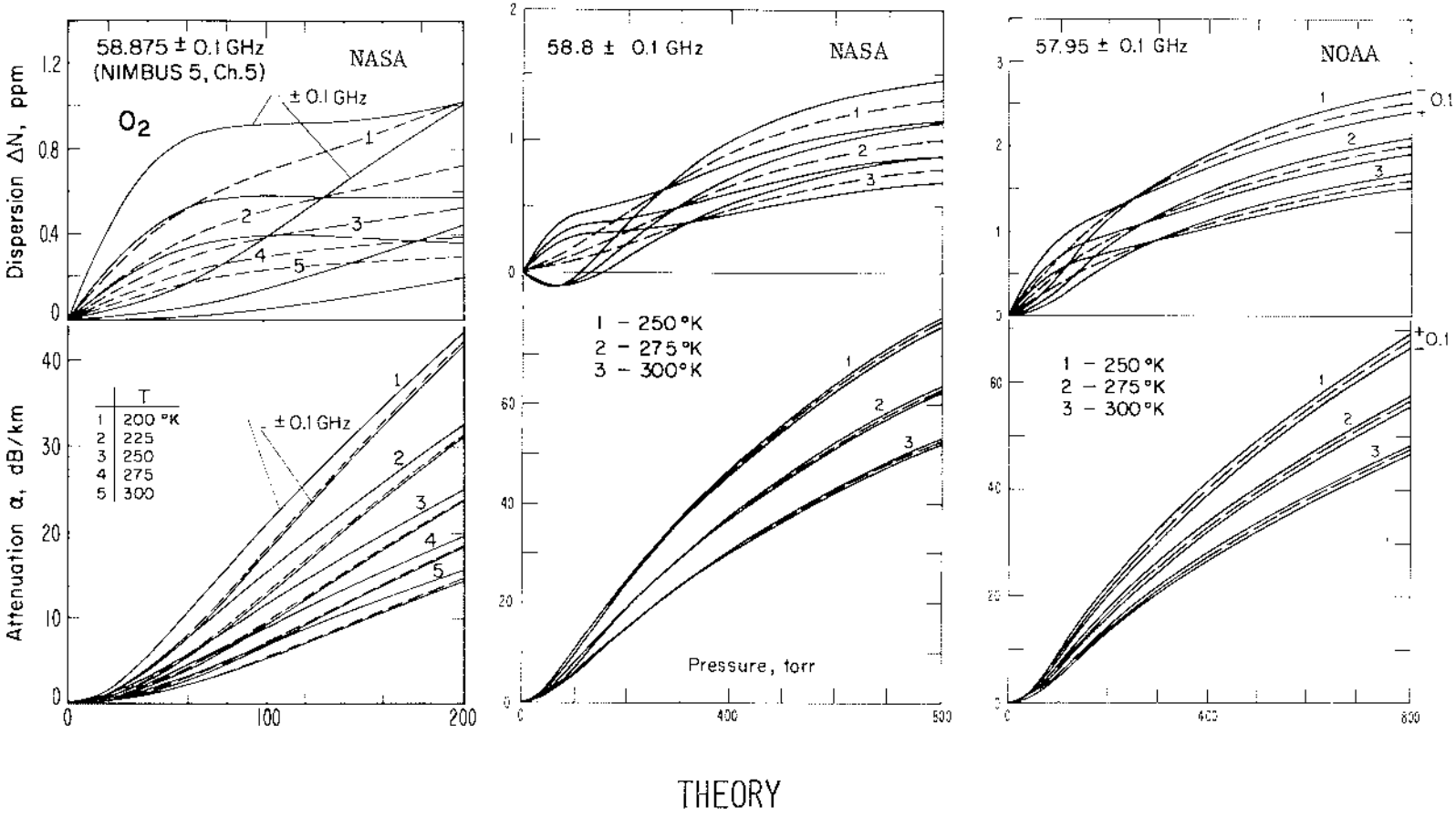

Figure 31a. Computer plot of experimental O_2-MS continuum pressure profiles at 58.875 GHz (CH. 5 - NIMBUS 5), 58.8 GHz, and 57.95 GHz (±0.1 GHz) at various temperatures and pressure ranges. For AIR multiply vertical scales by 0.225.

Linear Theory , $I_N^o = 0$.

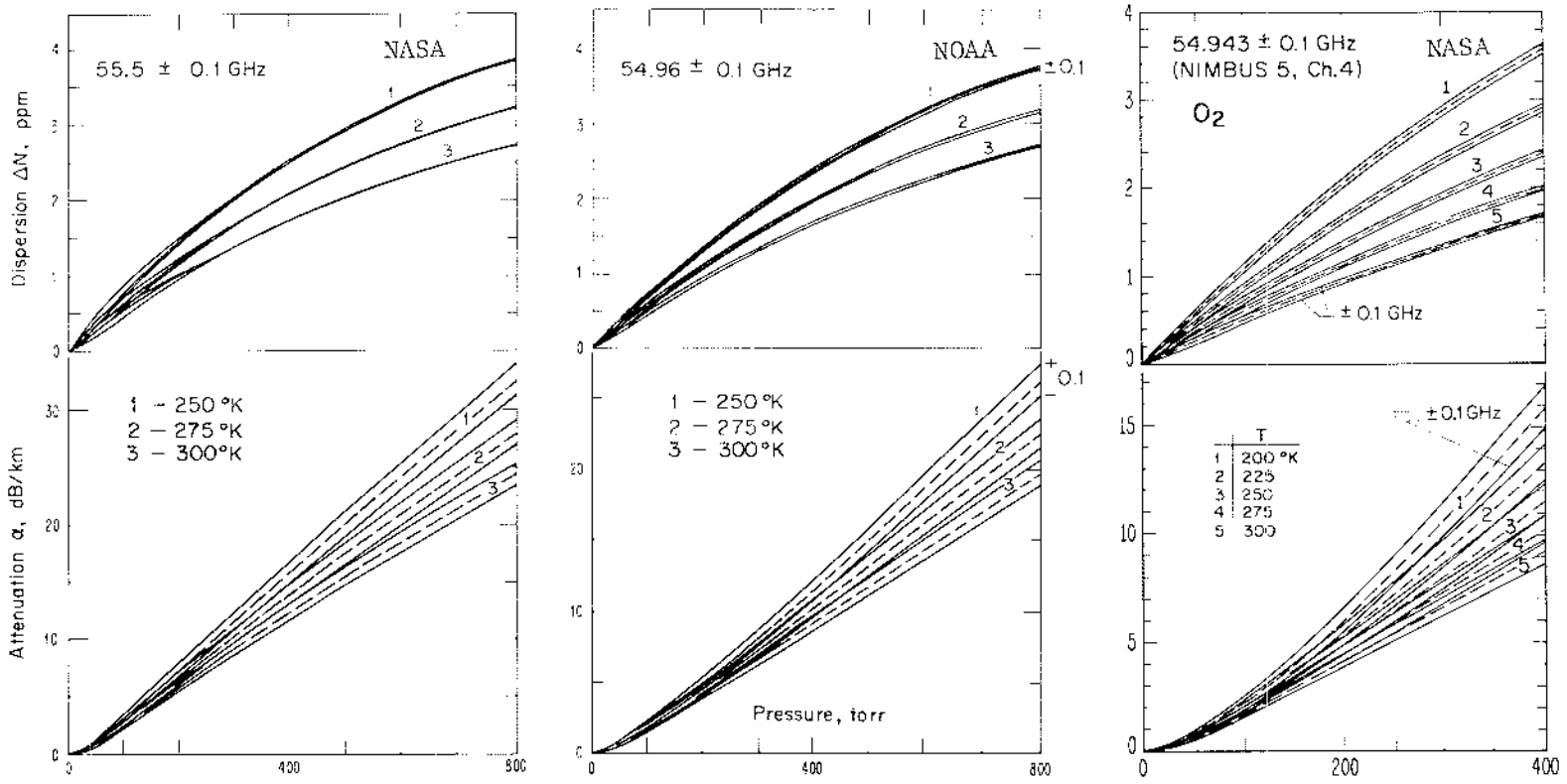

Figure 31b. Computer plots of experimental O_2-MS continuum pressure profiles at 55.5 GHz, 54.96 GHz, and 54.943 GHz (Ch. 4 - NIMBUS 5) (±0.1 GHz) at various temperatures and pressure ranges. For AIR multiply vertical scales by 0.225.

Linear Theory , $\Gamma_N^o = 0$.

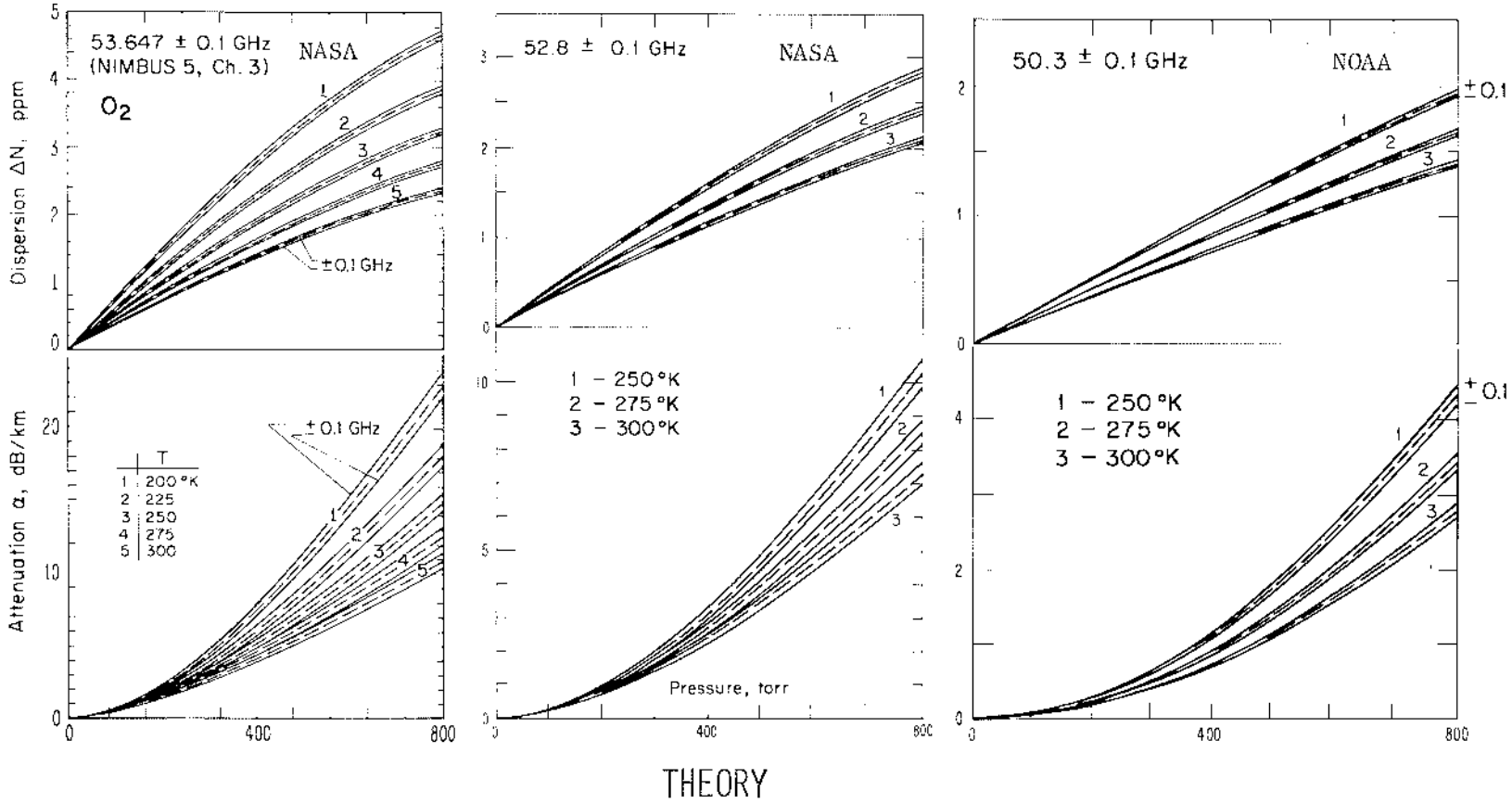

Figure 31c. Computer plots of experimental O_2-MS continuum pressure profiles at 53.647 GHz (Ch. 3 - NIMBUS 5), 52.8 GHz, and 50.3 GHz (±0.1 GHz) at various temperatures. For AIR multiply vertical scales by 0.225.

Linear Theory , $l_N^o = 0$.

Table 15. The O_2-MS Attenuation Rate in Air, α' [Np/km], for Channel 3 of NIMBUS 5.

ν = 53.647 GHz $\quad I_N^o = 0$

Pressure [torr]	200°K		225°K		250°K		275°K		300°K	
	ALPHA		ALPHA		ALPHA		ALPHA		ALPHA	
0	0.000	+000	0.000	+000	0.000	+000	0.000	+000	0.000	+000
2	3.374	-005	4.216	-005	4.930	-005	5.459	-005	5.796	-005
	1.318	-004	1.652	-004	1.937	-004	2.149	-004	2.286	-004
	2.857	-004	3.595	-004	4.233	-004	4.716	-004	5.032	-004
	4.835	-004	6.113	-004	7.238	-004	8.102	-004	8.682	-004
	7.125	-004	9.055	-004	1.078	-003	1.213	-003	1.307	-003
	9.617	-004	1.227	-003	1.470	-003	1.664	-003	1.802	-003
	1.221	-003	1.564	-003	1.884	-003	2.146	-003	2.336	-003
	1.486	-003	1.936	-003	2.308	-003	2.644	-003	2.894	-003
	1.752	-003	2.247	-003	2.732	-003	3.147	-003	3.462	-003
20	2.017	-003	2.585	-003	3.150	-003	3.645	-003	4.030	-003
	2.288	-003	2.911	-003	3.558	-003	4.133	-003	4.590	-003
	2.542	-003	3.231	-003	3.952	-003	4.606	-003	5.137	-003
	2.802	-003	3.542	-003	4.333	-003	5.062	-003	5.665	-003
	3.064	-003	3.848	-003	4.701	-003	5.501	-003	6.175	-003
	3.326	-003	4.144	-003	5.055	-003	5.923	-003	6.664	-003
	3.592	-003	4.437	-003	5.398	-003	6.327	-003	7.133	-003
	3.861	-003	4.727	-003	5.732	-003	6.716	-003	7.582	-003
	4.134	-003	5.014	-003	6.056	-003	7.092	-003	8.013	-003
	4.413	-003	5.300	-003	6.374	-003	7.454	-003	8.427	-003
40	4.698	-003	5.587	-003	6.686	-003	7.806	-003	8.826	-003
	4.990	-003	5.875	-003	6.993	-003	8.148	-003	9.211	-003
	5.289	-003	6.164	-003	7.298	-003	8.482	-003	9.583	-003
	5.596	-003	6.457	-003	7.600	-003	8.810	-003	9.944	-003
	5.911	-003	6.754	-003	7.902	-003	9.132	-003	1.029	-002
	6.234	-003	7.054	-003	8.204	-003	9.450	-003	1.064	-002
	6.567	-003	7.359	-003	8.506	-003	9.765	-003	1.097	-002
	6.909	-003	7.670	-003	8.810	-003	1.007	-002	1.130	-002
	7.260	-003	7.986	-003	9.116	-003	1.038	-002	1.163	-002
	7.620	-003	8.308	-003	9.424	-003	1.070	-002	1.195	-002
60	7.990	-003	8.636	-003	9.736	-003	1.101	-002	1.227	-002
	8.370	-003	8.971	-003	1.005	-002	1.132	-002	1.259	-002
	8.760	-003	9.313	-003	1.037	-002	1.163	-002	1.291	-002
	9.160	-003	9.661	-003	1.069	-002	1.194	-002	1.322	-002
	9.570	-003	1.001	-002	1.102	-002	1.226	-002	1.354	-002
	9.989	-003	1.038	-002	1.135	-002	1.258	-002	1.385	-002
	1.041	-002	1.075	-002	1.169	-002	1.290	-002	1.417	-002
	1.085	-002	1.112	-002	1.203	-002	1.322	-002	1.448	-002
	1.130	-002	1.151	-002	1.238	-002	1.355	-002	1.480	-002
	1.176	-002	1.190	-002	1.273	-002	1.388	-002	1.512	-002
80	1.223	-002	1.230	-002	1.309	-002	1.422	-002	1.544	-002
	1.272	-002	1.271	-002	1.345	-002	1.456	-002	1.577	-002
	1.321	-002	1.312	-002	1.382	-002	1.490	-002	1.609	-002
	1.371	-002	1.355	-002	1.420	-002	1.525	-002	1.642	-002
	1.422	-002	1.398	-002	1.458	-002	1.560	-002	1.675	-002
	1.474	-002	1.441	-002	1.497	-002	1.595	-002	1.709	-002
	1.527	-002	1.486	-002	1.536	-002	1.632	-002	1.743	-002
	1.581	-002	1.531	-002	1.576	-002	1.668	-002	1.777	-002
	1.636	-002	1.578	-002	1.617	-002	1.705	-002	1.811	-002
	1.692	-002	1.624	-002	1.658	-002	1.742	-002	1.846	-002
100	1.749	-002	1.672	-002	1.700	-002	1.780	-002	1.881	-002
	1.807	-002	1.721	-002	1.742	-002	1.819	-002	1.917	-002
	1.866	-002	1.770	-002	1.785	-002	1.857	-002	1.953	-002
	1.926	-002	1.820	-002	1.829	-002	1.897	-002	1.989	-002
	1.987	-002	1.870	-002	1.873	-002	1.936	-002	2.026	-002
	2.048	-002	1.922	-002	1.918	-002	1.977	-002	2.063	-002
	2.111	-002	1.974	-002	1.963	-002	2.018	-002	2.100	-002
	2.175	-002	2.027	-002	2.009	-002	2.059	-002	2.138	-002
	2.240	-002	2.080	-002	2.056	-002	2.100	-002	2.176	-002
	2.305	-002	2.135	-002	2.103	-002	2.143	-002	2.215	-002
120	2.372	-002	2.190	-002	2.151	-002	2.185	-002	2.254	-002
	2.440	-002	2.246	-002	2.199	-002	2.228	-002	2.293	-002
	2.508	-002	2.302	-002	2.248	-002	2.272	-002	2.333	-002
	2.577	-002	2.360	-002	2.297	-002	2.316	-002	2.373	-002
	2.648	-002	2.418	-002	2.347	-002	2.361	-002	2.414	-002
	2.719	-002	2.476	-002	2.398	-002	2.406	-002	2.455	-002
	2.791	-002	2.536	-002	2.449	-002	2.451	-002	2.496	-002
	2.864	-002	2.596	-002	2.501	-002	2.497	-002	2.538	-002
	2.938	-002	2.657	-002	2.553	-002	2.543	-002	2.580	-002
	3.013	-002	2.718	-002	2.606	-002	2.590	-002	2.622	-002

0.001

0.01

Table 15. (continued)

Pressure	200°K		225°K		250°K		275°K		300°K	
140	3.689	-002	2.780	-002	2.059	-002	2.638	-002	2.705	-002
	3.106	-002	2.843	-002	2.713	-002	2.685	-002	2.708	-002
	3.243	-002	2.907	-002	2.778	-002	2.734	-002	2.752	-002
	3.322	-002	2.971	-002	2.823	-002	2.787	-002	2.796	-002
	3.401	-002	3.036	-002	2.878	-002	2.831	-002	2.840	-002
	3.481	-002	3.102	-002	2.935	-002	2.881	-002	2.885	-002
	3.563	-002	3.168	-002	2.991	-002	2.931	-002	2.930	-002
	3.645	-002	3.235	-002	3.048	-002	2.981	-002	2.975	-002
	3.727	-002	3.302	-002	3.106	-002	3.032	-002	3.021	-002
	3.811	-002	3.371	-002	3.164	-002	3.084	-002	3.067	-002
160	3.896	-002	3.440	-002	3.223	-002	3.135	-002	3.114	-002
	3.981	-002	3.509	-002	3.282	-002	3.187	-002	3.161	-002
	4.067	-002	3.579	-002	3.342	-002	3.240	-002	3.208	-002
	4.155	-002	3.650	-002	3.402	-002	3.293	-002	3.256	-002
	4.243	-002	3.722	-002	3.463	-002	3.346	-002	3.303	-002
	4.331	-002	3.794	-002	3.524	-002	3.400	-002	3.352	-002
	4.421	-002	3.867	-002	3.586	-002	3.454	-002	3.400	-002
	4.512	-002	3.940	-002	3.648	-002	3.509	-002	3.449	-002
	4.603	-002	4.014	-002	3.711	-002	3.564	-002	3.499	-002
	4.695	-002	4.089	-002	3.775	-002	3.619	-002	3.548	-002
180	4.788	-002	4.164	-002	3.838	-002	3.675	-002	3.598	-002
	4.882	-002	4.240	-002	3.903	-002	3.731	-002	3.648	-002
	4.977	-002	4.316	-002	3.967	-002	3.788	-002	3.699	-002
	5.072	-002	4.394	-002	4.032	-002	3.845	-002	3.750	-002
	5.168	-002	4.471	-002	4.098	-002	3.902	-002	3.801	-002
	5.265	-002	4.550	-002	4.164	-002	3.960	-002	3.853	-002
	5.363	-002	4.629	-002	4.231	-002	4.018	-002	3.905	-002
	5.462	-002	4.708	-002	4.298	-002	4.076	-002	3.957	-002
	5.561	-002	4.788	-002	4.366	-002	4.135	-002	4.009	-002
	5.662	-002	4.869	-002	4.434	-002	4.194	-002	4.062	-002
200	5.763	-002	4.950	-002	4.502	-002	4.254	-002	4.115	-002
	5.865	-002	5.032	-002	4.571	-002	4.314	-002	4.169	-002
	5.967	-002	5.115	-002	4.640	-002	4.374	-002	4.222	-002
	6.071	-002	5.198	-002	4.710	-002	4.435	-002	4.276	-002
	6.175	-002	5.282	-002	4.780	-002	4.496	-002	4.331	-002
	6.280	-002	5.366	-002	4.851	-002	4.557	-002	4.385	-002
	6.385	-002	5.451	-002	4.922	-002	4.619	-002	4.440	-002
	6.492	-002	5.536	-002	4.994	-002	4.681	-002	4.495	-002
	6.599	-002	5.622	-002	5.066	-002	4.744	-002	4.551	-002
	6.707	-002	5.709	-002	5.139	-002	4.806	-002	4.606	-002
220	6.816	-002	5.795	-002	5.211	-002	4.870	-002	4.662	-002
	6.926	-002	5.883	-002	5.285	-002	4.933	-002	4.719	-002
	7.036	-002	5.972	-002	5.359	-002	4.997	-002	4.775	-002
	7.147	-002	6.060	-002	5.433	-002	5.061	-002	4.832	-002
	7.259	-002	6.150	-002	5.507	-002	5.126	-002	4.889	-002
	7.371	-002	6.240	-002	5.583	-002	5.190	-002	4.947	-002
	7.484	-002	6.330	-002	5.658	-002	5.256	-002	5.004	-002
	7.596	-002	6.421	-002	5.734	-002	5.321	-002	5.062	-002
	7.713	-002	6.513	-002	5.810	-002	5.387	-002	5.120	-002
	7.829	-002	6.605	-002	5.887	-002	5.453	-002	5.179	-002
240	7.946	-002	6.697	-002	5.964	-002	5.520	-002	5.237	-002
	8.062	-002	6.790	-002	6.042	-002	5.586	-002	5.296	-002
	8.179	-002	6.884	-002	6.120	-002	5.653	-002	5.356	-002
	8.296	-002	6.978	-002	6.198	-002	5.721	-002	5.415	-002
	8.417	-002	7.073	-002	6.277	-002	5.789	-002	5.475	-002
	8.537	-002	7.169	-002	6.356	-002	5.857	-002	5.535	-002
	8.657	-002	7.264	-002	6.436	-002	5.925	-002	5.595	-002
	8.778	-002	7.361	-002	6.516	-002	5.994	-002	5.656	-002
	8.900	-002	7.459	-002	6.596	-002	6.063	-002	5.716	-002
	9.023	-002	7.555	-002	6.677	-002	6.132	-002	5.777	-002
260	9.146	-002	7.653	-002	6.758	-002	6.202	-002	5.839	-002
	9.270	-002	7.751	-002	6.840	-002	6.272	-002	5.900	-002
	9.395	-002	7.850	-002	6.922	-002	6.342	-002	5.962	-002
	9.520	-002	7.950	-002	7.004	-002	6.412	-002	6.024	-002
	9.646	-002	8.050	-002	7.087	-002	6.483	-002	6.086	-002
	9.773	-002	8.150	-002	7.170	-002	6.554	-002	6.148	-002
	9.901	-002	8.251	-002	7.253	-002	6.626	-002	6.211	-002
	1.002	-001	8.353	-002	7.337	-002	6.697	-002	6.274	-002
	1.015	-001	8.455	-002	7.421	-002	6.769	-002	6.337	-002
	1.028	-001	8.557	-002	7.506	-002	6.842	-002	6.401	-002

0.05

Table 15. (continued)

Pressure	200°K		225°K		250°K		275°K		300°K	
280	1.041	-001	8.660	-002	7.591	-002	6.914	-002	6.464	-002
	1.054	-001	8.764	-002	7.677	-002	6.987	-002	6.528	-002
	1.067	-001	8.868	-002	7.762	-002	7.060	-002	6.592	-002
	1.081	-001	8.972	-002	7.849	-002	7.134	-002	6.656	-002
	1.094	-001	9.077	-002	7.935	-002	7.208	-002	6.721	-002
	1.107	-001	9.182	-002	8.022	-002	7.282	-002	6.786	-002
	1.121	-001	9.288	-002	8.109	-002	7.356	-002	6.850	-002
	1.134	-001	9.395	-002	8.197	-002	7.431	-002	6.916	-002
	1.148	-001	9.502	-002	8.285	-002	7.505	-002	6.981	-002
	1.161	-001	9.609	-002	8.373	-002	7.581	-002	7.047	-002
300	1.175	-001	9.717	-002	8.462	-002	7.656	-002	7.112	-002
	1.189	-001	9.825	-002	8.551	-002	7.732	-002	7.179	-002
	1.203	-001	9.934	-002	8.640	-002	7.808	-002	7.245	-002
	1.218	-001	1.004	-001	8.730	-002	7.884	-002	7.311	-002
	1.232	-001	1.015	-001	8.820	-002	7.960	-002	7.378	-002
	1.246	-001	1.026	-001	8.911	-002	8.037	-002	7.445	-002
	1.259	-001	1.037	-001	9.002	-002	8.114	-002	7.512	-002
	1.272	-001	1.048	-001	9.093	-002	8.192	-002	7.579	-002
	1.287	-001	1.059	-001	9.184	-002	8.269	-002	7.647	-002
	1.301	-001	1.070	-001	9.276	-002	8.347	-002	7.715	-002
320	1.315	-001	1.082	-001	9.368	-002	8.425	-002	7.782	-002
	1.329	-001	1.093	-001	9.461	-002	8.504	-002	7.851	-002
	1.344	-001	1.104	-001	9.554	-002	8.582	-002	7.919	-002
	1.359	-001	1.116	-001	9.647	-002	8.661	-002	7.988	-002
	1.373	-001	1.127	-001	9.741	-002	8.740	-002	8.056	-002
	1.387	-001	1.139	-001	9.835	-002	8.820	-002	8.125	-002
	1.402	-001	1.150	-001	9.929	-002	8.900	-002	8.194	-002
	1.417	-001	1.162	-001	1.002	-001	8.980	-002	8.264	-002
	1.432	-001	1.173	-001	1.011	-001	9.060	-002	8.333	-002
	1.446	-001	1.185	-001	1.021	-001	9.140	-002	8.403	-002
340	1.461	-001	1.197	-001	1.030	-001	9.221	-002	8.473	-002
	1.476	-001	1.208	-001	1.040	-001	9.302	-002	8.543	-002
	1.491	-001	1.220	-001	1.050	-001	9.383	-002	8.614	-002
	1.506	-001	1.232	-001	1.059	-001	9.465	-002	8.684	-002
	1.521	-001	1.244	-001	1.069	-001	9.546	-002	8.755	-002
	1.537	-001	1.256	-001	1.079	-001	9.628	-002	8.825	-002
	1.552	-001	1.268	-001	1.089	-001	9.710	-002	8.897	-002
	1.567	-001	1.280	-001	1.098	-001	9.793	-002	8.968	-002
	1.582	-001	1.292	-001	1.108	-001	9.876	-002	9.040	-002
	1.598	-001	1.304	-001	1.118	-001	9.959	-002	9.111	-002
360	1.613	-001	1.316	-001	1.128	-001	1.004	-001	9.183	-002
	1.629	-001	1.328	-001	1.138	-001	1.012	-001	9.255	-002
	1.644	-001	1.340	-001	1.148	-001	1.020	-001	9.327	-002
	1.660	-001	1.352	-001	1.158	-001	1.029	-001	9.400	-002
	1.676	-001	1.365	-001	1.168	-001	1.037	-001	9.472	-002
	1.691	-001	1.377	-001	1.178	-001	1.046	-001	9.545	-002
	1.707	-001	1.389	-001	1.188	-001	1.054	-001	9.618	-002
	1.723	-001	1.402	-001	1.198	-001	1.063	-001	9.691	-002
	1.739	-001	1.414	-001	1.208	-001	1.071	-001	9.765	-002
	1.755	-001	1.427	-001	1.218	-001	1.080	-001	9.838	-002
380	1.771	-001	1.439	-001	1.228	-001	1.088	-001	9.912	-002
	1.787	-001	1.452	-001	1.239	-001	1.097	-001	9.986	-002
	1.803	-001	1.464	-001	1.249	-001	1.105	-001	1.006	-001
	1.819	-001	1.477	-001	1.259	-001	1.114	-001	1.013	-001
	1.835	-001	1.490	-001	1.269	-001	1.123	-001	1.020	-001
	1.851	-001	1.502	-001	1.280	-001	1.131	-001	1.028	-001
	1.868	-001	1.515	-001	1.290	-001	1.140	-001	1.035	-001
	1.884	-001	1.528	-001	1.301	-001	1.149	-001	1.043	-001
	1.900	-001	1.541	-001	1.311	-001	1.157	-001	1.050	-001
	1.917	-001	1.554	-001	1.321	-001	1.166	-001	1.058	-001
400	1.933	-001	1.567	-001	1.332	-001	1.175	-001	1.065	-001

0.1

Table 16. The O_2-MS Attenuation Rate in Air, α' [Np/km], for Channel 4 of NIMBUS 5.

ν = 54.943 GHz $\quad T_N^O = 0$

Pressure [torr]	200°K		225°K		250°K		275°K		300°K	
	ALPHA		ALPHA		ALPHA		ALPHA		ALPHA	
0	0.000	+000	0.000	+000	0.000	+000	0.000	+000	0.000	+000
1	7.680	-006	9.185	-006	6.519	-006	5.878	-006	5.269	-006
	3.151	-005	3.873	-005	2.606	-005	2.349	-005	2.106	-005
	7.088	-005	8.463	-005	5.862	-005	5.284	-005	4.736	-005
	1.259	-004	1.498	-004	1.041	-004	9.392	-005	8.422	-005
	1.967	-004	1.793	-004	1.627	-004	1.467	-004	1.315	-004
	2.831	-004	2.581	-004	2.342	-004	2.111	-004	1.893	-004
	3.851	-004	3.512	-004	3.186	-004	2.873	-004	2.576	-004
	5.026	-004	4.584	-004	4.159	-004	3.750	-004	3.363	-004
	6.356	-004	5.797	-004	5.260	-004	4.743	-004	4.254	-004
10	7.839	-004	7.150	-004	6.489	-004	5.852	-004	5.248	-004
	9.475	-004	8.644	-004	7.845	-004	7.076	-004	6.347	-004
	1.126	-003	1.027	-003	9.328	-004	8.414	-004	7.548	-004
	1.320	-003	1.204	-003	1.093	-003	9.866	-004	8.852	-004 0.001
	1.529	-003	1.395	-003	1.267	-003	1.143	-003	1.025	-003
	1.752	-003	1.599	-003	1.452	-003	1.310	-003	1.176	-003
	1.991	-003	1.817	-003	1.650	-003	1.489	-003	1.337	-003
	2.244	-003	2.048	-003	1.861	-003	1.679	-003	1.507	-003
	2.511	-003	2.293	-003	2.083	-003	1.880	-003	1.688	-003
	2.793	-003	2.550	-003	2.318	-003	2.092	-003	1.879	-003
20	3.089	-003	2.821	-003	2.564	-003	2.315	-003	2.079	-003
	3.398	-003	3.105	-003	2.822	-003	2.549	-003	2.290	-003
	3.722	-003	3.401	-003	3.092	-003	2.793	-003	2.509	-003
	4.059	-003	3.710	-003	3.374	-003	3.048	-003	2.739	-003
	4.410	-003	4.031	-003	3.667	-003	3.314	-003	2.978	-003
	4.774	-003	4.364	-003	3.971	-003	3.589	-003	3.225	-003
	5.151	-003	4.710	-003	4.286	-003	3.876	-003	3.484	-003
	5.540	-003	5.068	-003	4.613	-003	4.171	-003	3.751	-003
	5.943	-003	5.437	-003	4.950	-003	4.478	-003	4.027	-003
	6.358	-003	5.818	-003	5.298	-003	4.794	-003	4.312	-003
30	6.785	-003	6.210	-003	5.657	-003	5.119	-003	4.606	-003
	7.225	-003	6.614	-003	6.026	-003	5.455	-003	4.909	-003
	7.676	-003	7.028	-003	6.406	-003	5.800	-003	5.221	-003
	8.139	-003	7.454	-003	6.796	-003	6.154	-003	5.542	-003
	8.613	-003	7.893	-003	7.195	-003	6.518	-003	5.871	-003
	9.099	-003	8.337	-003	7.605	-003	6.891	-003	6.208	-003
	9.596	-003	8.794	-003	8.024	-003	7.273	-003	6.554	-003
	1.010	-002	9.262	-003	8.453	-003	7.664	-003	6.907	-003
	1.062	-002	9.739	-003	8.891	-003	8.063	-003	7.269	-003
	1.115	-002	1.022	-002	9.338	-003	8.471	-003	7.639	-003
40	1.168	-002	1.072	-002	9.795	-003	8.888	-003	8.017	-003
	1.223	-002	1.122	-002	1.026	-002	5.313	-003	8.403	-003
	1.279	-002	1.174	-002	1.073	-002	9.748	-003	8.796	-003
	1.336	-002	1.226	-002	1.121	-002	1.018	-002	9.197	-003
	1.394	-002	1.280	-002	1.170	-002	1.063	-002	9.605	-003
	1.452	-002	1.334	-002	1.220	-002	1.109	-002	1.002	-002 0.01
	1.512	-002	1.389	-002	1.271	-002	1.155	-002	1.044	-002
	1.572	-002	1.445	-002	1.322	-002	1.202	-002	1.087	-002
	1.634	-002	1.501	-002	1.375	-002	1.250	-002	1.130	-002
	1.696	-002	1.559	-002	1.428	-002	1.299	-002	1.175	-002
50	1.759	-002	1.617	-002	1.481	-002	1.348	-002	1.220	-002
	1.823	-002	1.676	-002	1.536	-002	1.398	-002	1.265	-002
	1.887	-002	1.736	-002	1.591	-002	1.449	-002	1.312	-002
	1.953	-002	1.796	-002	1.647	-002	1.500	-002	1.359	-002
	2.019	-002	1.857	-002	1.703	-002	1.552	-002	1.406	-002
	2.086	-002	1.919	-002	1.761	-002	1.605	-002	1.454	-002
	2.153	-002	1.981	-002	1.818	-002	1.658	-002	1.503	-002
	2.221	-002	2.045	-002	1.877	-002	1.712	-002	1.552	-002
	2.290	-002	2.108	-002	1.936	-002	1.767	-002	1.602	-002
	2.360	-002	2.173	-002	1.996	-002	1.822	-002	1.652	-002
60	2.431	-002	2.236	-002	2.056	-002	1.877	-002	1.703	-002
	2.501	-002	2.303	-002	2.117	-002	1.933	-002	1.755	-002
	2.572	-002	2.369	-002	2.178	-002	1.990	-002	1.807	-002
	2.644	-002	2.436	-002	2.240	-002	2.047	-002	1.859	-002
	2.717	-002	2.503	-002	2.302	-002	2.104	-002	1.912	-002
	2.790	-002	2.571	-002	2.365	-002	2.163	-002	1.966	-002
	2.864	-002	2.639	-002	2.428	-002	2.222	-002	2.020	-002
	2.938	-002	2.708	-002	2.492	-002	2.281	-002	2.074	-002
	3.013	-002	2.777	-002	2.557	-002	2.340	-002	2.129	-002
	3.089	-002	2.847	-002	2.621	-002	2.400	-002	2.184	-002

Table 16. (Continued)

Pressure	200°K		225°K		250°K		275°K		300°K	
70	3.165	-002	2.917	-002	2.687	-002	2.461	-002	2.248	-002
	3.241	-002	2.987	-002	2.752	-002	2.522	-002	2.296	-002
	3.318	-002	3.058	-002	2.818	-002	2.583	-002	2.353	-002
	3.395	-002	3.130	-002	2.885	-002	2.645	-002	2.410	-002
	3.473	-002	3.203	-002	2.952	-002	2.707	-002	2.467	-002
	3.552	-002	3.274	-002	3.019	-002	2.769	-002	2.525	-002
	3.630	-002	3.347	-002	3.087	-002	2.832	-002	2.583	-002
	3.710	-002	3.420	-002	3.154	-002	2.895	-002	2.641	-002
	3.789	-002	3.493	-002	3.223	-002	2.959	-002	2.700	-002
	3.869	-002	3.567	-002	3.291	-002	3.022	-002	2.759	-002
80	3.950	-002	3.641	-002	3.360	-002	3.087	-002	2.818	-002
	4.031	-002	3.715	-002	3.430	-002	3.151	-002	2.878	-002
	4.112	-002	3.790	-002	3.499	-002	3.216	-002	2.938	-002
	4.194	-002	3.865	-002	3.569	-002	3.281	-002	2.998	-002
	4.276	-002	3.940	-002	3.639	-002	3.346	-002	3.059	-002
	4.358	-002	4.016	-002	3.710	-002	3.412	-002	3.120	-002
	4.441	-002	4.092	-002	3.780	-002	3.478	-002	3.181	-002
	4.524	-002	4.168	-002	3.851	-002	3.544	-002	3.242	-002
	4.608	-002	4.245	-002	3.922	-002	3.610	-002	3.304	-002
	4.692	-002	4.322	-002	3.994	-002	3.677	-002	3.366	-002
90	4.776	-002	4.399	-002	4.065	-002	3.743	-002	3.428	-002
	4.861	-002	4.476	-002	4.137	-002	3.810	-002	3.490	-002
	4.945	-002	4.554	-002	4.209	-002	3.878	-002	3.553	-002
	5.031	-002	4.632	-002	4.282	-002	3.945	-002	3.615	-002
	5.116	-002	4.710	-002	4.354	-002	4.013	-002	3.678	-002
	5.202	-002	4.788	-002	4.427	-002	4.081	-002	3.742	-002
	5.288	-002	4.866	-002	4.500	-002	4.149	-002	3.805	-002
	5.375	-002	4.945	-002	4.573	-002	4.217	-002	3.868	-002
	5.462	-002	5.024	-002	4.646	-002	4.285	-002	3.932	-002
	5.549	-002	5.103	-002	4.720	-002	4.354	-002	3.996	-002
100	5.636	-002	5.183	-002	4.793	-002	4.422	-002	4.060	-002
	5.724	-002	5.262	-002	4.867	-002	4.491	-002	4.124	-002
	5.812	-002	5.342	-002	4.941	-002	4.560	-002	4.188	-002
	5.900	-002	5.422	-002	5.015	-002	4.629	-002	4.253	-002
	5.989	-002	5.502	-002	5.089	-002	4.698	-002	4.317	-002
	6.078	-002	5.582	-002	5.164	-002	4.768	-002	4.382	-002
	6.167	-002	5.663	-002	5.238	-002	4.837	-002	4.447	-002
	6.256	-002	5.744	-002	5.313	-002	4.907	-002	4.512	-002
	6.346	-002	5.824	-002	5.387	-002	4.977	-002	4.577	-002
	6.436	-002	5.906	-002	5.462	-002	5.046	-002	4.642	-002
110	6.526	-002	5.987	-002	5.537	-002	5.116	-002	4.707	-002
	6.617	-002	6.068	-002	5.612	-002	5.186	-002	4.773	-002
	6.708	-002	6.150	-002	5.688	-002	5.256	-002	4.838	-002
	6.799	-002	6.231	-002	5.763	-002	5.327	-002	4.904	-002
	6.890	-002	6.313	-002	5.838	-002	5.397	-002	4.969	-002
	6.982	-002	6.395	-002	5.914	-002	5.467	-002	5.035	-002
	7.073	-002	6.477	-002	5.990	-002	5.538	-002	5.101	-002
	7.165	-002	6.560	-002	6.065	-002	5.608	-002	5.167	-002
	7.258	-002	6.642	-002	6.141	-002	5.679	-002	5.233	-002
	7.351	-002	6.725	-002	6.217	-002	5.749	-002	5.299	-002
120	7.443	-002	6.808	-002	6.293	-002	5.820	-002	5.365	-002
	7.537	-002	6.891	-002	6.369	-002	5.891	-002	5.431	-002
	7.630	-002	6.974	-002	6.445	-002	5.962	-002	5.497	-002
	7.724	-002	7.057	-002	6.522	-002	6.033	-002	5.563	-002
	7.817	-002	7.140	-002	6.598	-002	6.104	-002	5.629	-002
	7.912	-002	7.224	-002	6.674	-002	6.175	-002	5.696	-002
	8.006	-002	7.307	-002	6.751	-002	6.246	-002	5.762	-002
	8.101	-002	7.391	-002	6.827	-002	6.317	-002	5.828	-002
	8.196	-002	7.475	-002	6.904	-002	6.388	-002	5.895	-002
	8.291	-002	7.559	-002	6.981	-002	6.459	-002	5.961	-002
130	8.386	-002	7.643	-002	7.057	-002	6.530	-002	6.028	-002
	8.482	-002	7.727	-002	7.134	-002	6.601	-002	6.094	-002
	8.578	-002	7.812	-002	7.211	-002	6.673	-002	6.161	-002
	8.674	-002	7.896	-002	7.288	-002	6.744	-002	6.227	-002
	8.770	-002	7.981	-002	7.365	-002	6.815	-002	6.294	-002
	8.867	-002	8.066	-002	7.442	-002	6.887	-002	6.360	-002
	8.964	-002	8.151	-002	7.520	-002	6.958	-002	6.427	-002
	9.061	-002	8.236	-002	7.597	-002	7.029	-002	6.494	-002
	9.158	-002	8.321	-002	7.674	-002	7.101	-002	6.560	-002
	9.256	-002	8.407	-002	7.751	-002	7.172	-002	6.627	-002

0.05

Table 16. (Continued)

Pressure	200°K		225°K		250°K		275°K		300°K	
140	9.35	-002	8.492	-002	7.625	-002	7.244	-002	6.693	-002
	9.45	-002	8.578	-002	7.906	-002	7.315	-002	6.760	-002
	9.55	-002	8.663	-002	7.984	-002	7.387	-002	6.827	-002
	9.64	-002	8.749	-002	8.061	-002	7.458	-002	6.893	-002
	9.74	-002	8.835	-002	8.139	-002	7.530	-002	6.960	-002
	9.841	-002	8.921	-002	8.217	-002	7.602	-002	7.026	-002
	9.945	-002	9.007	-002	8.294	-002	7.673	-002	7.093	-002
	1.004	-001	9.094	-002	8.372	-002	7.745	-002	7.160	-002
	1.014	-001	9.180	-002	8.450	-002	7.816	-002	7.226	-002
	1.024	-001	9.267	-002	8.528	-002	7.888	-002	7.293	-002
150	1.034	-001	9.354	-002	8.606	-002	7.960	-002	7.360	-002
	1.044	-001	9.440	-002	8.684	-002	8.031	-002	7.426	-002
	1.054	-001	9.527	-002	8.762	-002	8.103	-002	7.493	-002
	1.064	-001	9.614	-002	8.840	-002	8.175	-002	7.559	-002
	1.074	-001	9.702	-002	8.918	-002	8.247	-002	7.626	-002
	1.084	-001	9.789	-002	8.997	-002	8.318	-002	7.693	-002
	1.095	-001	9.876	-002	9.075	-002	8.390	-002	7.759	-002
	1.105	-001	9.964	-002	9.153	-002	8.462	-002	7.826	-002
	1.115	-001	1.005	-001	9.232	-002	8.533	-002	7.892	-002
	1.125	-001	1.013	-001	9.310	-002	8.605	-002	7.959	-002
160	1.136	-001	1.022	-001	9.388	-002	8.677	-002	8.025	-002
	1.146	-001	1.031	-001	9.467	-002	8.748	-002	8.092	-002
	1.156	-001	1.040	-001	9.546	-002	8.821	-002	8.158	-002
	1.166	-001	1.049	-001	9.624	-002	8.892	-002	8.225	-002
	1.177	-001	1.058	-001	9.703	-002	8.964	-002	8.291	-002
	1.187	-001	1.066	-001	9.782	-002	9.036	-002	8.357	-002
	1.198	-001	1.075	-001	9.860	-002	9.108	-002	8.424	-002
	1.208	-001	1.084	-001	9.939	-002	9.180	-002	8.490	-002
	1.218	-001	1.093	-001	1.001	-001	9.251	-002	8.557	-002
	1.229	-001	1.102	-001	1.009	-001	9.323	-002	8.623	-002
170	1.239	-001	1.111	-001	1.017	-001	9.395	-002	8.689	-002
	1.250	-001	1.120	-001	1.025	-001	9.467	-002	8.756	-002
	1.260	-001	1.129	-001	1.033	-001	9.539	-002	8.822	-002
	1.271	-001	1.138	-001	1.041	-001	9.611	-002	8.888	-002
	1.281	-001	1.147	-001	1.049	-001	9.683	-002	8.955	-002
	1.292	-001	1.156	-001	1.057	-001	9.754	-002	9.021	-002
	1.303	-001	1.165	-001	1.065	-001	9.826	-002	9.087	-002
	1.313	-001	1.174	-001	1.073	-001	9.898	-002	9.153	-002
	1.324	-001	1.183	-001	1.081	-001	9.970	-002	9.219	-002
	1.335	-001	1.192	-001	1.089	-001	1.004	-001	9.286	-002
180	1.345	-001	1.201	-001	1.096	-001	1.011	-001	9.352	-002
	1.356	-001	1.210	-001	1.104	-001	1.018	-001	9.418	-002
	1.367	-001	1.219	-001	1.112	-001	1.025	-001	9.484	-002
	1.378	-001	1.228	-001	1.120	-001	1.033	-001	9.550	-002
	1.388	-001	1.237	-001	1.128	-001	1.040	-001	9.616	-002
	1.399	-001	1.246	-001	1.136	-001	1.047	-001	9.682	-002
	1.410	-001	1.255	-001	1.144	-001	1.054	-001	9.748	-002
	1.421	-001	1.264	-001	1.152	-001	1.061	-001	9.815	-002
	1.432	-001	1.274	-001	1.160	-001	1.069	-001	9.881	-002
	1.443	-001	1.283	-001	1.168	-001	1.076	-001	9.947	-002
190	1.454	-001	1.292	-001	1.176	-001	1.083	-001	1.001	-001
	1.465	-001	1.301	-001	1.184	-001	1.090	-001	1.007	-001
	1.476	-001	1.310	-001	1.192	-001	1.097	-001	1.014	-001
	1.487	-001	1.319	-001	1.200	-001	1.105	-001	1.021	-001
	1.498	-001	1.329	-001	1.208	-001	1.112	-001	1.027	-001
	1.509	-001	1.338	-001	1.217	-001	1.119	-001	1.034	-001
	1.520	-001	1.347	-001	1.225	-001	1.126	-001	1.040	-001
	1.531	-001	1.356	-001	1.233	-001	1.133	-001	1.047	-001
	1.542	-001	1.366	-001	1.241	-001	1.141	-001	1.054	-001
	1.553	-001	1.375	-001	1.249	-001	1.148	-001	1.060	-001
200	1.564	-001	1.384	-001	1.257	-001	1.155	-001	1.067	-001

0.1

Table 17. The O_2-MS Attenuation Rate in Air, α' [Np/km], for Channel 5 of NIMBUS 5.

ν = 58.875 GHz $\quad I_N^o = 0$

Pressure [torr]	200°K	225°K	250°K	275°K	300°K
0	ALPHA	ALPHA	ALPHA	ALPHA	ALPHA
	0.0000000+000	0.0000000+000	0.0000000+000	0.0000000+000	0.0000000+000
.5	1.715 -005	1.158 -005	8.117 -006	5.643 -006	4.345 -006
	6.855 -005	4.629 -005	3.242 -005	2.341 -005	1.734 -005
	1.542 -004	1.041 -004	7.294 -005	5.267 -005	3.901 -005
	2.741 -004	1.851 -004	1.296 -004	9.362 -005	6.935 -005
	4.282 -004	2.892 -004	2.025 -004	1.462 -004	1.083 -004
	6.166 -004	4.164 -004	2.916 -004	2.106 -004	1.560 -004
	8.391 -004	5.667 -004	3.969 -004	2.866 -004	2.123 -004
	1.095 -003	7.400 -004	5.184 -004	3.743 -004	2.773 -004
5	1.386 -003	9.364 -004	6.560 -004	4.737 -004	3.509 -004
	1.711 -003	1.155 -003	8.097 -004	5.847 -004	4.331 -004
	2.070 -003	1.398 -003	9.796 -004	7.074 -004	5.240 -004
	2.463 -003	1.663 -003	1.165 -003	8.417 -004	6.236 -004
	2.889 -003	1.952 -003	1.367 -003	9.877 -004	7.317 -004
	3.350 -003	2.263 -003	1.585 -003	1.145 -003	8.485 -004
	3.844 -003	2.597 -003	1.819 -003	1.314 -003	9.738 -004
	4.372 -003	2.954 -003	2.070 -003	1.495 -003	1.107 -003
	4.934 -003	3.333 -003	2.338 -003	1.687 -003	1.250 -003
	5.529 -003	3.736 -003	2.618 -003	1.891 -003	1.401 -003
	6.157 -003	4.161 -003	2.916 -003	2.106 -003	1.561 -003
10	6.819 -003	4.609 -003	3.230 -003	2.333 -003	1.729 -003
	7.514 -003	5.079 -003	3.566 -003	2.572 -003	1.906 -003
	8.242 -003	5.572 -003	3.906 -003	2.822 -003	2.091 -003
	9.003 -003	6.087 -003	4.267 -003	3.083 -003	2.285 -003
	9.797 -003	6.625 -003	4.645 -003	3.356 -003	2.487 -003
	1.062 -002	7.184 -003	5.038 -003	3.640 -003	2.698 -003
	1.146 -002	7.767 -003	5.446 -003	3.936 -003	2.917 -003
	1.237 -002	8.371 -003	5.871 -003	4.243 -003	3.145 -003
	1.330 -002	8.997 -003	6.311 -003	4.561 -003	3.381 -003
	1.425 -002	9.646 -003	6.766 -003	4.891 -003	3.626 -003
15	1.524 -002	1.031 -002	7.237 -003	5.231 -003	3.879 -003
	1.626 -002	1.100 -002	7.724 -003	5.584 -003	4.140 -003
	1.731 -002	1.172 -002	8.226 -003	5.947 -003	4.410 -003
	1.840 -002	1.246 -002	8.743 -003	6.321 -003	4.688 -003
	1.951 -002	1.321 -002	9.275 -003	6.707 -003	4.974 -003
	2.066 -002	1.399 -002	9.823 -003	7.104 -003	5.269 -003
	2.184 -002	1.479 -002	1.038 -002	7.512 -003	5.572 -003
	2.305 -002	1.561 -002	1.096 -002	7.931 -003	5.883 -003
	2.429 -002	1.646 -002	1.155 -002	8.361 -003	6.202 -003
	2.556 -002	1.732 -002	1.216 -002	8.802 -003	6.530 -003
20	2.686 -002	1.820 -002	1.279 -002	9.254 -003	6.866 -003
	2.819 -002	1.911 -002	1.342 -002	9.717 -003	7.210 -003
	2.955 -002	2.004 -002	1.408 -002	1.019 -002	7.562 -003
	3.095 -002	2.099 -002	1.474 -002	1.067 -002	7.922 -003
	3.237 -002	2.195 -002	1.543 -002	1.117 -002	8.290 -003
	3.382 -002	2.294 -002	1.612 -002	1.167 -002	8.667 -003
	3.530 -002	2.395 -002	1.684 -002	1.219 -002	9.051 -003
	3.681 -002	2.498 -002	1.756 -002	1.272 -002	9.444 -003
	3.835 -002	2.603 -002	1.830 -002	1.325 -002	9.844 -003
	3.991 -002	2.710 -002	1.906 -002	1.380 -002	1.025 -002
25	4.151 -002	2.819 -002	1.983 -002	1.436 -002	1.066 -002
	4.313 -002	2.930 -002	2.061 -002	1.493 -002	1.109 -002
	4.478 -002	3.043 -002	2.141 -002	1.551 -002	1.152 -002
	4.646 -002	3.158 -002	2.222 -002	1.610 -002	1.196 -002
	4.817 -002	3.274 -002	2.305 -002	1.670 -002	1.241 -002
	4.991 -002	3.393 -002	2.389 -002	1.731 -002	1.286 -002
	5.167 -002	3.514 -002	2.474 -002	1.794 -002	1.333 -002
	5.346 -002	3.636 -002	2.561 -002	1.857 -002	1.380 -002
	5.527 -002	3.761 -002	2.649 -002	1.921 -002	1.428 -002
	5.711 -002	3.887 -002	2.739 -002	1.986 -002	1.476 -002
30	5.898 -002	4.015 -002	2.829 -002	2.052 -002	1.526 -002
	6.088 -002	4.145 -002	2.922 -002	2.119 -002	1.576 -002
	6.280 -002	4.277 -002	3.015 -002	2.188 -002	1.627 -002
	6.474 -002	4.411 -002	3.110 -002	2.257 -002	1.678 -002
	6.671 -002	4.546 -002	3.206 -002	2.327 -002	1.731 -002
	6.871 -002	4.683 -002	3.304 -002	2.398 -002	1.784 -002
	7.073 -002	4.823 -002	3.402 -002	2.470 -002	1.838 -002
	7.277 -002	4.963 -002	3.502 -002	2.543 -002	1.892 -002
	7.484 -002	5.106 -002	3.604 -002	2.617 -002	1.948 -002
	7.694 -002	5.250 -002	3.706 -002	2.692 -002	2.004 -002

0.001

0.01

0.05

Table 17. (Continued)

Pressure	200°K		225°K		250°K		275°K		300°K	
35	7.905	-002	5.496	-002	3.810	-002	2.768	-002	2.060	-002
	8.119	-002	5.644	-002	3.916	-002	2.845	-002	2.118	-002
	8.336	-002	5.793	-002	4.023	-002	2.923	-002	2.178	-002
	8.554	-002	5.944	-002	4.130	-002	3.002	-002	2.239	-002
	8.775	-002	6.097	-002	4.238	-002	3.081	-002	2.299	-002
	8.999	-002	6.252	-002	4.349	-002	3.162	-002	2.359	-002
	9.224	-002	6.408	-002	4.460	-002	3.244	-002	2.416	-002
	9.452	-002	6.566	-002	4.572	-002	3.326	-002	2.478	-002
	9.682	-002	6.725	-002	4.686	-002	3.409	-002	2.540	-002
	9.914	-002	6.885	-002	4.801	-002	3.494	-002	2.604	-002
40	1.014	-001	6.948	-002	4.917	-002	3.579	-002	2.667	-002
	1.038	-001	7.112	-002	5.034	-002	3.665	-002	2.732	-002
	1.062	-001	7.277	-002	5.153	-002	3.752	-002	2.797	-002
	1.086	-001	7.444	-002	5.272	-002	3.839	-002	2.863	-002
	1.110	-001	7.613	-002	5.393	-002	3.928	-002	2.930	-002
	1.135	-001	7.783	-002	5.515	-002	4.017	-002	2.997	-002
	1.159	-001	7.954	-002	5.638	-002	4.108	-002	3.065	-002
	1.184	-001	8.127	-002	5.762	-002	4.199	-002	3.133	-002
	1.209	-001	8.302	-002	5.887	-002	4.291	-002	3.202	-002
	1.234	-001	8.478	-002	6.013	-002	4.384	-002	3.272	-002
45	1.260	-001	8.655	-002	6.140	-002	4.478	-002	3.343	-002
	1.285	-001	8.834	-002	6.269	-002	4.572	-002	3.414	-002
	1.311	-001	9.014	-002	6.398	-002	4.668	-002	3.486	-002
	1.337	-001	9.195	-002	6.529	-002	4.764	-002	3.558	-002
	1.363	-001	9.378	-002	6.660	-002	4.861	-002	3.631	-002
	1.389	-001	9.562	-002	6.793	-002	4.958	-002	3.705	-002
	1.416	-001	9.748	-002	6.926	-002	5.057	-002	3.779	-002
	1.443	-001	9.934	-002	7.061	-002	5.156	-002	3.854	-002
	1.469	-001	1.012	-001	7.197	-002	5.256	-002	3.929	-002
	1.496	-001	1.031	-001	7.333	-002	5.357	-002	4.005	-002
50	1.523	-001	1.050	-001	7.471	-002	5.459	-002	4.082	-002
	1.551	-001	1.069	-001	7.609	-002	5.561	-002	4.159	-002
	1.578	-001	1.088	-001	7.749	-002	5.665	-002	4.237	-002
	1.606	-001	1.108	-001	7.889	-002	5.768	-002	4.316	-002
	1.634	-001	1.127	-001	8.031	-002	5.873	-002	4.395	-002
	1.661	-001	1.147	-001	8.173	-002	5.978	-002	4.474	-002
	1.690	-001	1.167	-001	8.316	-002	6.085	-002	4.555	-002
	1.718	-001	1.187	-001	8.460	-002	6.191	-002	4.635	-002
	1.746	-001	1.207	-001	8.605	-002	6.299	-002	4.717	-002
	1.775	-001	1.227	-001	8.751	-002	6.407	-002	4.799	-002
55	1.803	-001	1.247	-001	8.898	-002	6.516	-002	4.881	-002
	1.832	-001	1.267	-001	9.046	-002	6.626	-002	4.964	-002
	1.861	-001	1.288	-001	9.194	-002	6.736	-002	5.048	-002
	1.890	-001	1.308	-001	9.344	-002	6.847	-002	5.132	-002
	1.919	-001	1.329	-001	9.494	-002	6.959	-002	5.217	-002
	1.948	-001	1.350	-001	9.645	-002	7.071	-002	5.302	-002
	1.978	-001	1.371	-001	9.797	-002	7.184	-002	5.388	-002
	2.007	-001	1.392	-001	9.950	-002	7.298	-002	5.474	-002
	2.037	-001	1.413	-001	1.010	-001	7.412	-002	5.561	-002
	2.067	-001	1.434	-001	1.025	-001	7.527	-002	5.648	-002
60	2.097	-001	1.455	-001	1.041	-001	7.643	-002	5.736	-002
	2.127	-001	1.477	-001	1.056	-001	7.759	-002	5.824	-002
	2.157	-001	1.498	-001	1.072	-001	7.876	-002	5.913	-002
	2.187	-001	1.520	-001	1.088	-001	7.993	-002	6.002	-002
	2.217	-001	1.541	-001	1.104	-001	8.111	-002	6.092	-002
	2.248	-001	1.563	-001	1.120	-001	8.230	-002	6.182	-002
	2.278	-001	1.585	-001	1.135	-001	8.349	-002	6.273	-002
	2.309	-001	1.607	-001	1.152	-001	8.469	-002	6.364	-002
	2.340	-001	1.629	-001	1.168	-001	8.590	-002	6.456	-002
	2.371	-001	1.651	-001	1.184	-001	8.711	-002	6.548	-002
65	2.402	-001	1.673	-001	1.200	-001	8.832	-002	6.641	-002
	2.433	-001	1.695	-001	1.216	-001	8.954	-002	6.734	-002
	2.464	-001	1.717	-001	1.233	-001	9.077	-002	6.828	-002
	2.495	-001	1.740	-001	1.249	-001	9.200	-002	6.922	-002
	2.526	-001	1.762	-001	1.266	-001	9.324	-002	7.017	-002
	2.558	-001	1.785	-001	1.282	-001	9.449	-002	7.112	-002
	2.589	-001	1.808	-001	1.299	-001	9.574	-002	7.207	-002
	2.621	-001	1.830	-001	1.316	-001	9.699	-002	7.303	-002
	2.652	-001	1.853	-001	1.332	-001	9.825	-002	7.399	-002
	2.684	-001	1.876	-001	1.349	-001	9.951	-002	7.496	-002

0.05

0.1

Table 17. (Continued)

Pressure	200°K		225°K		250°K		275°K		300°K	
70	2.716	-001	1.899	-001	1.366	-001	1.007	-001	7.593	-002
	2.748	-001	1.922	-001	1.383	-001	1.020	-001	7.691	-002
	2.780	-001	1.945	-001	1.400	-001	1.033	-001	7.789	-002
	2.812	-001	1.968	-001	1.417	-001	1.046	-001	7.887	-002
	2.844	-001	1.991	-001	1.434	-001	1.059	-001	7.986	-002
	2.876	-001	2.014	-001	1.451	-001	1.072	-001	8.085	-002
	2.908	-001	2.038	-001	1.469	-001	1.085	-001	8.185	-002
	2.940	-001	2.061	-001	1.486	-001	1.098	-001	8.285	-002
	2.973	-001	2.084	-001	1.503	-001	1.111	-001	8.385	-002
75	3.005	-001	2.108	-001	1.521	-001	1.124	-001	8.486	-002
	3.037	-001	2.132	-001	1.538	-001	1.137	-001	8.587	-002
	3.070	-001	2.155	-001	1.556	-001	1.150	-001	8.688	-002
	3.103	-001	2.179	-001	1.573	-001	1.164	-001	8.791	-002
	3.135	-001	2.203	-001	1.591	-001	1.177	-001	8.893	-002
	3.168	-001	2.226	-001	1.608	-001	1.190	-001	8.996	-002
	3.201	-001	2.250	-001	1.626	-001	1.204	-001	9.099	-002
	3.233	-001	2.274	-001	1.644	-001	1.217	-001	9.202	-002
	3.266	-001	2.298	-001	1.662	-001	1.230	-001	9.306	-002
	3.299	-001	2.322	-001	1.680	-001	1.244	-001	9.410	-002
	3.332	-001	2.346	-001	1.697	-001	1.258	-001	9.514	-002
80	3.365	-001	2.370	-001	1.715	-001	1.271	-001	9.619	-002
	3.398	-001	2.394	-001	1.733	-001	1.285	-001	9.724	-002
	3.431	-001	2.418	-001	1.751	-001	1.298	-001	9.830	-002
	3.464	-001	2.442	-001	1.769	-001	1.312	-001	9.936	-002
	3.497	-001	2.467	-001	1.787	-001	1.326	-001	1.004	-001
	3.530	-001	2.491	-001	1.806	-001	1.340	-001	1.014	-001
	3.564	-001	2.515	-001	1.824	-001	1.353	-001	1.025	-001
	3.597	-001	2.540	-001	1.842	-001	1.367	-001	1.036	-001
	3.630	-001	2.564	-001	1.860	-001	1.381	-001	1.046	-001
	3.663	-001	2.588	-001	1.879	-001	1.395	-001	1.057	-001
85	3.697	-001	2.613	-001	1.897	-001	1.409	-001	1.068	-001
	3.730	-001	2.637	-001	1.915	-001	1.423	-001	1.079	-001
	3.763	-001	2.662	-001	1.934	-001	1.437	-001	1.090	-001
	3.797	-001	2.687	-001	1.952	-001	1.451	-001	1.101	-001
	3.830	-001	2.711	-001	1.971	-001	1.465	-001	1.112	-001
	3.864	-001	2.736	-001	1.989	-001	1.479	-001	1.122	-001
	3.897	-001	2.761	-001	2.008	-001	1.494	-001	1.133	-001
	3.931	-001	2.785	-001	2.026	-001	1.508	-001	1.144	-001
	3.964	-001	2.810	-001	2.045	-001	1.522	-001	1.156	-001
	3.998	-001	2.835	-001	2.063	-001	1.536	-001	1.167	-001
90	4.031	-001	2.860	-001	2.082	-001	1.550	-001	1.178	-001
	4.065	-001	2.884	-001	2.101	-001	1.565	-001	1.189	-001
	4.099	-001	2.909	-001	2.119	-001	1.579	-001	1.200	-001
	4.132	-001	2.934	-001	2.138	-001	1.593	-001	1.211	-001
	4.166	-001	2.959	-001	2.157	-001	1.608	-001	1.222	-001
	4.199	-001	2.984	-001	2.176	-001	1.622	-001	1.233	-001
	4.233	-001	3.009	-001	2.195	-001	1.637	-001	1.245	-001
	4.267	-001	3.034	-001	2.213	-001	1.651	-001	1.256	-001
	4.300	-001	3.059	-001	2.232	-001	1.666	-001	1.267	-001
	4.334	-001	3.084	-001	2.251	-001	1.680	-001	1.279	-001
95	4.368	-001	3.109	-001	2.270	-001	1.695	-001	1.290	-001
	4.402	-001	3.134	-001	2.289	-001	1.709	-001	1.301	-001
	4.436	-001	3.159	-001	2.308	-001	1.724	-001	1.313	-001
	4.469	-001	3.184	-001	2.327	-001	1.738	-001	1.324	-001
	4.503	-001	3.209	-001	2.346	-001	1.753	-001	1.335	-001
	4.536	-001	3.234	-001	2.365	-001	1.768	-001	1.347	-001
	4.570	-001	3.260	-001	2.384	-001	1.782	-001	1.358	-001
	4.604	-001	3.285	-001	2.403	-001	1.797	-001	1.370	-001
	4.638	-001	3.310	-001	2.422	-001	1.812	-001	1.381	-001
	4.671	-001	3.335	-001	2.441	-001	1.827	-001	1.393	-001
100	4.705	-001	3.360	-001	2.461	-001	1.841	-001	1.404	-001

0.1

0.2

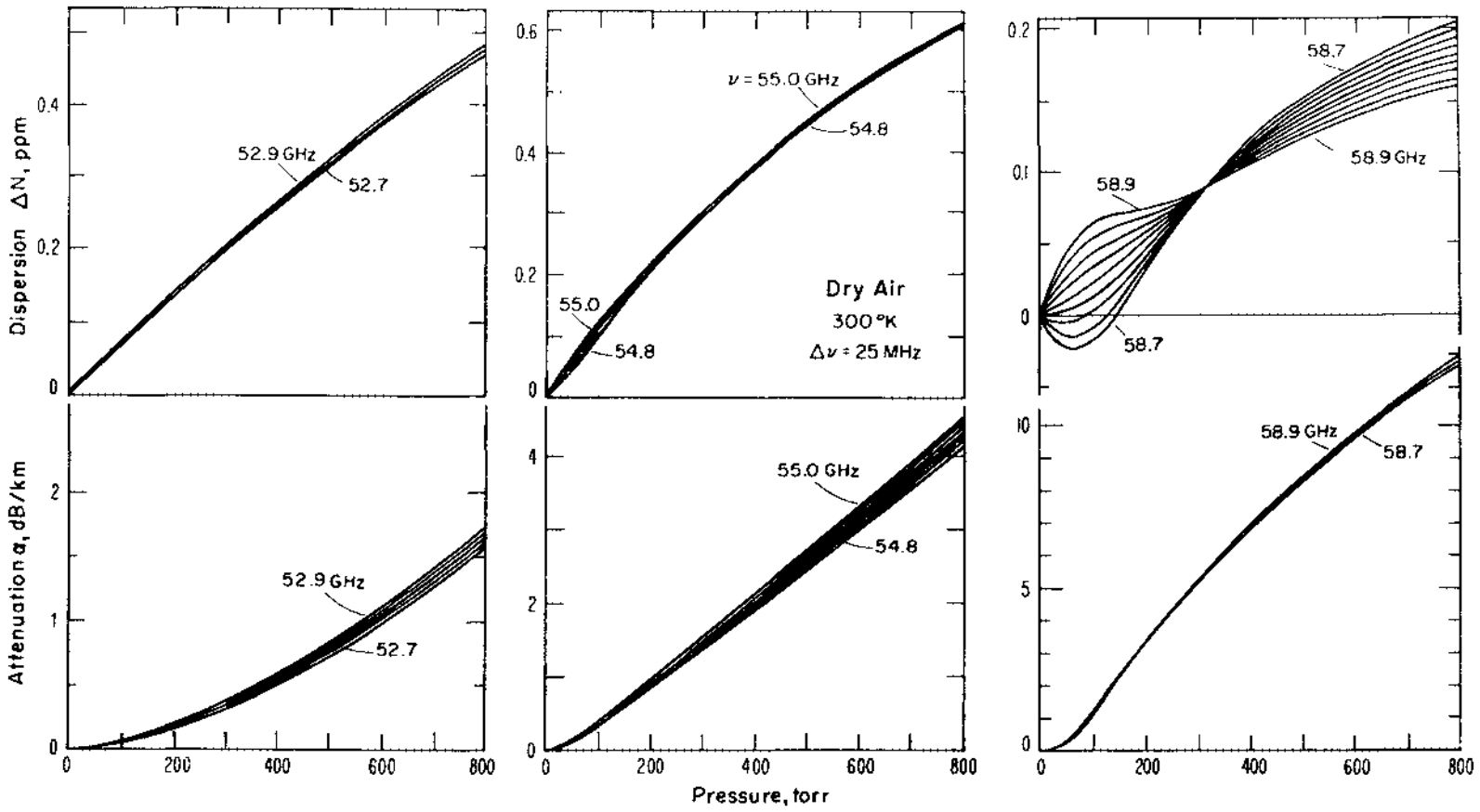

Figure 32. Computer plots of O_2-MS continuum pressure profiles in AIR at 52.8 GHz, 54.9 GHz, and 58.8 GHz (±0.1 GHz).

Linear Theory , $I_N^o = 0$.

2.6 Atmospheric O_2-MS Properties (40-140 GHz)

The transfer function of a homogeneous atmosphere is characterized by the complex refractivity $N = N' - jN''$ that has been treated in depth for the O_2-MS in terms of dispersion ΔN[ppm] and attenuation α [dB/km]. A turbulent atmosphere introduces random contributions to the refractivity N. Turbulence can be expressed by statistics of temperature and pressure fields; thus, a general transfer function calls for the evaluation of temperature and pressure sensitivities (Ott, 1975),

$$\begin{aligned} a_T &= \partial\alpha/\partial T\alpha \quad , \quad b_T = \partial(\Delta N)/\partial T\Delta N \quad [\%/^\circ K] \ , \\ a_p &= \partial\alpha/\partial p\alpha \quad , \quad b_p = \partial(\Delta N)/\partial p\Delta N \quad [\%/\text{torr}] \ , \end{aligned} \tag{60}$$

across the O_2-MS band (Fig. 25). A "modulation" of turbulence-induced signal fluctuations occurs when the sensitivities $a_{T,p}$ and $b_{T,p}$ depend upon frequency. A broadband signal (several GHz) can experience decorrelation or, in other words, the turbulent atmosphere may exhibit an ultimate bandwidth.

The frequency dependence of $a_{T,p}$, $b_{T,p}$ can reveal information about the state of the atmosphere via a differential measurement of amplitude and/or phase of a (coherent) signal pair at selected frequencies. Peckham (1974) proposes to measure with a satellite-based radar the ground-reflected signal strength at several frequencies located in the low frequency wing of the O_2-MS. If no precipitation is present, the differential signal strengths are expected to be indicative of atmospheric ground level (mainly over oceans) pressure. Wykes (1974) reported the supporting calculations of O_2-MS transfer characteristics between 47 and 54 GHz.

2.6.1 Temperature and Pressure Sensitivities

The potential applications triggered our interest to find out what extremes of $a_{T,p}$ and $b_{T,p}$ can be expected for typical atmospheric conditions up to 10 kilometers height (300-200°K, 760-190 torr). The linear O_2-MS model ($I_N^o = 0$) was used in a computer calculation, and the results are presented in graphical form (Figs. 33 to 38). The dispersion sensitivities are given by the partial derivatives $\partial(\Delta N)/\partial T$ and $\partial(\Delta N)/\partial p$ since the division by $\Delta N=0$ poses a problem. The dispersive O_2-MS term is contributing 0 to ± 1 percent to dry air refractivity, an amount sufficient to justify its consideration. Attenuation is generally more important and, at a fixed frequency ν, we use equation (59c) to describe the variability around p_o and T_o. O_2-MS attenuation $\alpha(\nu,p_o,T_o)$ is depicted in figure 33, and the associated exponents are listed in Table 18. The example (below) of dry air at 760 torr, 300°K gives an overview of what to expect:

ν , GHz	50	55	60	115	119	Reference
			REFRACTION			
N_o , ppm			262.2			Eq. 2, T.9
$b_o(T)$, %/°K			-0.33			
$b_o^o(p)$, %/torr			0.13			
			DISPERSION			
ΔN , ppm	0.3	0.7	0	-0.23	-0.30	Fig. 34
b(T) , %/°K	-0.6	-0.6	-	-0.6	-0.65	Fig. 37
b(p) , %/torr	0.13	0.09	-	0.14	0.13	Fig. 38
			ATTENUATION			
α , dB/km	0.5	4.0	11.9	0.25	1.35	Fig. 33
a(T) , %/°K	-0.80	-0.50	- 0.73	-1.13	-0.71	Fig. 35
y	-2.37	-1.50	- 2.20	-3.42	-2.19	T. 18
a(p) , %/torr	0.26	0.14	0.09	0.24	0.01	Fig. 36
x	1.91	1.05	0.71	1.77	0.13	T. 18

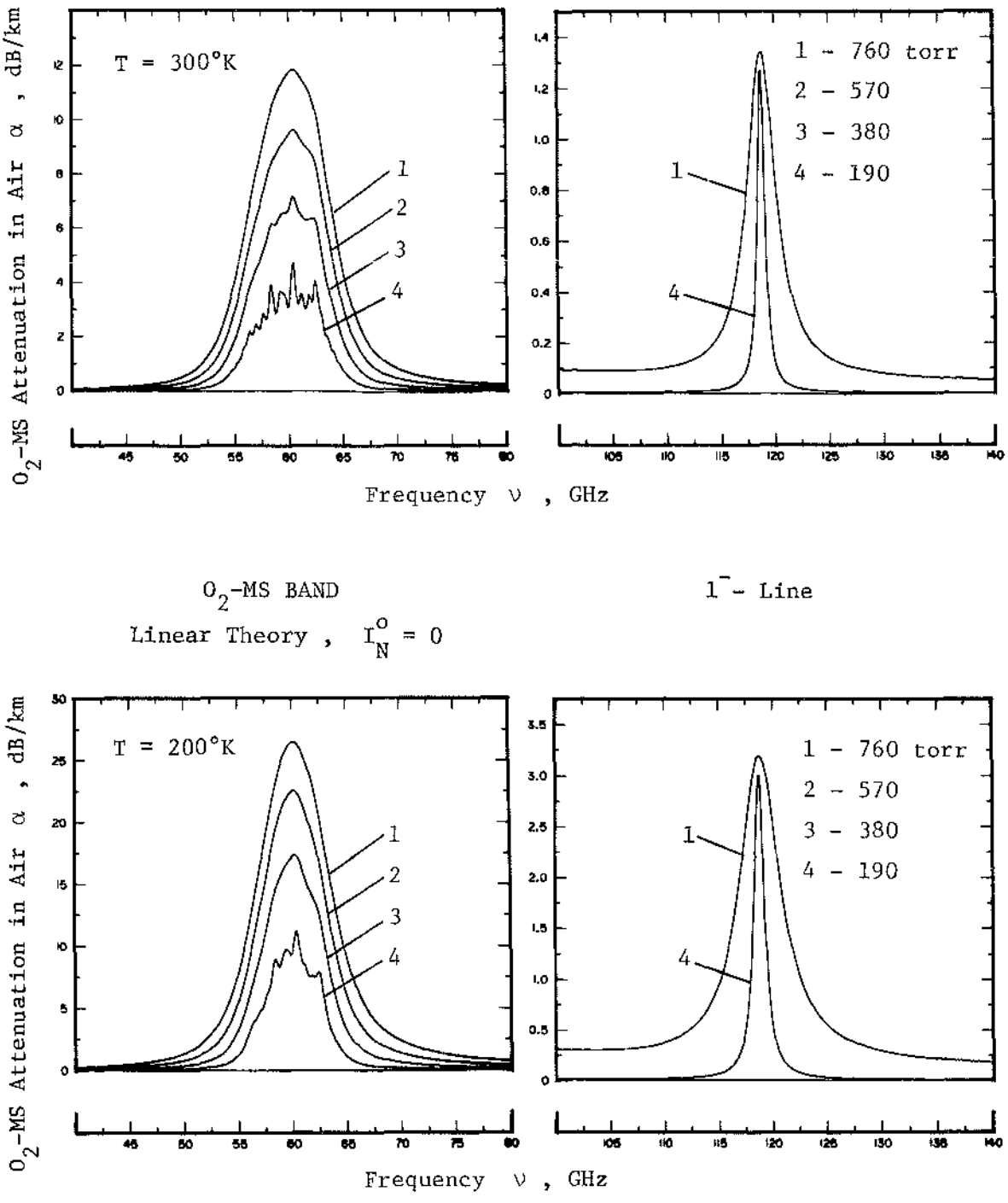

Figure 33. Dry AIR attenuation due to the O_2-MS at 300° and 200°K for four pressure parameters (190-760 torr).

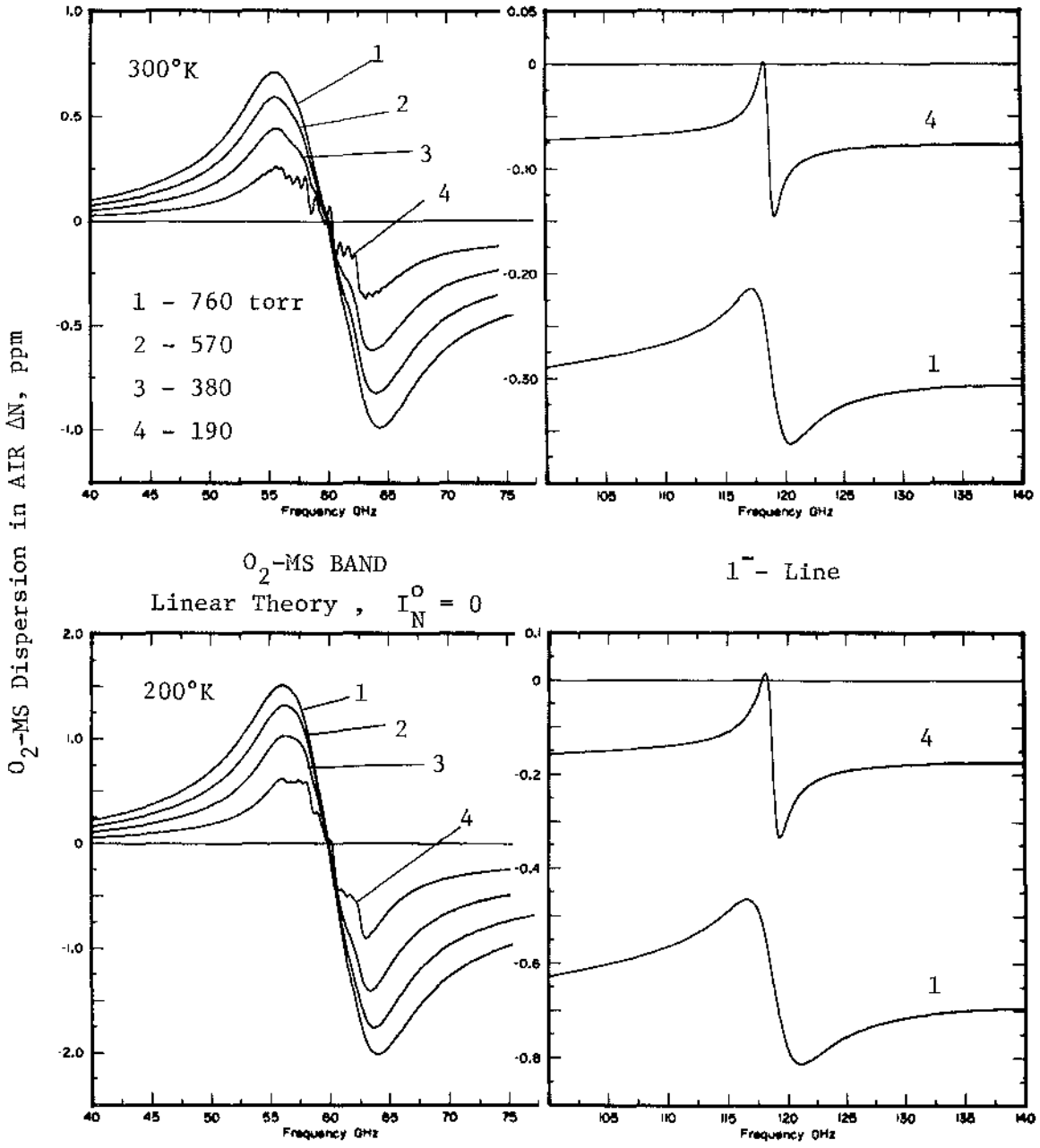

Figure 34. Dry AIR dispersion due to the O_2-MS at 300° and 200°K for four pressure parameters (190-760 torr).

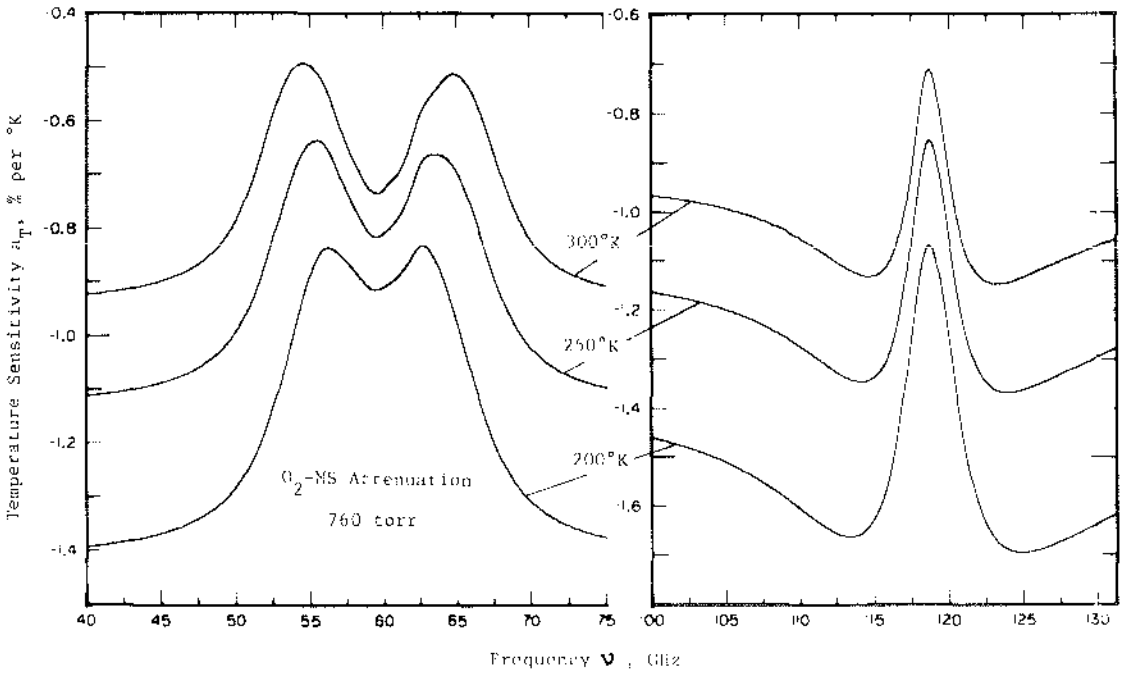

$$I_N^o = 0$$

Figure 35. Temperature sensitivity $a_T = \partial\alpha/\partial T\alpha$ of O_2-MS attenuation (see Fig. 33) at 760, 380, and 190 torr for three temperature parameters (200-300°K).

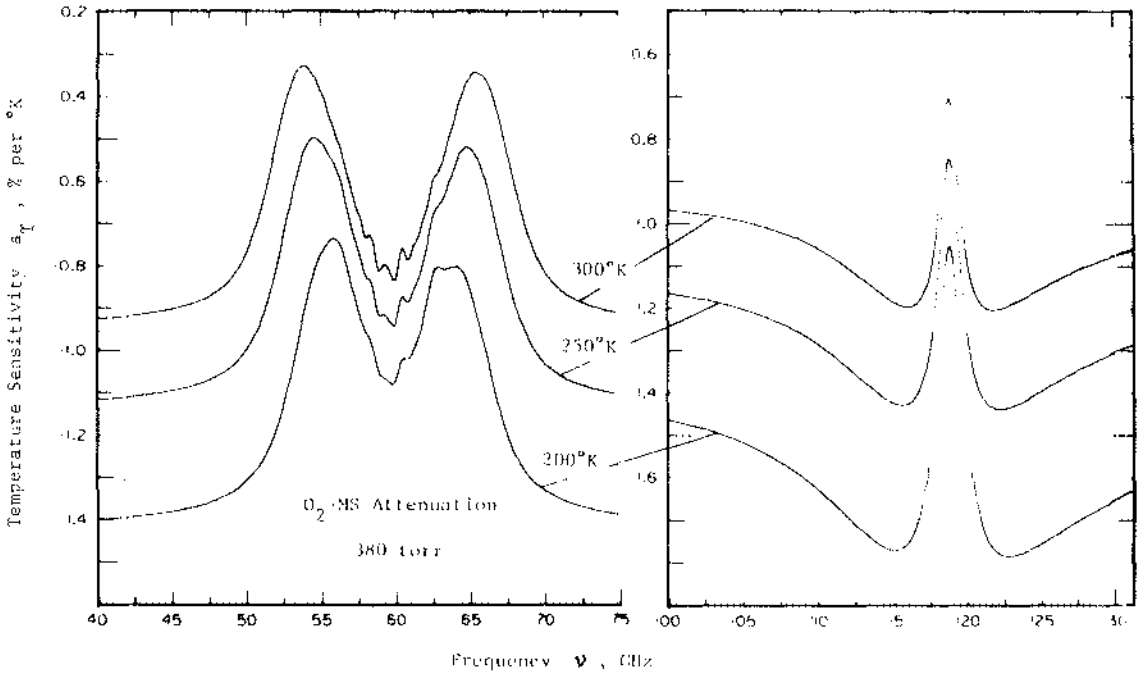
Temperature Sensitivity a_T , % per °K
300°K
250°K
200°K
O_2-MS Attenuation
380 torr
Frequency ν , GHz

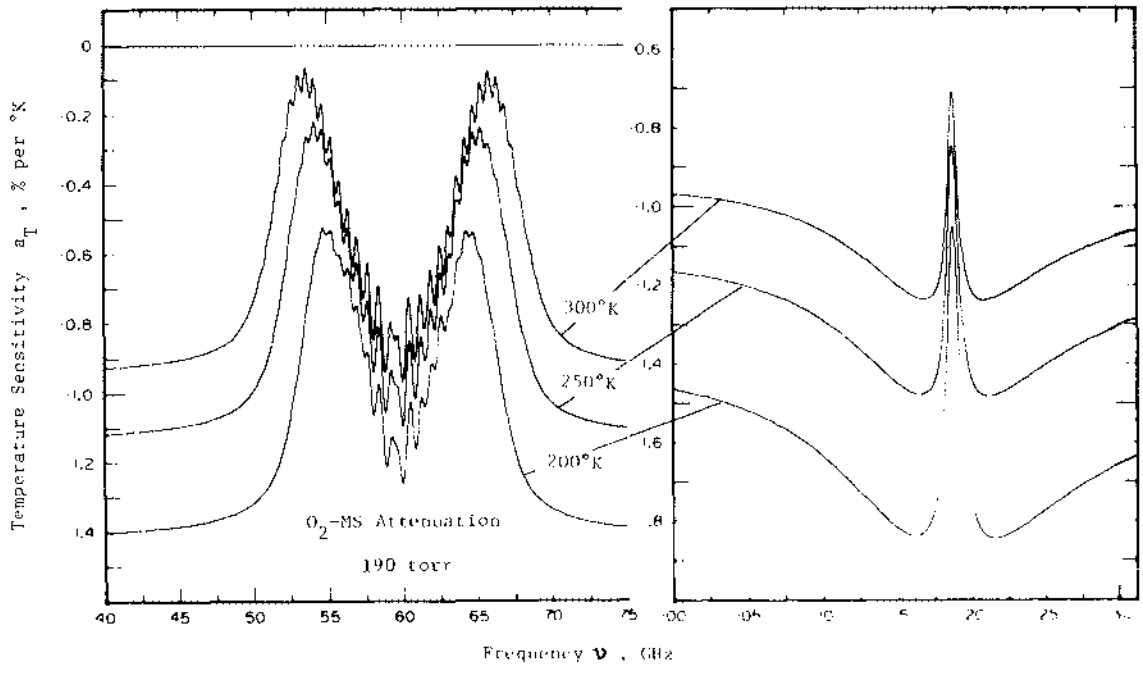
Temperature Sensitivity a_T , % per °K
300°K
250°K
200°K
O_2-MS Attenuation
190 torr
Frequency ν , GHz

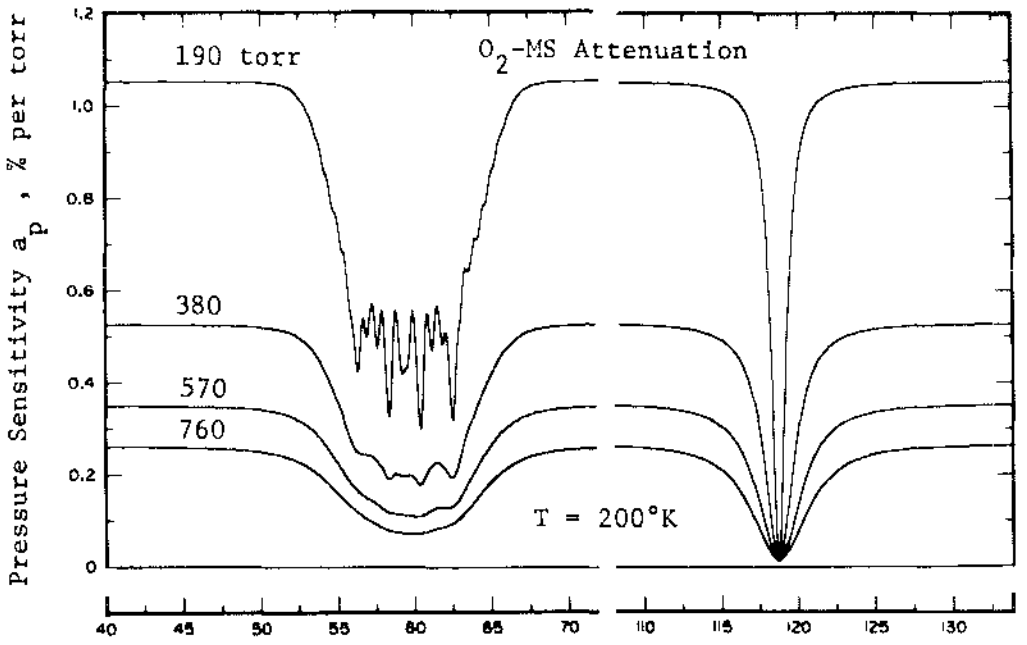
190 torr
O_2-MS Attenuation
380
570
760
T = 200°K
Pressure Sensitivity a_p, % per torr
1.2
1.0
0.8
0.6
0.4
0.2
0
40
45
50
55
60
65
70
110
115
120
125
130

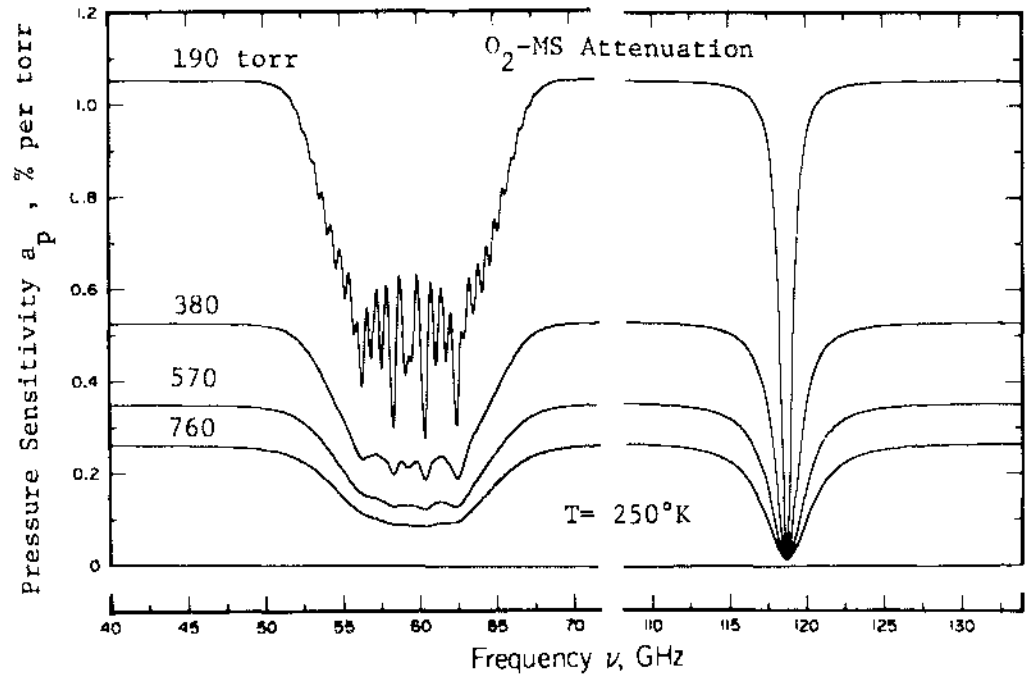
190 torr
O_2-MS Attenuation
380
570
760
T= 250°K
Pressure Sensitivity a_p, % per torr
1.2
1.0
0.8
0.6
0.4
0.2
0
40
45
50
55
60
65
70
110
115
120
125
130
Frequency ν, GHz

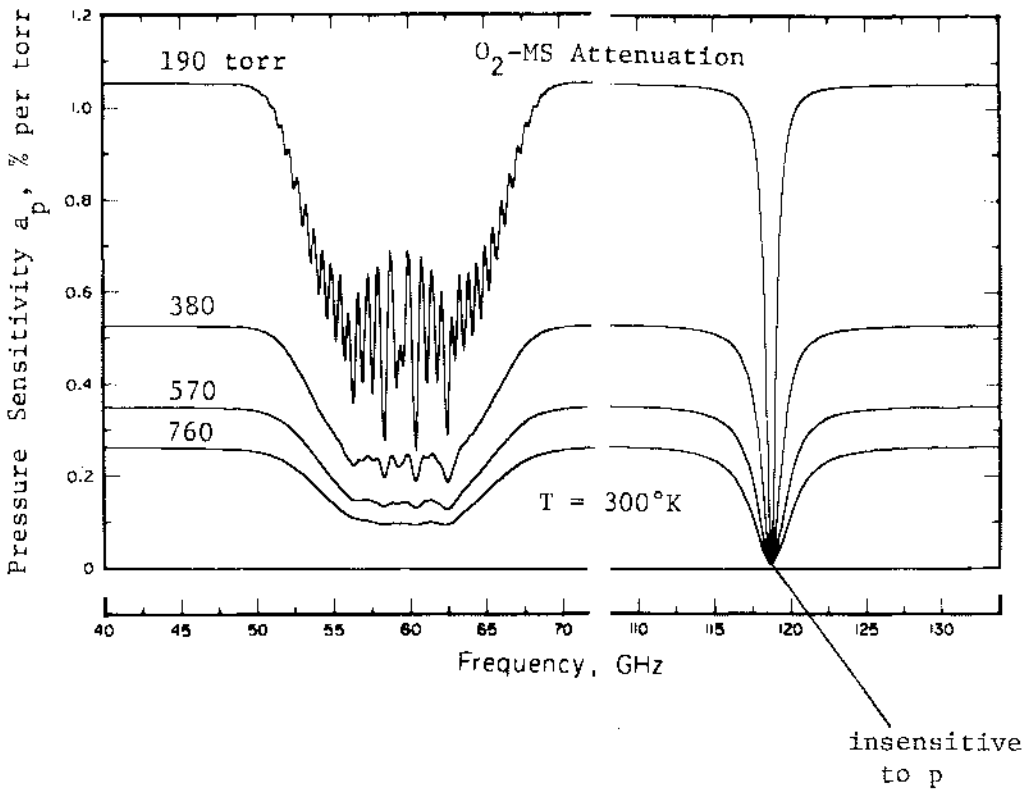

$$I_N^o = 0$$

Figure 36. Pressure sensitivity $a_p = \partial\alpha/\partial p\alpha$ of O_2-MS attenuation (see Fig. 33) at 200, 250, and 300°K for four parameters (190-760 torr).

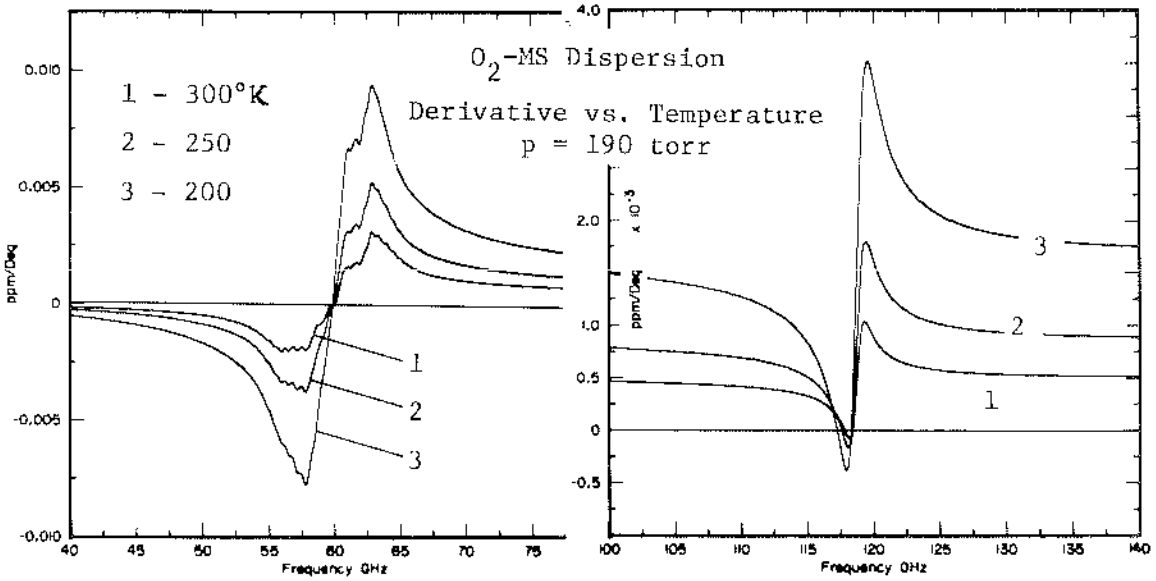
O_2-MS Dispersion
Derivative vs. Temperature
p = 190 torr
1 - 300°K
2 - 250
3 - 200
ppm/Deg
Frequency GHz
1
2
3

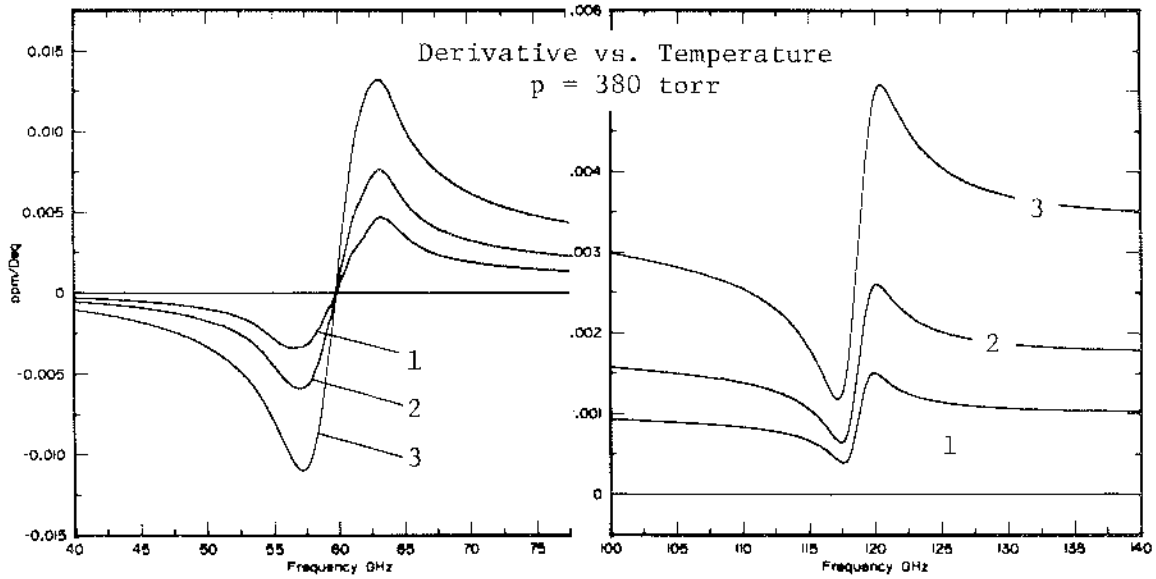
Derivative vs. Temperature
p = 380 torr
ppm/Deg
Frequency GHz
1
2
3

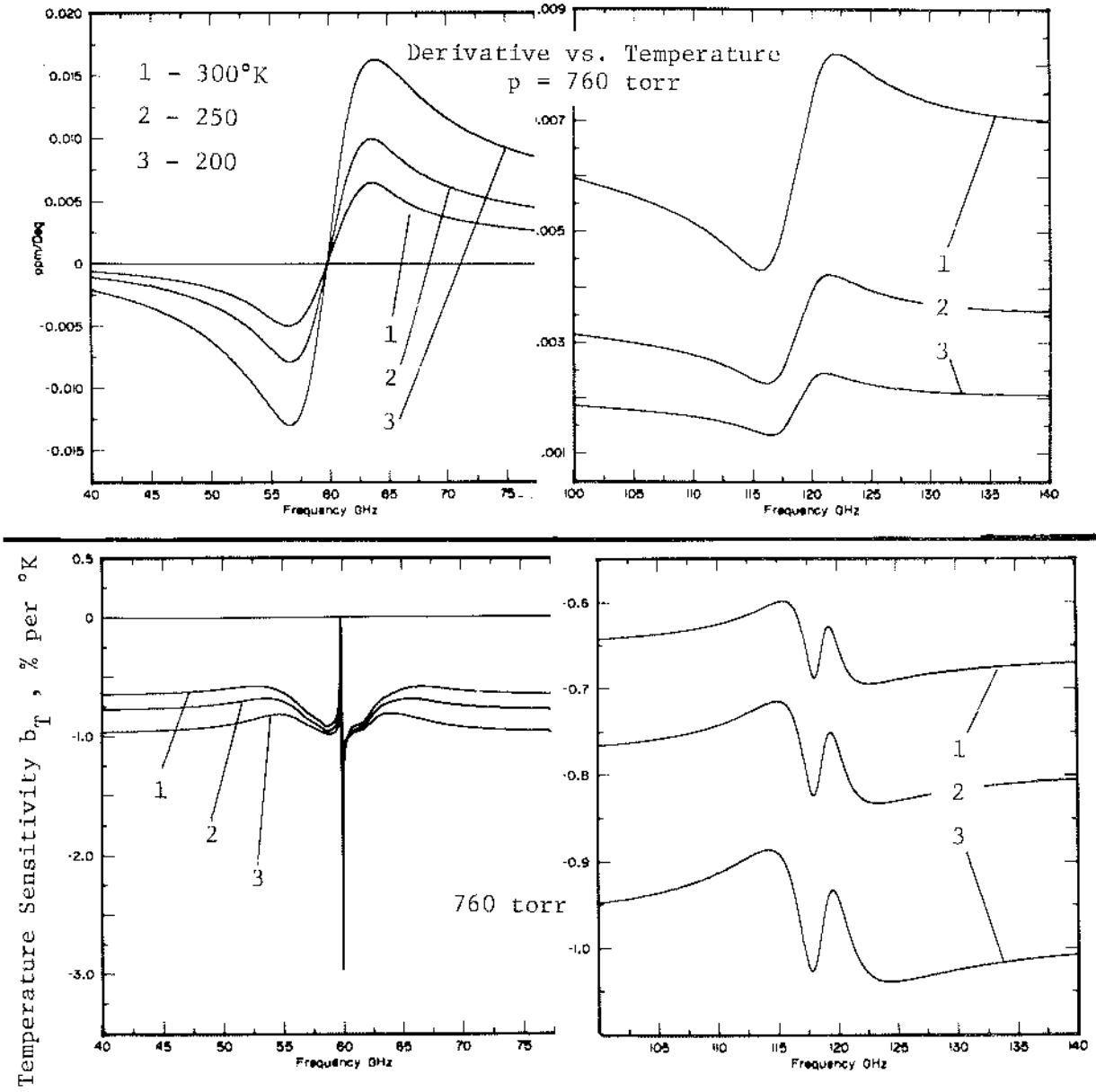

$$I_N^o = 0$$

Figure 37. Temperature derivative $\partial\ \Delta N/\partial T$ and temperature sensitivity $b_T = \partial\ \Delta N/\partial T \cdot \Delta N$ at 190, 380, and 760 torr for three temperature parameters (200-300°K).

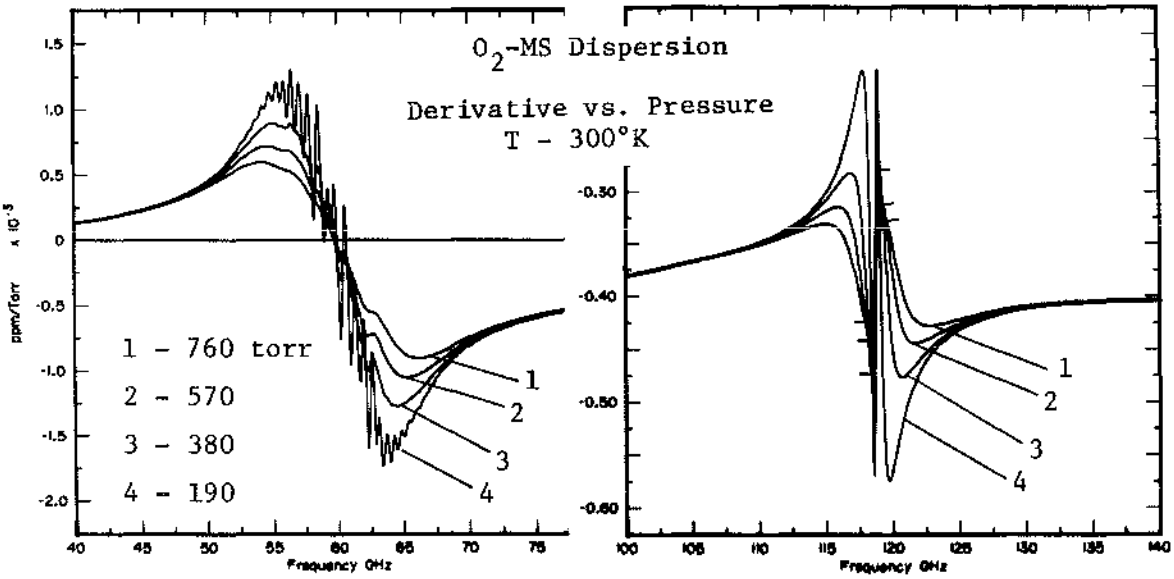
O_2-MS Dispersion
Derivative vs. Pressure
T - 300°K
1 - 760 torr
2 - 570
3 - 380
4 - 190
ppm/Torr x 10^{-3}
Frequency GHz

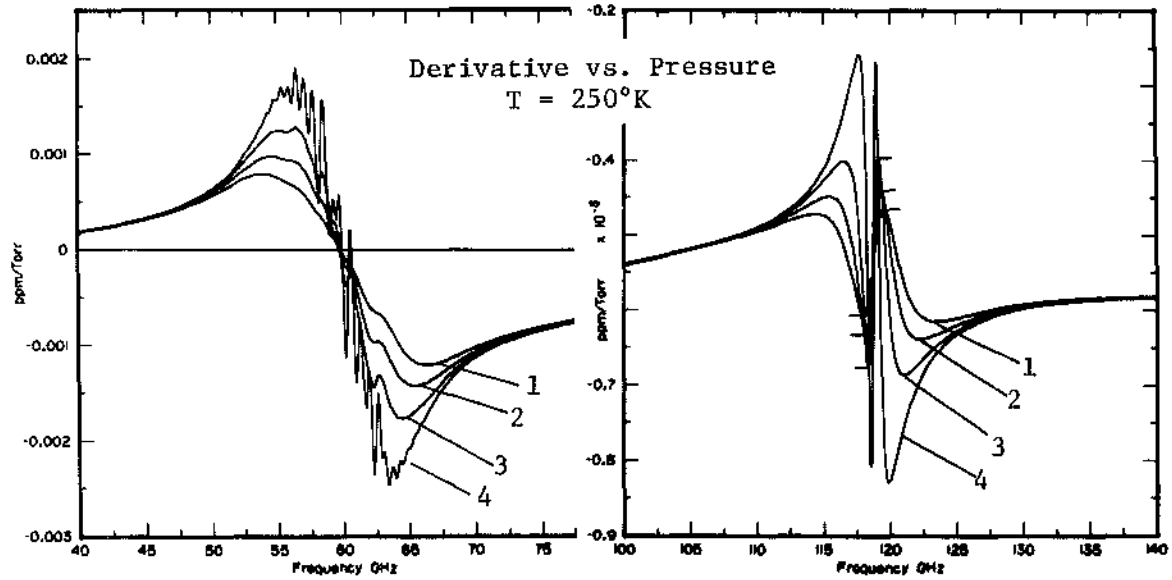
Derivative vs. Pressure
T = 250°K
ppm/Torr
Frequency GHz

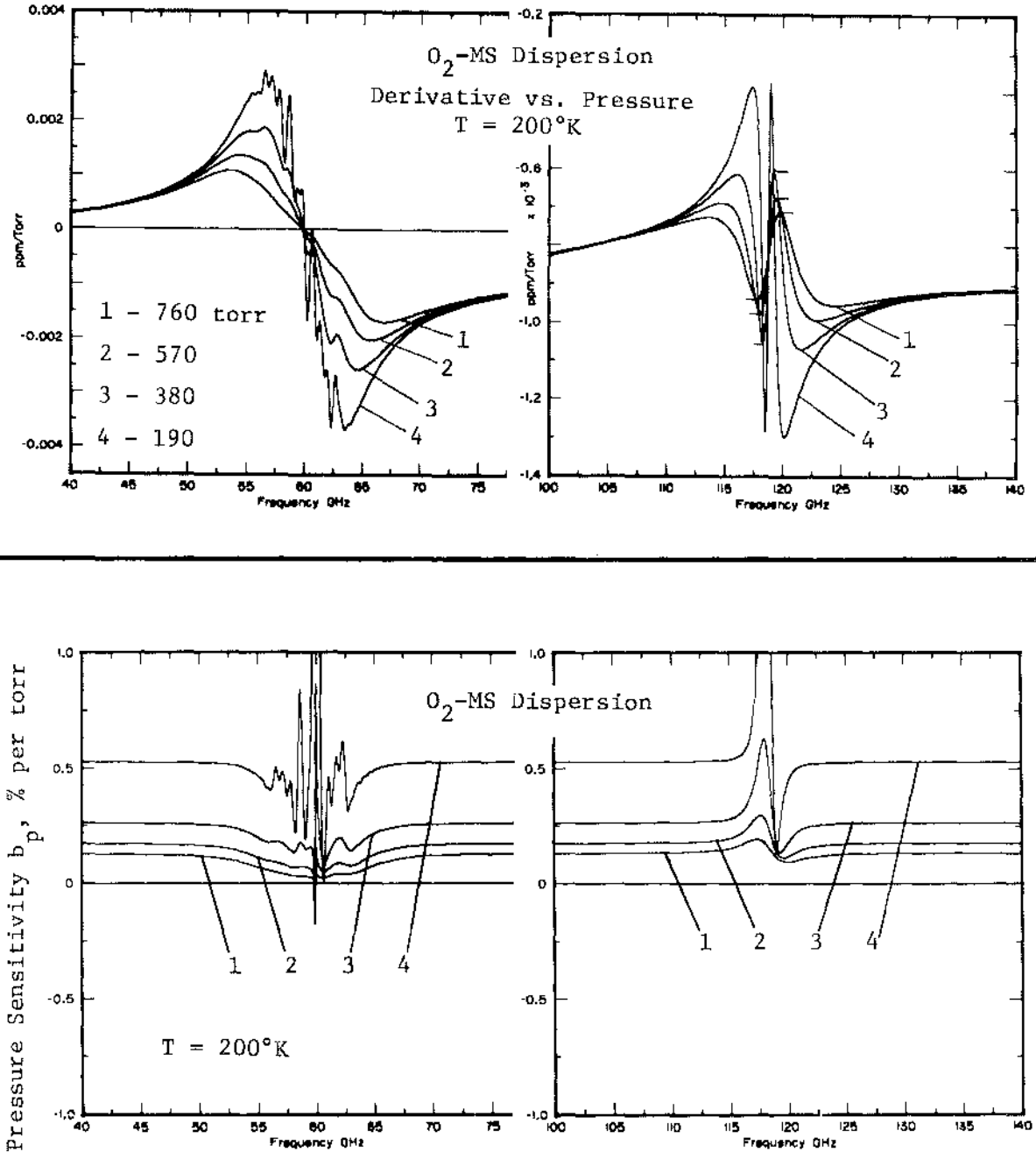

Figure 38. Pressure derivative $\partial \Delta N/\partial p$ and pressure sensitivity $b_p = \partial \Delta N/\partial p \cdot \Delta N$ at 300, 250, and 200°K for four pressure parameters (190-760 torr).

Table 18. Pressure exponents x and temperature exponents y of the O_2-MS attenuation α for two pressure (760, 570 torr) and two temperature (300, 200°K) parameters

Freq. ν	x				-y				p_o / T_o
	760 torr		570 torr		760 torr		570 torr		
	300°K	200°K	300°K	200°K	300°K	200°K	300°K	200°K	
GHz									
40	1.99	1.98	2.00	1.99	2.79	2.81	2.79	2.82	
45	1.98	1.96	1.99	1.98	2.71	2.76	2.72	2.78	
50	1.91	1.88	1.94	1.93	2.37	2.59	2.36	2.62	
51	1.84	1.84	1.88	1.90	2.17	2.50	2.12	2.53	
52	1.72	1.76	1.76	1.84	1.91	2.37	1.79	2.39	
53	1.53	1.63	1.57	1.73	1.66	2.19	1.47	2.19	
54	1.30	1.44	1.33	1.54	1.51	1.98	1.32	1.93	
55	1.05	1.18	1.09	1.26	1.50	1.79	1.37	1.72	
56	0.85	0.93	0.87	0.97	1.61	1.69	1.55	1.62	
57	0.78	0.75	0.83	0.82	1.82	1.71	1.84	1.72	
58	0.73	0.61	0.78	0.68	2.03	1.77	2.11	1.85	
59	0.72	0.54	0.80	0.63	2.18	1.83	2.30	1.97	
60	0.71	0.52	0.78	0.60	2.20	1.83	2.32	1.97	
61	0.72	0.56	0.80	0.66	2.11	1.79	2.21	1.91	
62	0.71	0.63	0.76	0.70	1.90	1.71	1.95	1.76	
63	0.76	0.78	0.80	0.83	1.70	1.68	1.70	1.66	
64	1.00	1.07	1.05	1.18	1.59	1.79	1.50	1.75	
65	1.23	1.36	1.26	1.47	1.55	1.97	1.37	1.92	
66	1.47	1.58	1.50	1.69	1.64	2.16	1.44	2.14	
67	1.67	1.73	1.71	1.82	1.85	2.34	1.70	2.36	
68	1.81	1.82	1.85	1.88	2.11	2.48	2.03	2.51	
69	1.89	1.87	1.92	1.92	2.33	2.58	2.30	2.61	
70	1.93	1.90	1.96	1.94	2.48	2.64	2.48	2.67	
75	1.98	1.96	1.99	1.98	2.74	2.78	2.74	2.79	
80	1.99	1.98	2.00	1.99	2.80	2.82	2.81	2.83	
100	2.00	1.99	2.00	2.00	2.92	2.95	2.92	2.95	
110	1.98	1.94	1.99	1.97	3.18	3.25	3.19	3.27	
112	1.95	1.88	1.97	1.93	3.30	3.33	3.32	3.39	
114	1.87	1.73	1.92	1.83	3.41	3.36	3.46	3.46	
115	1.77	1.57	1.86	1.72	3.42	3.29	3.51	3.44	
116	1.58	1.30	1.73	1.51	3.34	3.12	3.49	3.32	
117	1.18	0.86	1.41	1.09	3.05	2.78	3.28	3.01	
118	0.45	0.31	0.61	0.39	2.46	2.32	2.62	2.42	
119	0.13	0.14	0.13	0.11	2.19	2.17	2.21	2.17	
120	0.84	0.57	1.09	0.76	2.79	2.54	3.02	2.73	
121	1.40	1.09	1.60	1.33	3.24	2.97	3.43	3.20	
122	1.68	1.43	1.80	1.62	3.42	3.23	3.54	3.42	
123	1.81	1.64	1.89	1.77	3.46	3.36	3.54	3.50	
124	1.88	1.76	1.93	1.85	3.46	3.42	3.51	3.51	
125	1.92	1.84	1.96	1.90	3.43	3.43	3.46	3.50	
126	1.95	1.88	1.97	1.93	3.39	3.42	3.41	3.47	
128	1.97	1.94	1.99	1.96	3.30	3.37	3.32	3.40	
130	1.99	1.96	1.99	1.98	3.23	3.31	3.24	3.33	
140	2.00	1.99	2.00	2.00	3.05	3.11	3.05	3.11	

Scanning Table 18 for decorrelations of pressure and temperature sensitivities, only the 1^- line center attenuation at 119 GHz proves to be fairly insensitive to pressure variations (x = 0.13), hence the strength of a radio signal at this frequency is a good indicator of integrated temperature fluctuations along a line-of-sight path (y = -2.2). Picking O_2-MS attenuation as a pressure indicator seems to be a poor choice since the variability with temperature dominates at ground levels for all frequencies. The variation of both exponents, x and y, with the mean pressure or mean temperature is relatively small compared to the changes with frequency (Table 18). The value of O_2-MS dispersion (Figs. 34, 37, and 38) to sensing the state of the atmosphere was discussed briefly in Section 3.1.2 of Part 1.

The results of figures 33 to 38 depend upon the line shape and width (e.g., Wykes, 1974) and they will be slightly different for the "Overlap" model (I_N^o - Table 1).

3. WATER VAPOR STUDIES

Water vapor exhibits a rich rotational spectrum of which two lines appear below 200 GHz. The influence of water vapor upon microwave transfer characteristics can be analyzed by (Eqs. 1 to 3)

$$\alpha_w = 0.1820\nu[(SF'')_1 + (SF'')_2 + q''] \quad [dB/km], \qquad (61)$$

$$\Delta N_w = (SF')_1 + (SF')_2 + q' \quad [ppm] .$$

The terms $(SF)_{1,2}$ identify the two H_2O^{16} microwave lines, and $q = q' - jq''$ all contributions in excess of these two lines. A few remarks are made regarding difficulties encountered when studying α_w and ΔN_w either in the laboratory or the free atmosphere. All results, especially anomalies that are discussed in section 3.2, should be judged in light of these remarks.

Water vapor is a difficult test gas inside a vacuum vessel since it strongly adsorbs upon all surfaces. The exchange process with the wall is reversible for isothermic conditions, but the time period to reach equilibrium is in the order of 0.5 to 5 hours depending upon T and how close p_w is to saturation (Liebe, P-8). No sure means have been found to eliminate adsorption. Mrowinski (P-9) experimented with Teflon coatings but only with partial success. Forming water layers alter homogeneous gas conditions and the detection capability of the resonance spectrometer.

Water vapor in the free atmosphere is known to vary considerably, both in time and space, making point measurements of p_w highly unreliable to represent the moisture content along a radio path.

3.1 Water Vapor Microwave Line Spectrum

The two microwave H_2O lines are centered at 22.2 and 183.3 GHz. Their strengths are given by (Sect. 2.5 - Part 1)

$$S = (\nu/\nu_o)\, S^o_{1,2}(300/T)^{3.5}\, p_w \exp[w_{1,2}(1 - \tfrac{300}{T})] \ . \qquad (62)$$

The line parameters at 300°K are

Line	1	2	
ν_o - center frequency	22.23515	183.31012	GHz
S^o - strength parameter	13.9	322	Hz/torr
w - temperature exponent	2.14	0.653	
γ^o_w - width parameter	18.0	19	MHz/torr .

The line shape in moist air that fitted laboratory data (Becker and Autler, 1946) best, was the Van Vleck-Weisskopf shape, which follows from equations (5), (6) when assuming $I^o = 0$. The linewidth is

$$\gamma_w = \gamma^o_w\, [0.21\ (300/T)^{0.6}\ p + (300/T)p_w] \qquad [\text{MHz}], \qquad (63)$$

whereby p is the dry air pressure in torr. The formulation, so far, does

not yield correct answers for α_w and ΔN_w since the nonresonant term q needs to be added.

3.2 Nonresonant Water Vapor Microwave Spectrum

A nonresonant excess q_1 is expected from the far wings of all higher frequency lines. It is a weakness of the Van Vleck-Weisskopf shape that it does not describe the intensity distribution in the far wing ($\gtrsim 10\gamma$). For this reason one tends to adapt the Gross shape (Liebe, 1969),

$$F''_G = 4\nu^2\gamma/[(\nu_o^2 - \nu^2)^2 + 4\nu^2\gamma^2] \quad \text{and}$$
$$F'_G = 2\nu_o(\nu_o^2 - \nu^2)/[(\nu_o^2 - \nu^2)^2 + 4\nu^2\gamma^2] \,, \tag{64}$$

for calculations of the H_2O spectrum between 1 and 1500 GHz since it predicts higher intensities in the low frequency wings (Hall, 1970). The wing contribution q_1 is expected to be proportional to the pressure p_w.

Laboratory attenuation data taken between 18 and 42 GHz at $p \doteq 760$ torr and $p_w = 0$ to 50 torr were fitted when

$$\alpha_{excess} \approx 1.4 \cdot 10^{-3}\, \nu^2 p_w/T \qquad [dB/km] \,, \tag{65}$$

which is about five times as large if the Van Vleck-Weisskopf shape is used for the wing contributions of all higher frequency lines (Becker and Autler, 1946). Similar high wing attenuation was measured for H_2O and H_2O+N_2 mixtures between 120 and 300 GHz (Frenkel and Wood, 1966).

Deviations from a pressure-linear dependence of q lead to the introduction of a second contribution proportional to p_w^2. Such quadratic term $q_2(p_w^2)$ presents evidence of pressure-induced (involving pairs of H_2O molecules) polarization effects, which can occur from a spectrum of a dimer H_2OOH_2 (e.g., Braun, P-15; Dyke and Muenter, 1974) and/or as a consequence of quenching of the rotational motion of the H_2O molecule by intermolecular forces. Indications of nonlinear behavior of $\alpha_w(\Delta N_w)$ with respect to p_w

exist from a variety of experimental studies:

(i) Line-of-sight radio path attenuation

(70 and 79 GHz - Hogg, 1971; 179 and 184 GHz - Whaley, P-5; 222 GHz - Malyshenko, 1969).

(ii) Zenith path attenuation

(36 GHz - Hogg, 1971; 80 to 130 GHz - Gibbins et al., 1975).

(iii) Spectroscopic absorption and dispersion

(22 GHz - Mrowinski, 1970; 119 GHz - Tolbert et al., 1964; 184 GHz - Hemmi and Straiton, 1969; 225 GHz - Harries et al., 1969; 22.2 and 23.6 GHz - Dillon and Liebe, 1971).

We report some α_w and ΔN_w measurements with the PRS at frequencies between 22.2 and 61.2 GHz using pure water vapor. Extreme temperature control ($< \pm 0.01°K$) throughout the system was essential to approach saturation pressures in a reproducible manner. Water vapor generation in a double-walled hard-glass bulb and inlet tubing, where the jacket was part of the temperature circulator flow, enabled to reach 99 percent saturation as checked with an integrated dew point hygrometer.

Results of the types shown in figures 39b, 40, and 41 are roughly described by

$$\Delta N_w = N(\nu_R) - N(\nu_R/2) \approx [2.3(17)p_w(300/T)^{10} + 1.2(3)p_w^2(300/T)^{18}] \cdot 10^{-3} \text{[ppm]}, \quad (66)$$

$$\alpha_w \approx [4(1)p_w(\nu/60)^2(300/T)^{2.5} + 0.8(1)p_w^2(\nu/60)^{2.6}(300/T)^{12}] \cdot 10^{-3} \text{ [dB/km]}, \quad (67)$$

where ν is the frequency in gigahertz.

The theory of $(H_2O)_2$ dimer microwave attenuation was treated in some detail by Poon (1974). His theoretical findings can be expressed as

$$\alpha_{Dimer} \approx 0.2\ p_w^2 (\nu/60)^{2.4}\ (300/T)^{16} \cdot 10^{-3} \quad [dB/km]\ . \qquad (68)$$

Noteworthy are certain similarities between equations (67) and (68) in respect to a strong temperature and some frequency dependencies. An Arrhenius plot (Harries et al., 1969) of α_w at 61.2 GHz (Fig. 40) yields as gradient of constant pressure data the value 4.5 kcal/mole. The same procedure of the dispersion data delivers 8.5 kcal/mole. We believe that dispersion pressure profiles are erroneous due to surface adsorption effects while attenuation profiles are much less affected. More evidence of anomalous water vapor polarization is given in figures 39c, and d. The deviations from equation (2) in figure 39d are attributed to the real gas law (van der Waals equation), which relates p_w to the number of molecules per unit volume,

$$M \doteq 9.66 \cdot 10^{18}\ p_w/(T - p_w B_2/62366) \qquad [1/cm^3]\ . \qquad (69)$$

The second virial coefficient $B_2[cm^3/mole]$ is discussed by Bohlander and Gebbie (1975).

All data are only sketchy evidence of anomalies in the microwave spectrum of water vapor, which warrant more systematic studies of α_w and ΔN_w over a wider range of temperatures, frequencies, and close to saturation. At present, there is no satisfactory theory to account for the experimentally observed excess q.

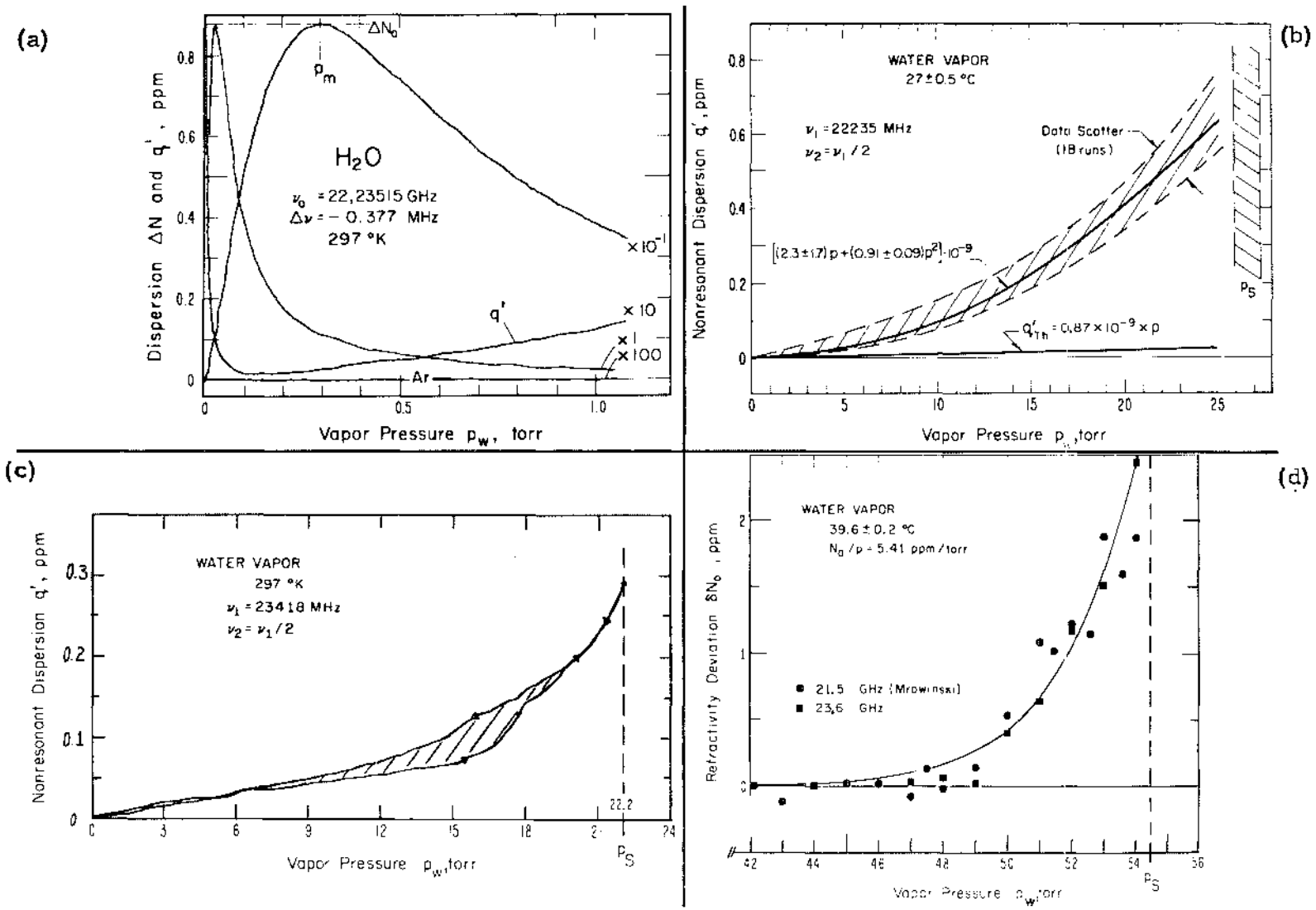
(a)
ΔN0
pm
H2O
ν0 = 22,23515 GHz
Δν = − 0.377 MHz
297 °K
× 10⁻¹
q'
× 10
× 1
× 100
Ar
Dispersion ΔN and q', ppm
Vapor Pressure pw, torr
(b)
WATER VAPOR
27±0.5 °C
ν1 = 22235 MHz
ν2 = ν1 / 2
Data Scatter (18 runs)
[(2.3±1.7) p + (0.91 ± 0.09) p²] · 10⁻⁹
q'Th = 0.87 × 10⁻⁹ × p
PS
Nonresonant Dispersion q', ppm
Vapor Pressure pw, torr
(c)
WATER VAPOR
297 °K
ν1 = 23418 MHz
ν2 = ν1 / 2
22.2
PS
Nonresonant Dispersion q', ppm
Vapor Pressure pw, torr
(d)
WATER VAPOR
39.6 ± 0.2 °C
N0 / p = 5.41 ppm / torr
21.5 GHz (Mrowinski)
23.6 GHz
PS
Refractivity Deviation δN0, ppm
Vapor Pressure pw, torr

Figure 39. Examples of various anomalous behaviors of K-band water vapor refractivity. These results were obtained with the bimodal spectrometer cell shown in figure 3.10 - Part 2.

(a) Resonance dispersion ΔN in the vicinity of the 22 GHz H_2O line. The 10 torr scale shows the nonresonant dispersion q' between ν = 22,235 MHz and $\nu/2$. The multipliers refer to the pressure scale.

(b) The nonresonant dispersion q' of (a) for 18 runs and an analytical expression describing the data (Dillon and Liebe, 1971).

(c) The nonresonant dispersion q' between ν = 23,418 MHz and $\nu/2$ for increasing and decreasing vapor pressure (p_s-saturation pressure for the temperature of the experiment).

(d) Deviations from the refractivity N^o/p (Eq.2, N^o/p = 5.41 ppm/torr at 313°K) when approaching the saturation pressure p_s (● - Mrowinski, 1970).

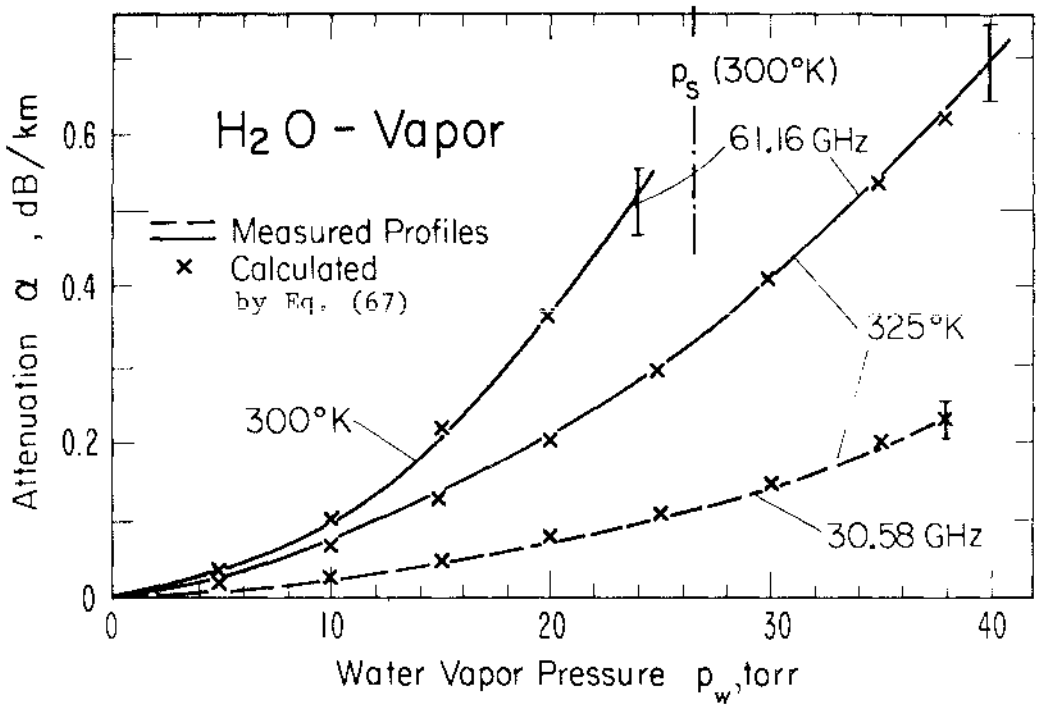

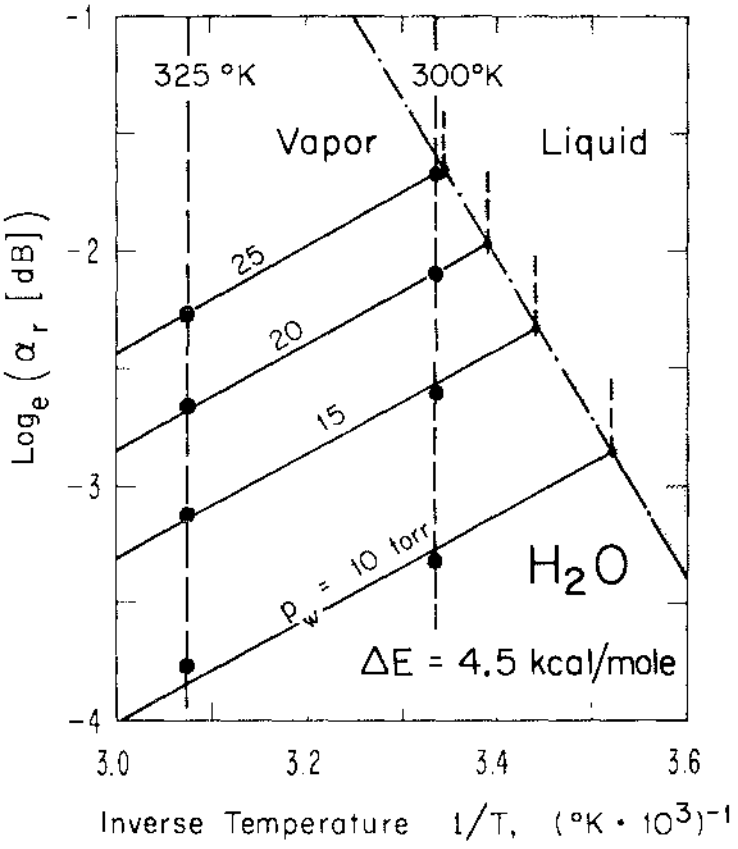

Figure 40.

Water vapor attenuation versus pressure for two temperatures at 61.16 and 30.58 GHz (see Fig. 12 in Part 1), and an Arrhenius plot of the data (Harries et al., 1969).

● 61.16 GHz data

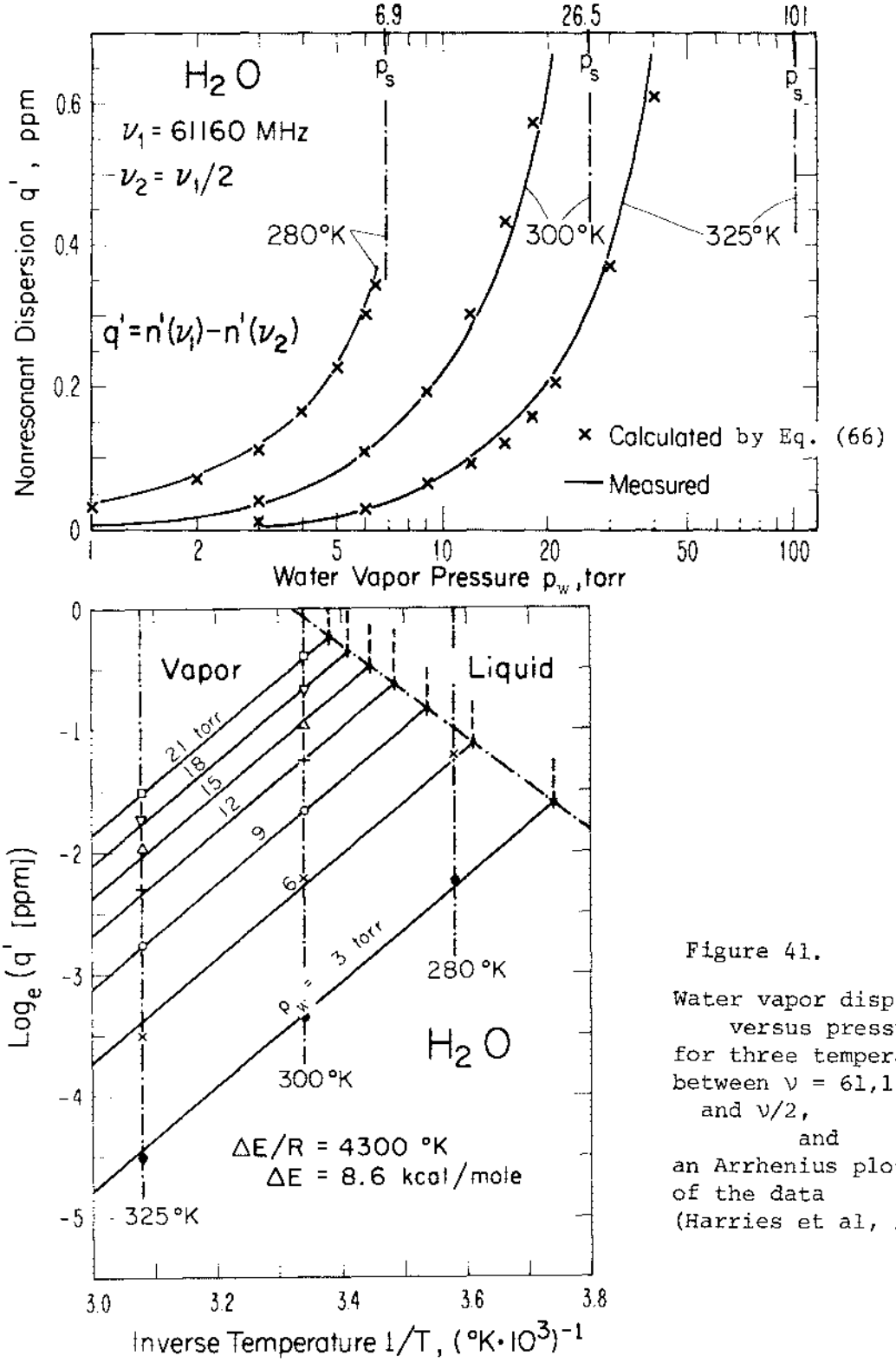

Figure 41.

Water vapor dispersion versus pressure for three temperatures between ν = 61,160 MHz and $\nu/2$, and an Arrhenius plot of the data (Harries et al, 1969).

4. CONCLUSIONS

The 60 GHz oxygen multiplet spectrum (O_2-MS) was studied under a very diverse range of simulated atmospheric conditions with a new experimental technique based upon dispersion pressure profiles. Emphasis was on quantitative intensity information. The studies are categorized into three pressure ranges:

i) 0 to 1 torr, Doppler and Zeeman-broadened isolated lines;

ii) 1 to 100 torr, pressure-broadened line or doublet plus pressure linear continuum;

iii) 100 to 800 torr, pressure-broadened band structure of more than thirty overlapping lines;

and they did not produce any contradictions in the grand O_2-MS scheme, such as might be expected from channel 5 data of NIMBUS 5 (Poon, 1974). The results are encouraging in that dispersion spectroscopy produces in the laboratory credible and reproducible data that can be deduced to accurate line parameters which, in turn, are applied to reliable analytical treatments of molecular transfer and emission characteristics.

The comprehensive measurement program anticipated originally had to be cut short for funding reasons. Nevertheless, more than 300 pressure profiles have been recorded under a wide variety of atmospheric conditions, however, inadequate support given to the data analysis phase limited their conversion to general parameters. Because of the major role that O_2 plays in many areas, particularly in the atmosphere, greater accuracy and better understanding of its intensity function is desirable. Recommendations are expressed to further perfect the experimental technique and continue with the analysis of existing and to be accrued

data. The end product will be a well checked, confirmed, and documented O_2-MS.

Water vapor studies at 61.2 and 30.6 GHz yielded anomalous high dispersion and attenuation rates when saturation pressures were approached. The sketchy experimental evidence of possible molecular complexes in water vapor warrants further work. Much more data at different temperatures and frequencies need to be gathered before more definite conclusions can be drawn.

Summarizing Parts 1 to 3 of this final report, we conclude that the review and translation of molecular theory on millimeter wave properties of air into engineering terms, the description of analytical schemes to predict propagation phenomena on the basis of meteorological variables and their experimental verification on several accounts, together with many examples of unique transfer properties shall provide a basis for the development of system concepts operating in the 40- to 140-GHz frequency range.

Acknowledgment

Everybody named in APPENDICES B and D is gratefully acknowledged for his valuable contributions. The author also thanks Ms. J. Mollard for the meticulous typing.

V. REFERENCES

Artman, J. O., and H. P. Gordon (1954), Absorption of microwaves by oxygen in mm wavelength region, Phys. Rev. 96, 1237-1241 (see P-1).

Becker, G. E., and S. H. Autler (1946), Water vapor absorption of em radiation in the centimeter wave-length range, Phys. Rev. 70, 300-307.

Bohlander, R. A., and H. A. Gebbie (1975), Molecular complexity of water vapour and the speed of sound, Nature 253, no. 5492, 523-525.

Boudouris, G. (1963), On the refractive index of air, and absorption and dispersion of centimeter waves by gases, J. Res. NBS 67D, 631-684.

Dillon, T. A., and J. T. Godfrey (1972), Pressure broadening of the O_2 microwave spectrum, Phys. Rev. A5 599-605 (see P-7).

Dillon, T. A., and H. J. Liebe (1971), Dispersion studies of the 22 GHz water vapor line shape - Part II, J. Quant. Spectrosc. Radiat. Transfer 11, 1803-1817.

Dyke, T. R., and J. S. Muenter (1974), Microwave spectrum and structure of hydrogen bonded water dimer, J. Chem. Phys. 60, 2929-2930.

Frenkel, L., and D. Woods (1966), The microwave absorption by H_2O vapor and its mixtures with other gases between 100 and 300 GHz, Proc. IEEE 54, 498-505.

Gardiner, Jr., W. C., H. M. Pickett, and M. H. Proffitt (1975), Cross sections for reorientation and rotational relaxation of oxygen, J. Chem. Phys. (submitted).

Gibbins, C. J., A. C. Gordon-Smith, and D. L. Croom (1975), Atmospheric emission measurements at 85 to 118 GHz, Planet. Space Sci. 23, 61-73.

Hall, J. T. (1970), Atmospheric effects on submillimeter radiation, Proc. Symp. Submm. Waves, PIB, 455-464.

Harries, J. E., W. J. Burroughs, and H. A. Gebbie (1969), Millimeter wavelength spectroscopic observations of the water dimer in the vapor phase, J. Quant. Spectrosc. Radiat. Transfer 9, 799-807.

Hemmi, C. O., and A. W. Straiton (1969), Pressure broadening of the 1.63-mm water vapor line, Radio Science 4, 9-15.

Hogg, D. C. (1971), Propagation through the atmosphere at frequencies greater than 10 GHz, Progress in Radio Science, 2, (edited by Lane, Findlay, and White), URSI-Brussels, 49-58.

Liebe, H. J. (1969), Calculated tropospheric dispersion and absorption due to the 22-GHz water vapor line, IEEE Trans. Ant. Prop., AP-17, 621-627.

Liebe, H. J., and W. M. Welch (1973), Molecular attenuation and phase dispersion between 40- and 140 GHz for path models from different altitudes, Office of Telecommunications, DoC, OT-Report No. 73-10 May (U.S. Gov't Printing Office, Washington, D.C.). Part 1

Liebe, H. J. (1974), A pressure-scanning refraction spectrometer for atmospheric gas studies at millimeter wavelengths, Office of Telecommunications, DoC, OT-Report No. 74-35, April (U.S. Gov't Printing Office, Washington, D.C.). Part 2

Lenoir, W. B. (1968), Microwave spectrum of molecular oxygen in the mesosphere, J. Geophys. Res. 73, 361-376 (see P-2).

Malota, F., and V. Stein (1974), Theoretical studies of atmospheric temperature profiles using multi-frequency measurements of thermal emission at 60 GHz (in German), Forschungsbericht BMFT-FB-W74-04, July, (Bundeministerium für Forschung und Technologie, Bonn, W. Germany).

Malyshenko, Y. I. (1969), Measurment of absorption coefficient of water vapor at 1.3 mm, Radio Eng. Electr. Phys. (Engl. transl.) 14, 447-448.

McGurk, J. C., T. G. Schmalz, and W. H. Flygare (1974), Fast passage in rotational spectroscopy: Theory and experiment, J. Chem. Phys. 60, 4181-4188.

Meeks, M. L., and A. E. Lilley (1963), The microwave spectrum of oxygen in the earth's atmosphere, J. Geophys. Res. 68, 1683-1703.

Mingelgrin, U. (1972), Classical scattering calculations for diatomic molecules and application to the microwave spectrum of O_2, Office of Telecommunications, DoC, OT/ITS Tech. Res. and Engrg. Rept., TRER 32, July (U.S. Gov't Printing Office, Washington, D.C.).

Mingelgrin, U.(1974), The microwave dispersion spectrum of O_2, Molecular Physics 28, 1591-1602 (see P-13).

Mrowinski, D. (1970), Refraktion und Absorption in atmosphaerischen Gasen in der Umgebung der 22 GHz-Wasserdampf-Linie, Z. Angew. Phys. 29, 323-330 (see P-9).

Newell, A. C., and R. C. Baird (1965), Absolute determination of refractive indices of gases at 47.7 GHz, J. Appl. Phys. 36, 79-83.

Ott, R. H. (1975), Bandwidth limitations in EM transmissions imposed by clear air turbulence, Proc. International Conf. on Communications, ICC 75, 15B, 1-4 (June).

Peckham, G. E. (1974), The measurement of surface pressure from a Satellite by active microwave techniques, NASA Handbook on Active Microwave Workshop, Section 4.4.1 (Houston, July).

Ph.D. Theses on Microwave Spectra of O_2 and H_2O (1953-1974)

P-1. Artman, J. O., "Absorption of microwaves by oxygen in the millimeter wavelength region," Columbia University, Radiation Laboratory, 1953 (84 pp.).

P-2. Lenoir, W. B., "Remote sounding of the upper atmosphere by microwave measurements," Massachusetts Institute of Technology, Dept. Electrical Engineering, 1965 (126 pp.).

P-3. West, B. G., "Absorption spectrum of the oxygen molecule in the 55-65 GHz region," University of Colorado, Dept. Physics, 1965 (58 pp.).

P-4. Gilbert, J., "Power saturation in the microwave spectroscopy of gases," Université Laval, Dept. Physique, Quebec, 1968 (264 pp.).

P-5. Whaley, Jr., T. W., "Characteristics of free space propagation near the 183 GHz H_2O line," University of Texas, Austin, Electrical Engineering, 1968 (76 pp.).

P-6. McKnight, J. S., "The submillimeter microwave spectrum of oxygen," Duke University, Dept. Physics, 1969 (67 pp.).

P-7. Dillon, T. A., "Theory of pressure broadening for isolated and overlapping spectral lines with a calculation on the 60 GHz oxygen lines," University of Colorado, Chemical Physics, 1969 (129 pp.).

P-8. Liebe, H. J., "Untersuchungen an Gasmischungen insbesondere Wasserdampf-Luft, mit einem digitalen Mikrowellen-Refraktometer, Technische Universitaet W-Berlin, Fakultaet Elektrotechnik, 1964 (80 pp.).

P-9. Mrowinski, D., "Refraktion und Absorption in atmosphaerischen Gasen in der Umgebung der 22 GHz H_2O Linie," Technische Universitaet W. Berlin, Inst. Hochfrequenztechnik, 1969 (78 pp.).

P-10. Wilheit, Jr., T. T., "Studies of microwave emission and absorption by atmospheric oxygen," Massachusetts Institute of Technology, Dept. Physics, 1970 (200 pp.).

P-11. Westwater, E. R., "Ground based determination of temperature profiles by microwaves," University of Colorado, Dept. Physics and Astrophysics, 1970 (121 pp.).

P-12. Waters, J. W., "Ground based microwave spectroscopic sensing of the stratosphere and mesosphere," Massachusetts Institute of Technology, Dept. Electrical Engineering, 1970 (238 pp.).

P-13. Mingelgrin, U., "The pressure broadening of the O_2 microwave spectrum," Harvard University, Dept. Chemistry, 1972 (130 pp.).

P-14. Link, F. C., "Molecular absorption of millimeter waves by atmospheric gases," Bucknell University, Pennsylvania, Electrical Engineering, 1973 (120 pp.).

P-15. Braun, C., "The vibration and rotation spectrum for the H_2O dimer," American University, Physics, 1973 (153 pp.).

P-16. Poon, R. K. K., "Atmospheric opacity near half centimeter wavelength," Massachusetts Institute of Technology, Dept. Electrical Engineering, 1974 (354 pp.).

P-17. Kaufman, I. A., "Microwave pressure broadening in O_2 and H_2O above one atmosphere," Columbia University, New York, 1967.

Poon, R. K. (1974), Atmospheric opacity near half centimeter wavelength, Ph.D. thesis, Massachusetts Institute of Technology, Dept. Electrical Engineering.

Pickett, H. M. (1975), General rotational relaxation matrix: Linewidth for oxygen, their interrelation and relation to theory, J. Chem. Phys. (submitted).

Rosenkranz, P. W. (1975), The shape of the 5mm oxygen band in the atmosphere, IEEE Trans. Ant. & Prop., AP-23, 001-029 (in press).

Sabatini, R. R.-editor (1972), the NIMBUS 5 user's guide, NASA Goddard Space Flight Center, ERTS/NIMBUS Project, 162 pp.

Stafford, L. G., and C. W. Tolbert (1963), Shapes of oxygen absorption lines in the microwave frequency region, J. Geophys. Res. 68, 3431-3435.

Tolbert, C. W., L. C. Krause, and A. W. Straiton (1964), Attenuation of the earth's atmosphere between the frequencies 100 and 140 GHz, J. Geophys. Res. 69, 1349-1357.

Waters, J. W. (1973), Ground-based measurement of millimeter wavelength emission by upper stratospheric O_2, Nature, 242, 506-508 (see P-12).

Wykes, C. (1974) Theoretical investigation of feasibility of pressure sounder, Report by Dept. of Physics, Heriot-Watt University, Edinburgh, June (26 pp.).

APPENDIX A

Abstract and Contents of Parts 1 and 2

OT-Report 73-10, Part 1

MOLECULAR ATTENUATION AND PHASE DISPERSION BETWEEN 40 AND 140 GHz FOR PATH MODELS FROM DIFFERENT ALTITUDES

Radio wave propagation in the 40 to 140 GHz band through the first hundred kilometers of the atmosphere is strongly influenced by the microwave spectrum of oxygen (O_2-MS). A unified treatment of molecular attenuation and phase dispersion is formulated. Results of molecular physics are translated into frequency, temperature, pressure, and magnetic field dependencies of a complex refractive index. The intensity distribution of the O_2-MS undergoes several changes with increasing altitudes: when h < 10 km, all lines but one at 119 GHz, are merged to a continuum spectrum under the influence of pressure-broadening; when h < 30 km, a line spectrum with isolated Lorentzians is displayed; when h > 40 km, Zeeman-splitting of each line occurs due to the influence of the earth's magnetic field; for h > 60 km, a Voigt profile governs the transition to a Gaussian line shape and eventually the Doppler-broadened line spectrum vanishes. The influence of water vapor is discussed separately.

Attenuation and dispersion rates for path models are evaluated by computer routines. Examples of computer plots are given as a function of altitude for homogeneous, zenith, and tangential path geometries. Molecular resonances of minor atmospheric gases are discussed briefly, as is the noise which originates from the O_2-MS.

A PRESSURE-SCANNING REFRACTION SPECTROMETER FOR ATMOSPHERIC GAS STUDIES AT MILLIMETER WAVELENGTHS

A differential refraction spectrometer was developed capable of measuring under simulated atmospheric conditions molecular EHF propagation factors, especially the intensity distribution of the oxygen microwave spectrum (O_2-MS). Dispersion and attenuation pressure profiles are measured between 10^{-3} and 10^{3} torr. The sensitivities are better than 1 part in 10^{9} and 0.01 dB/km. The multi-line (~43) structure of the O_2-MS around 60 GHz complicates the data analysis. Special diagnostics evolved from the data for deducing spectroscopic parameters. Experimental difficulties and their elimination are discussed. Examples of data taken for the 9^{+} line (61.15 GHz) and the $7^{+}/5^{-}$ doublet (60.4 GHz) are given.

APPENDIX B

Computer Programs For Studies Of The Atmospheric O_2 Microwave Spectrum

Variables:	Oxygen or Dry Air	Altitude	h = 0 - 100 km
	Quantum Number N = 1 to 43(63)	Temperature	T = 180 - 320°K
	Line Label i = 1 to 44	Pressure	p = 0 - 800 torr
		Magnetic Field Strength	H = 0 to 1 gauss
		Frequency	ν = 40 - 140 GHz
		Frequency Deviation	$\pm\Delta\nu(I)$ = 0 - 100 MHz

Programs are written in Fortran IV and executed on CDC 3800 computer with CRT plotting (6500)

Program					Examples in Final Report		
Name	No.	Developed by	Variable	Parameters	Part	Figure	Table
Line Center Frequencies	1	W. Welch	i	O_2 N	1 [3]		2 [A1]
Line Strengths	2	"	i	O_2 N, T	1 (2)	2	3, 7 (1)
Temperature Function	3	"	T	O_2 N	1	3	4
Line Widths	4	Mingelgrin (1972)	N	O_2 T	1 (2)[3]	5	6 (1) [6]
Interference Coeff.	5	J. Hopponen after Rosenkranz (1975)	N	T	[3]	[1]	[1]
DISPERSION (ΔN, $\Delta\phi$) and ATTENUATION (α) FREQUENCY and PRESSURE PROFILES							
1. General							
Pressure Broadening	6	W. Welch	ν	O_2 p, T	1 [3]	6 to 8 [25,32]	[11 to 13]
Nonlinear Overlap	7	Mingelgrin (1972)	ν	O_2 p, T	1	9, 21	
2. Experimental							
Lines	8	W. Welch	p	O_2 $\Delta\nu$, T	(2)[3]	(2.4) [3,8]	
Doublets	8	"	p	O_2 $\Delta\nu$, T	(2)[3]	(2.5)[10,11,13.14]	
Continuum	15	J. Hopponen	p	O_2 ν, T	(2)[3]	(2.6)[26,28 to 31]	
Zeeman Splitting	9	W. Welch	p	O_2 $\Delta\nu$,H,T	[3]	[17,18,23,24]	
Data Averaging	10	R.Chandler	p	O_2 AIR $\Delta\nu$,T	(2)		(7)
3. Analysis of Model Atmospheres (U.S. Std. Atm. 62)							
(a) Homogeneous Path							
Linear Model	11a	W. Welch	ν	AIR p,T(h)	1 [3]	20 [33,34]	10
CMR Model	11b	"	ν	" "	1	14-17	10
R Model	11c	"	ν	" "			10
Overlap Theory	16	J. Hopponen	ν	" "	[3]	[25]	
Zeeman Effect	12	"	ν	AIR H,p,T(h)	1	18,19	
Derivatives vs T and p	13	J. Hopponen	ν	AIR p,T	[3]	[35 to 38]	[14]
(b) Slant Path							
Zenith	14	W. Welch	ν	AIR h	1	25 to 37	10
Tangential	14	"	ν	AIR h	1	26 to 39	11

Table A1. Calculated O_2-MS Line Center Frequencies for N = 43 to 63 (Eq. 6 - Part 1). N = 1 to 43 see Tables 2,7 - Part 1 or Table 1 - Part 2.

N^+	ν_o [MHz]	N^-	ν_o [MHz]
43+	70545.0	43-	48942.4
45+	71072.9	45-	48434.5
47+	71600.8	47-	47927.7
49+	72128.9	49-	47421.7
51+	72657.1	51-	46916.5
53+	73185.7	53-	46412.1
55+	73714.7	55-	45908.3
57+	74244.1	57-	45405.0
59+	74774.1	59-	44902.2
61+	75304.6	61-	44399.8
63+	75835.8	63-	43897.7

The intensities of O_2-MS lines above $N^{\pm} = 31$ may become detectable in the upper atmosphere by limb-scanning from an orbiting laboratory (space shuttle) (J. Waters, private communication 1974).

APPENDIX C

The New Digital PRS Phase Meter

A. Diede and H. Liebe

The PRS data evaluation was improved by a completely new design consisting of six building blocks:

1. two linear, low-noise preamplifiers for the resonance pulses of R1 and R2;
2. two phase markers and peak detectors for dispersion and attenuation measurements (Fig. A1);
3. a digital phase meter with time period averaging of dispersion data (Fig. A2);
4. a linear ramp generator for ± klystron FM at rates, f_T = 1, 2.5, and 5 kHz;
5. a time period generator deriving the sweep rate f_T and 0.1 and 0.2μs time units from a 1 MHz standard frequency; and
6. extremely well regulated power supplies (±70, +15, +12, +5 V).

The circuit details are available upon request.

We mention a few of the design ideas that have been incorporated into the new instrument. The pulses, which are detected when sweeping the R1(R2) resonance (Sect. 3-Part 2), are amplified in two identical channels to a peak value of about $a_o \doteq -1$ V and fed into a comparator and peak detector (Fig. A1). The comparator generates rectangular pulses whose widths correspond to the width of the R1(R2) resonance at a predetermined level, say 0.8 a_o (actually variable between 0.1 a_o and 0.99 a_o). Leading and trailing edge of each rectangular pulse are transformed into a pair of

trigger pulses identified by A_1-A_2 and B_1-B_2. It is assumed that the resonance $\nu_{R1,\ R2}$ occurs timewise in the middle between the two triggers. The phase marking is very accurate due to high common gain and low hysteresis of the comparator (~1 mV uncertainty).

The decrease of the R2-channel signal amplitude due to O_2-MS attenuation from $a_o \rightarrow a_1$ (Eq. 39 - Part 2) is tracted by a peak detector which, in addition, keeps the comparator level at its preset level (0.8 a_1). This AGC-scheme proved to be best in avoiding additional phase errors introduced otherwise by O_2-MS attenuation.

Dispersion (refraction) data are obtained from the time sequence of the two pairs of triggers, A_1-A_2 and B_1-B_2, within one time frame of the FM sweep marked by S-S'. The Δt-measurment (Eqs. 44, 49 - Part 2) is performed by the gating logic (NAND gates G1-G9) shown in figure A2, which decides automatically for two cases possible in the sequence of triggers.

Case 1.

Time Duration	Count Unit, μs
S-A_1 or S-B_1	0
A_1-A_2 or B_1-B_2	0.2
A_2-B_1 or B_2-A_1	0.1
B_1-B_2 or A_1-A_2	0.2
B_2-S' or A_2-S'	0

The sequence B_1-A_1-A_2-B_2 when B_1-B_2 is wider than A_1-A_2 produces wrong results, but can easily be avoided by a slight offset of ν_{R1} against ν_{R2} ($\Delta t_o \approx 10\mu s$).

Case 2.

Time Duration	Count Unit, μs
$S-A_1$ or $S-B_1$	0
A_1-B_1 or B_1-A_1	0.2
B_1-A_2 or A_1-B_2	0
A_2-B_2 or B_2-A_2	0.2
B_2-S' or A_2-S'	0

The wanted time interval Δt is the total count over one sweep period. The result is displayed as an average of 10^3, 10^4, or 10^5 periods. For a sweep width u_M = 2.5 MHz, the sweep speed can be chosen between δ = 2.5 (f_T = 1 kHz) and 13 (f_T = 5 kHz) kHz/μs while the time for a Δt-reading varies between 0.2 s (f_T = 5 kHz, 10^3 periods) and 100 s (f_T = 1 kHz, 10^5 periods).

The performance of the new PRS phase meter is shown in figure A3 for dispersion and attenuation detection sensitivities at three sampling rates f_T. The most significant result is the satisfactory ΔN_{min} - detection at 1 kHz with a sweep speed δ = 2.55 kHz/μs. All dynamic detection problems (phase error, p.24; amplitude error, p. 29) are reduced by a factor of 5. The various combinations of sample number n, measurement time $t_{ob}/\Delta N$, and dispersion detection sensitivity $X = \Delta N/\Delta t$ give enough flexibility to adapt to different experimental requirements. In addition, for phase- and amplitude-true detection, the condition of equation (39) has to be fulfilled.

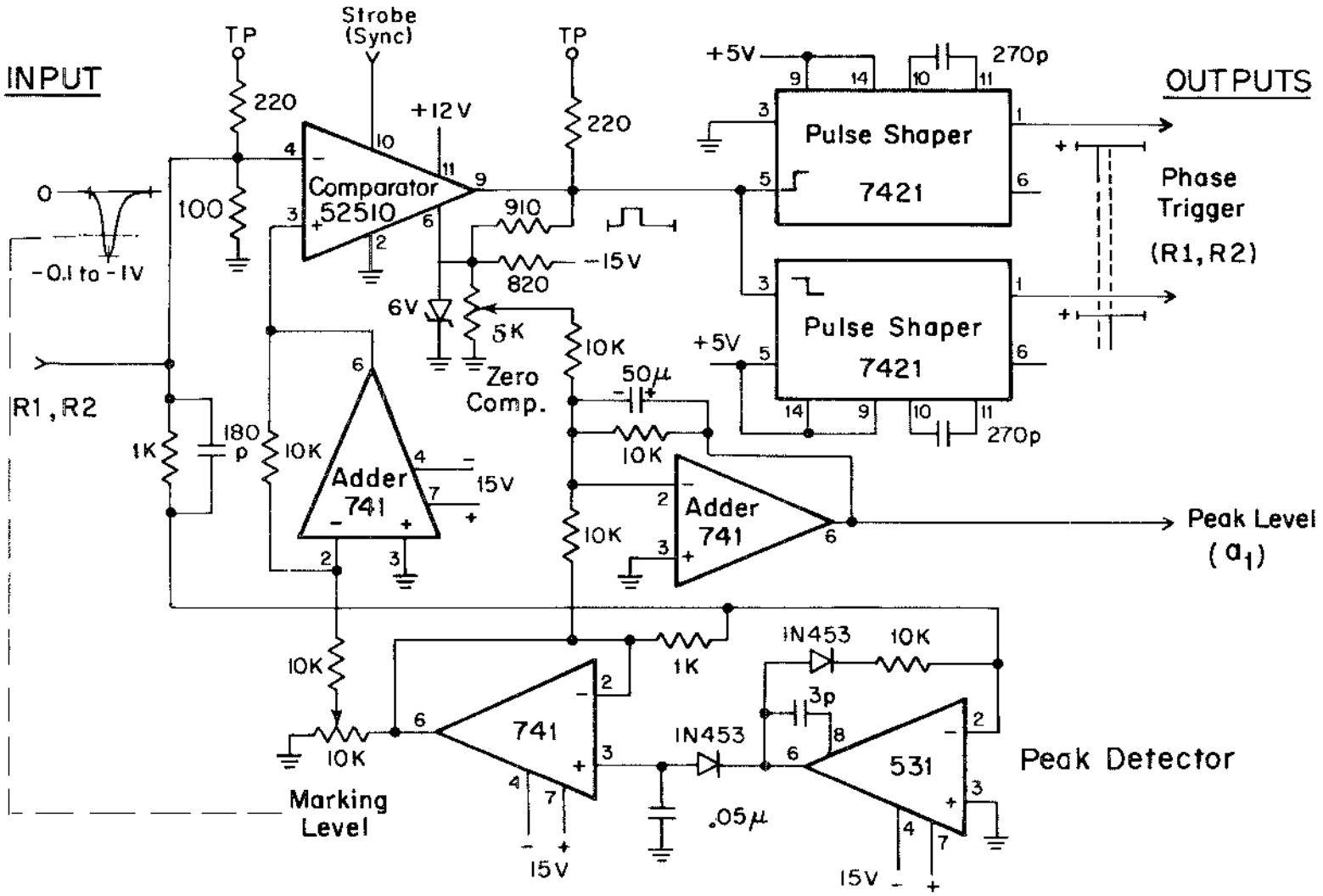

Figure A1. Circuit diagram of phase marker and peak level detector. Two identical channels for ν_R and $\nu_R/2$.

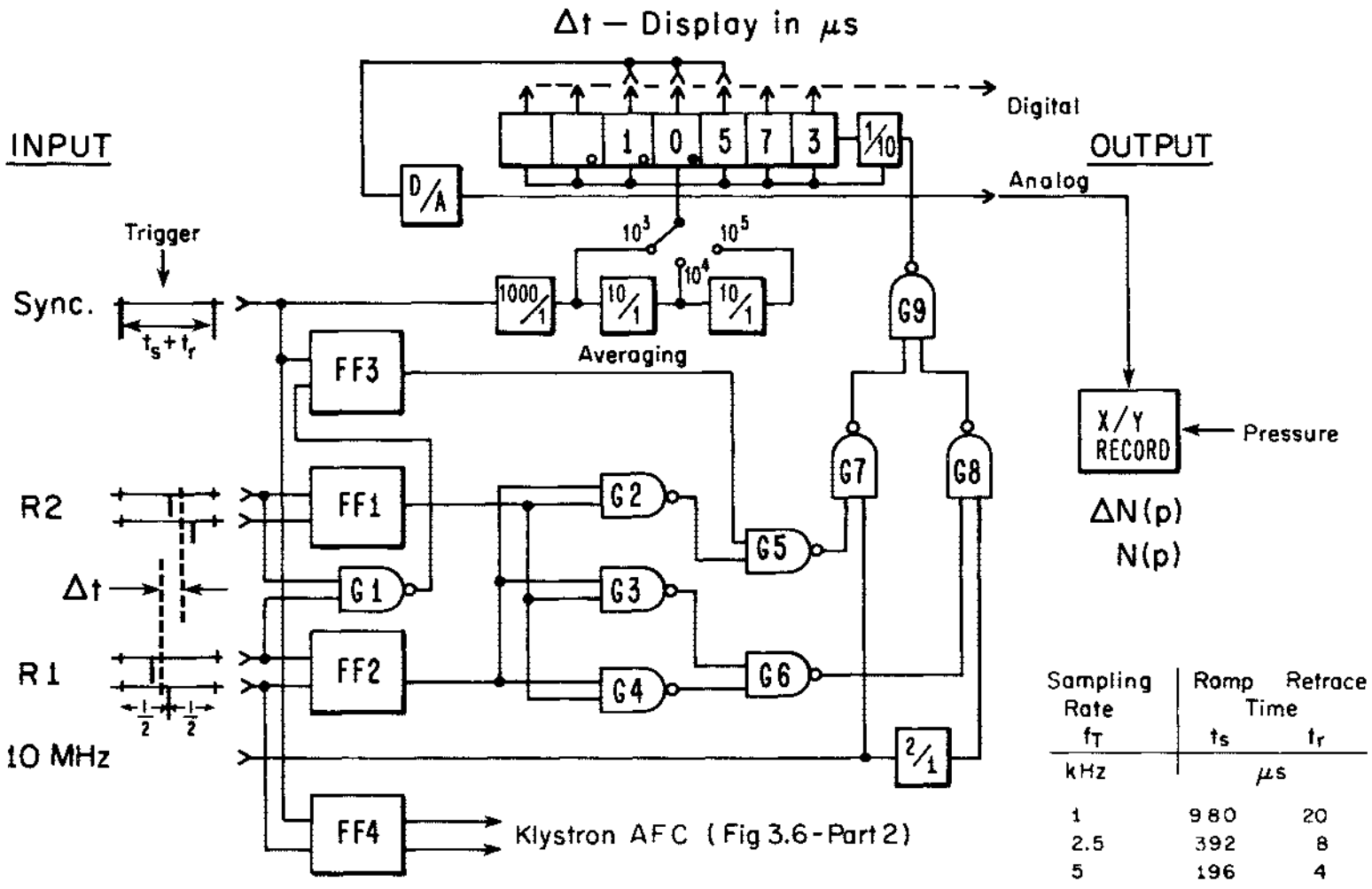

Sampling Rate f_T	Ramp Time t_s	Retrace Time t_r
kHz	μs	
1	980	20
2.5	392	8
5	196	4

Figure A2. Simplified block diagram of time interval averaging for refraction N(p) and dispersion ΔN(p) detection.

Experimental Conditions

$T = 300°K$, $p < 10^{-3}$ torr , $\nu_R = 58\ 436.60$ MHz ,

$Q = 392\ 000$, $\beta \approx 1.2$, $\Delta f_M = 1.25$ MHz

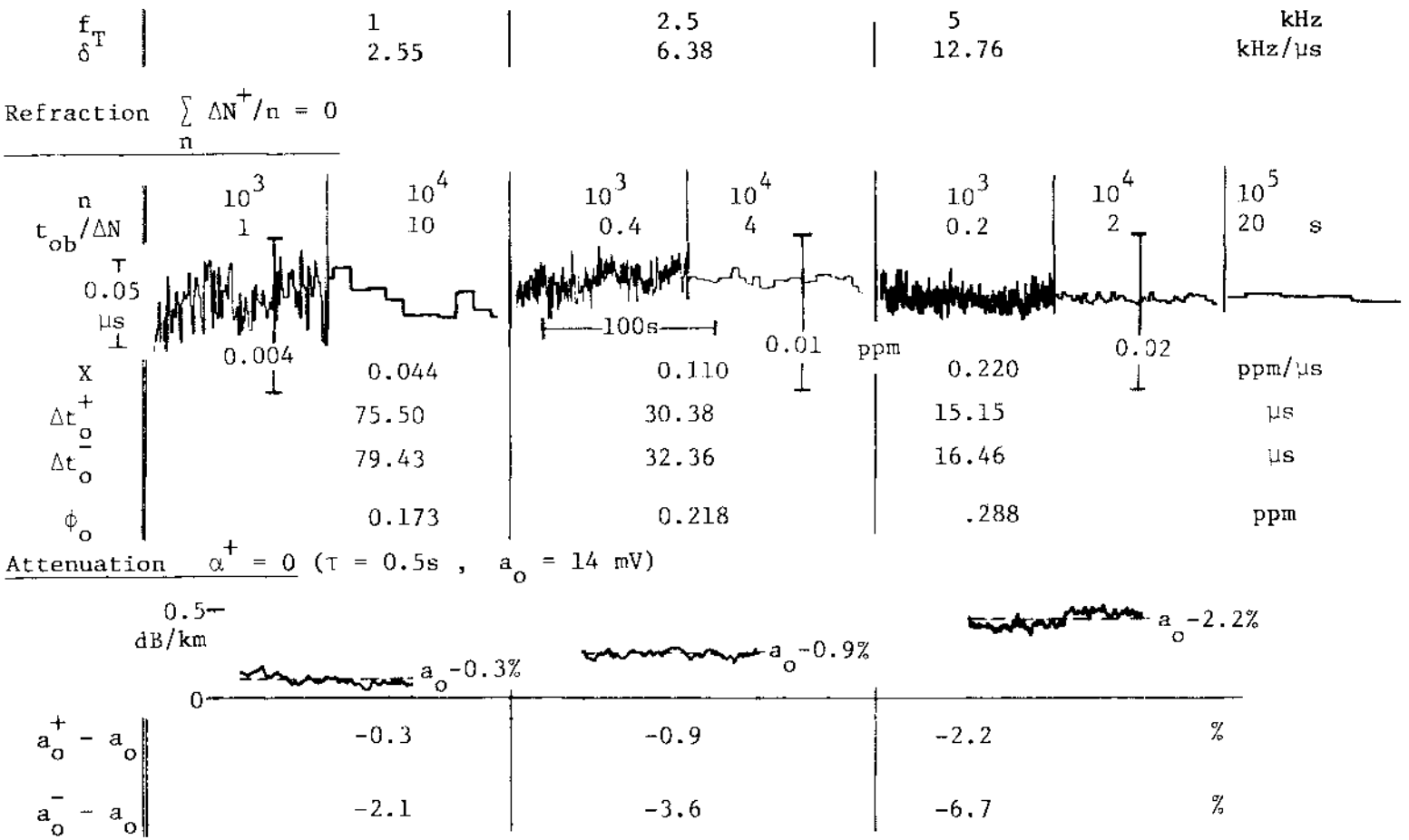

Figure A3. Noise and dynamic study for dispersion and attenuation detection at three sampling rates, f_T = 1, 2.5, 5 kHz.

APPENDIX D

Activities Under Joint Sponsorship (see Preface)

Research Period: 14 January 1971 to 28 February 1975

Personnel: The following made scientific and technical contributions to the work reported in the Final Report (Parts 1 to 3):

Principal Investigator:		H. J. Liebe
Research Associates	:	W. M. Welch U. Mingelgrin T. A. Dillon G. G. Gimmestad
Research Engineers	:	M. J. Vetter R. Chandler A. Diede R. May
Programmer	:	J. Hopponen

Reporting: 38 monthly progress letters have been written

Presentations at Meetings:*)

Liebe and Welch, "Atmospheric transmissivity between 48 and 72 GHz for vertical and horizontal path models at various altitudes," Symp. Antennas and Propagation, IEEE G-AP, Denver, CO, June, 1971.

Mingelgrin, "The effect of pressure and temperature on the O_2 microwave spectrum...," CIRES Seminar, Boulder, CO, November, 1971.

Liebe and Welch, "Complex atmospheric transmission factor between 48 and 72 GHz of various altitudes," URSI Fall Meeting, Los Angeles, September, 1971, (p. 14).

Mingelgrin and Gordon, "Study of some spectra and relaxation phenomena of O_2," 4th National Atomic and Molecular Physics Conf., London, April, 1972, (p. 12).

Welch, Mingelgrin, and Liebe, "Quantitative studies of the pressure-broadened microwave spectrum of O_2," First Internat. Conf. on Spectral Lines, APS, Knoxville, TN, August, 1972.

Liebe and Welch, "Pressure-scanning microwave spectroscopy for quantitative studies of resonant and nonresonant spectra," Second European Microwave Spectroscopy Conf., Bangor, Wales, September, 1972.

Liebe, Recommendations to NSF Workshop on "Future directions of electromagnetics of continuous media," Williamsburg, VA, December, 1972.

-- , "Laboratory measurements and analysis of propagation factors between 20 and 100 GHz," IEEE/AP-S Symposium, NCAR, Boulder, CO, May, 1974.

-- , "Laboratory studies of the atmospheric microwave spectrum of oxygen and water vapor," 5th Colloquium on Microwave Communication, Budapest, June, 1974.

-- , "Oxygen microwave attenuation from laboratory measurements," Third Annual Conf. Telecommunications for Government, Boulder, CO, October, 1974.

-- , "A pressure scanning EHF spectrometer for atmospheric gas studies," 1974 USNC/URSI-IEEE Meeting Boulder, CO, October, 1974.

-- , "Role of spectroscopy in microwave propagation," EM-Wave Seminar (OT-NOAA-CIRES-CU Series), Boulder, CO, February, 1975.

-- , "Absolute intensity measurements of the 60 GHz oxygen band under simulated atmospheric conditions," Inter-Union Commission on Radio Meteorology, URSI-IUGG Workshop, Bournemouth, England, May, 1975.

Also, see under Publications No. 1, 2, 6, 9, 11, and 15.

Publications*)

1. Liebe and Welch, "Phase delay and attenuation in the 50 to 70 GHz band for atmospheric path models at various altitudes," Proc. Internat. Symp. Ant. & Propagation, Sendai, Japan, September, 1971, 239-240 (published by IECE of Japan).

2. Liebe, "Precise measurements of atmospheric propagation parameters in the 50 to 75 GHz band using pressure scanning spectroscopy," Proc. NASA-AAFE Conference. October, 1971, 276-292 (published by NASA/LRC).

*) which carry an acknowledgement of NOAA, NASA, and/or DoD-ARO support (see Preface)

3. Dillon and Liebe, "Dispersion studies of the 22 GHz water vapor line shape. Part II," J. Quant. Spectr. Rad. Transf. 11, 1803-1817, 1971.

4. Welch and Mizushima, "Molecular parameters of the O_2 molecule," Phys. Rev. A-5, 2692-2696 (1972).

5. Welch, Liebe, and Dougherty, "W-Band study (50-75 GHz)," Final Report on ITS Project 910 1383, February 1972, 15 pp.

6. Liebe, Atmospheric transmissivity in the 48 to 72 GHz band. Analysis and Laboratory Measurements, "IEEE Internat. Conf. on Communications, Philadelphia, June, 1972; IEEE Cat. No. 72 CHD-622-1 Com, 41/16-22.

7. Mingelgrin, "Classical scattering calculations for diatomic molecules and application to microwave spectrum of O_2," TRE-32, July, 1972 (U.S. Govt. Printing Office, Washington, D.C.), 58 pp.

8. Liebe, "Complex atmospheric transmission response between 35 and 140 GHz - Programs I and II," OT-ITS Catalog of Telecommunication Related Computer Programs, November, 1971, 216-219.

9. Liebe and Welch, "Laboratory measurements and analysis of atmospheric propagation parameters in the 30 to 72 GHz band," NATO-AGARD Conference Print No. 107, 5/1-20 (18th Meeting of E.M. Wave Prop. Panel), Gausdal, Norway, September, 1972.

10. Mizushima, Wells, Evenson, and Welch, "Laser magnetic resonance of the O_2 molecule," Phys. Rev. L. 29, 831-833, 1972.

11. Liebe, Welch, and Chandler, "Laboratory measurments of e.m. properties of atmospheric gases at millimeter wavelengths, IEE Conference Publ. No. 98, 244-249 (Conf. on Propagation of Radio Waves Above 10 GHz) London, April, 1973.

12. Liebe and Welch, "Molecular attenuation and phase dispersion between 40 and 140 GHz for path models from different -Part 1- altitudes," OT-Report 73-10, May, 1973, 104 pp. (U.S. Govt. Printing Office, Washington, D.C.).

13. Liebe, "A pressure-scanning refraction spectrometer for atmospheric gas studies at millimeter wavelengths," -Part 2- OT-Report 74-35, April, 1974, 132 pp. (U.S. Govt. Printing Office, Washington, D.C.).

14. Mingelgrin, "The microwave dispersion spectrum of O_2," Molecular Physics, 28, 1591-1602, (1974).

15. Liebe and Welch, "Laboratory measurements and analysis of atmospheric propagation factors between 20 and 100 GHz," 1974 MmWaves Techniques Conference, NELC - San Diego, March, 1974, B2/1-6.

16. Liebe, "Molecular EHF transfer characteristics of air," Chapter C.VIII in Handbook "Multipath in the Air Traffic Control Frequencies," (W. J. Hartman, editor), Report No. FAA-74-75, vol. II, pp. 1-33, July, 1974 (available from NTIS, Springfield, Virginia 22151).

17. Liebe, "Transfer characteristics of clear air between 10 and 150 GHz," contribution to NASA Active Microwave Workshop Handbook, Sect. 4.4.4, pp. 205-236, July, 1974.

18. Liebe, "Molecular transfer characteristics of air between 40 and 140 GHz," IEEE Trans. MTT-23, 380-386, 1975.

19. Liebe, "Studies of oxygen and water vapor microwave spectra under simulated atmospheric conditions," OT Report 75-65, June, 1975, 150 pp. (this report). -Part 3-

20. Liebe, "A pressure-scanning millimeter-wave dispersion spectrometer," Rev. Sci. Instr. 46, July, 1975.

21. Liebe and Hopponen, "Temperature and pressure sensitivities of air transfer characteristics between 40 and 140 GHz," in preparation for Radio Science.

FORM OT-29
(3-73)

U.S. DEPARTMENT OF COMMERCE
OFFICE OF TELECOMMUNICATIONS

BIBLIOGRAPHIC DATA SHEET

	1. PUBLICATION OR REPORT NO.	2. Gov't Accession No.	3. Recipient's Accession No.
	OTR 75-65		

4. TITLE AND SUBTITLE
Studies of oxygen and water vapor microwave spectra under simulated atmospheric conditions.

5. Publication Date
June 1975

6. Performing Organization Code
OT/ITS, Div. 3

7. AUTHOR(S)
Hans J. Liebe

9. Project/Task/Work Unit No.
910 1411 (a)
910 1410 (b)
910 5204 (OT)

8. PERFORMING ORGANIZATION NAME AND ADDRESS
U.S. Department of Commerce
OT/ITS
325 Broadway
Boulder, CO 80302

10. Contract/Grant No.
(a) NASA-AAFE L58, 506
(b) NOAA-NESS 5-13155

11. Sponsoring Organization Name and Address
(a) NASA Langley Research Center, Hampton, VA 23365
(b) NOAA-National Environmental Satellite Service, Suitland, MD 20233

12. Type of Report and Period Covered
OT Report *
(Final Report, Part III)

13.

14. SUPPLEMENTARY NOTES
*Part I is OT Report 73-10, Part II is OT Report 74-35

15. ABSTRACT *(A 200-word or less factual summary of most significant information. If document includes a significant bibliography or literature survey, mention it here.)*

Atmospheric radio wave propagation in the 40 to 140 GHz band is influenced by microwave spectra of oxygen (O_2-MS) and water vapor. The report treats the complementary roles of controlled laboratory experiments and computer analysis for providing detailed molecular transfer characteristics. A pressure-scanning differential refractometer was operated at fixed frequencies between 58 and 61.5 GHz. The variability of O_2 and H_2O spectra with frequency, pressure, temperature, and magnetic field strength was studied under conditions which occur in the atmosphere. Results obtained (a) for oxygen and air on the 9^+ line, the $7^+/5^-$ and $3^+/9^-$ doublets, and the continuum spectrum, and (b) for water vapor on nonresonant effects, are reported. The experimental O_2-MS data are used in theoretical analyses of attenuation and dispersion rates which are extended to other lines, to frequencies identified for remote sensing applications, and to temperature and pressure sensitivities between 40 and 140 GHz.

16. Key words *(Alphabetical order, separated by semicolons)*
Atmospheric mm-wave propagation; attenuation profiles; dispersion profiles; EHF transfer characteristics; oxygen microwave spectrum; water vapor microwave spectrum.

17. AVAILABILITY STATEMENT

[X] UNLIMITED.

[ ] FOR OFFICIAL DISTRIBUTION.

18. Security Class *(This report)*	20. Number of pages
Unclassified	150
19. Security Class *(This page)*	**21. Price:**
Unclassified	

USCOMM-DC 29716-P73
USCOMM - EXL

U.S. GOVERNMENT PRINTING OFFICE 1975 - 680-794/232 Reg. 6